Acridinone-based anion transporters

Daniel A. McNaughton,[a] Lauren K. Macreadie [a] and Philip A. Gale [*a,b]

[a.] *School of Chemistry (F11), The University of Sydney, NSW 2006, Australia.*
[b.] *The University of Sydney Nano Institute (SydneyNano), The University of Sydney, NSW 2006, Australia.*

Characterisation Data
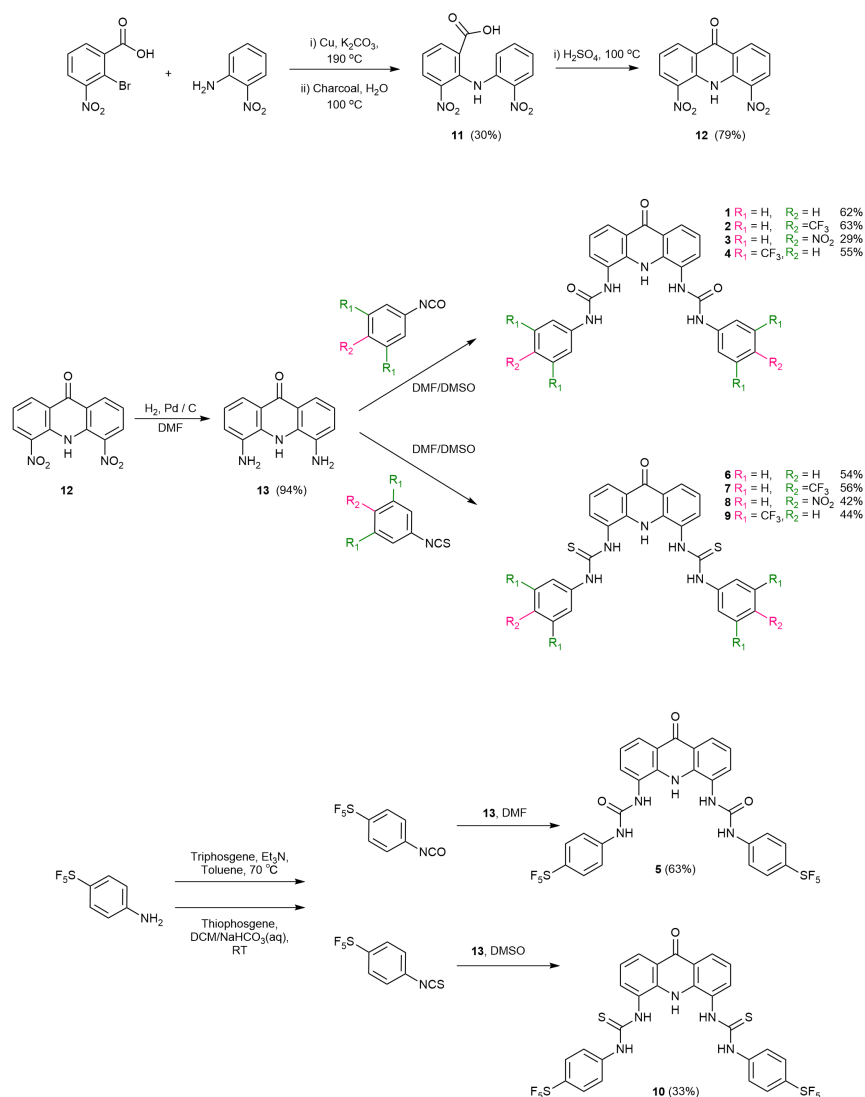
Scheme S1. General schematic for the synthesis of compounds **1**−**10** from commercial starting material. Methods can be found in the experimental section and characterisation of each compound can be found below.
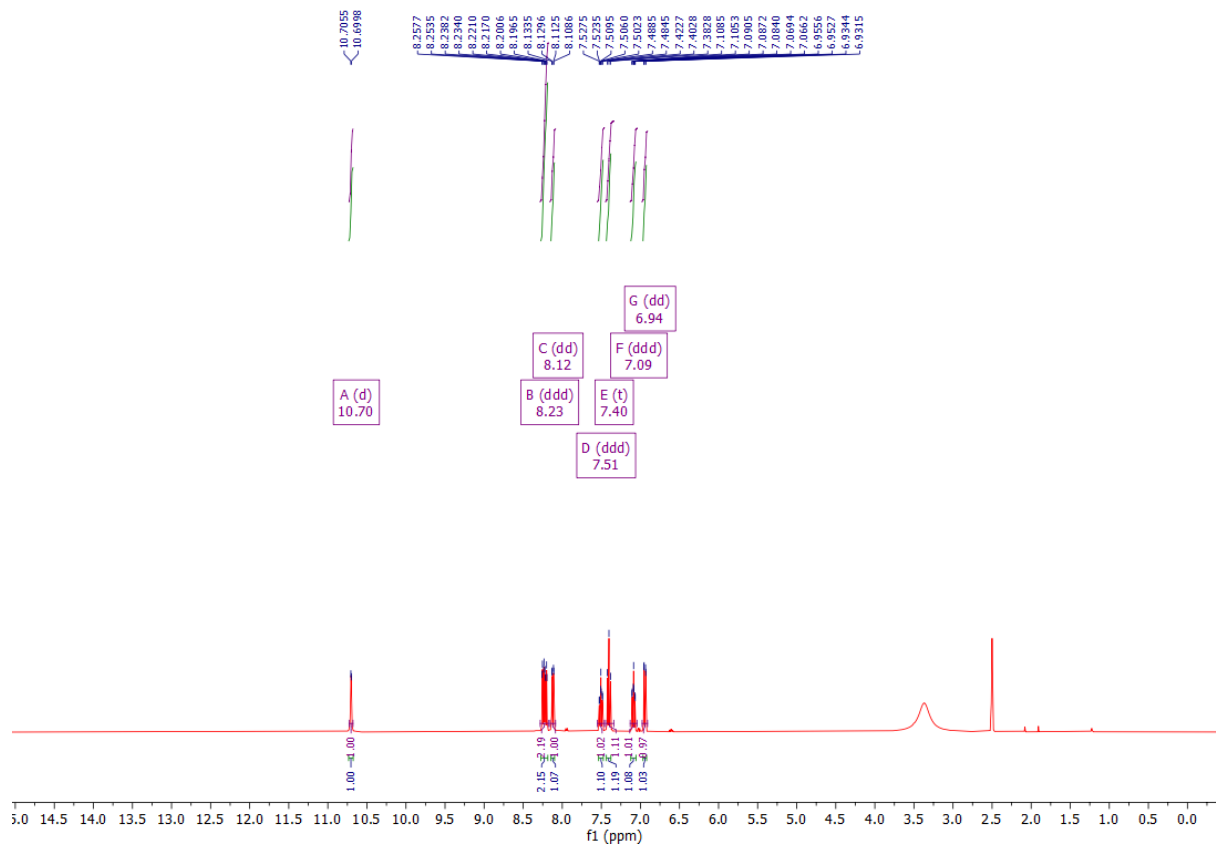
2,2'-Dinitrodiphenylamine-6-carboxylic acid
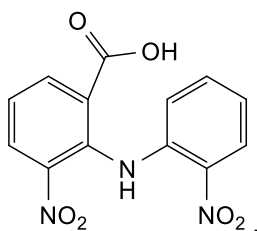
Figure S1. ¹H NMR (400 MHz) spectrum of 2,2'-dinitrodiphenylamine-6-carboxylic acid in $(CD_3)_2SO_3$ at 298 K.
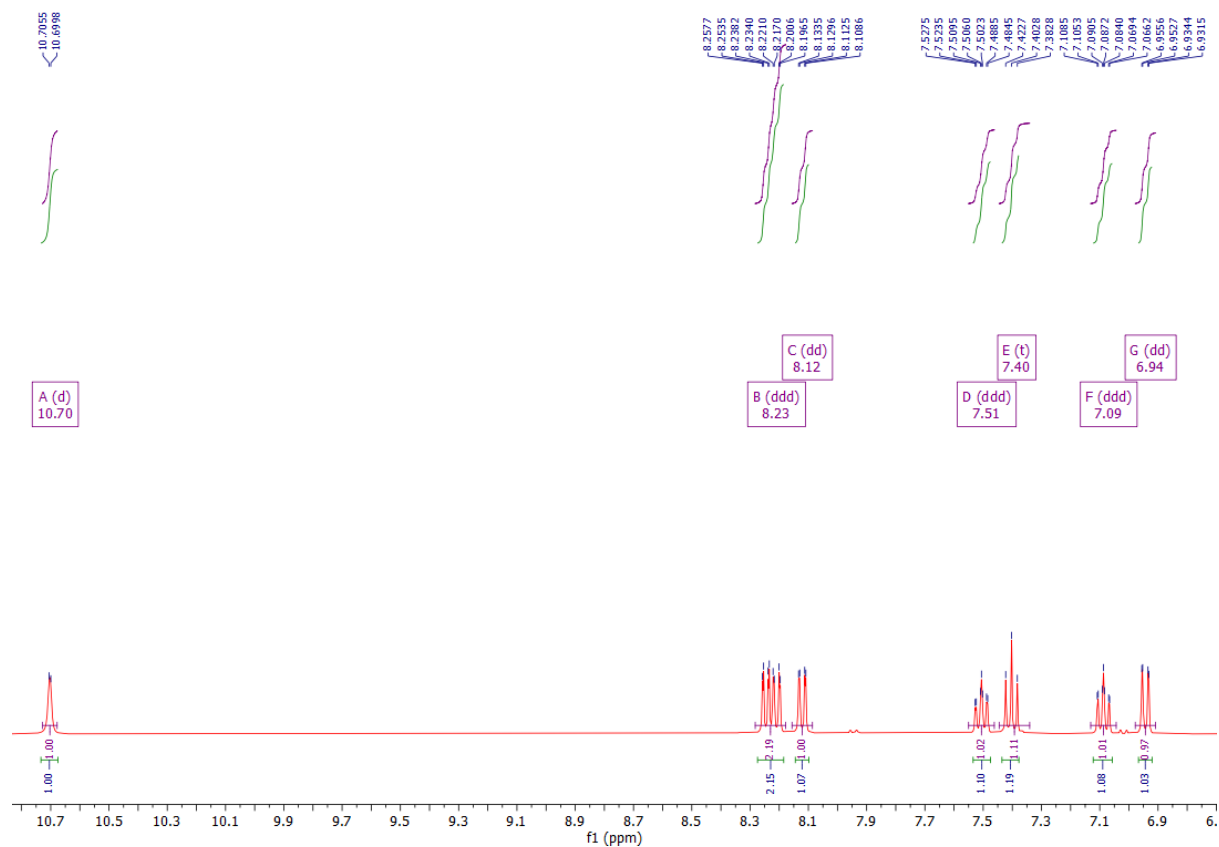
Figure S2. ^{1}H NMR (400 MHz) spectrum of 2,2'-dinitrodiphenylamine-6-carboxylic acid in $(CD_3)_2SO_3$ at 298 K. Zoomed in for clarity.
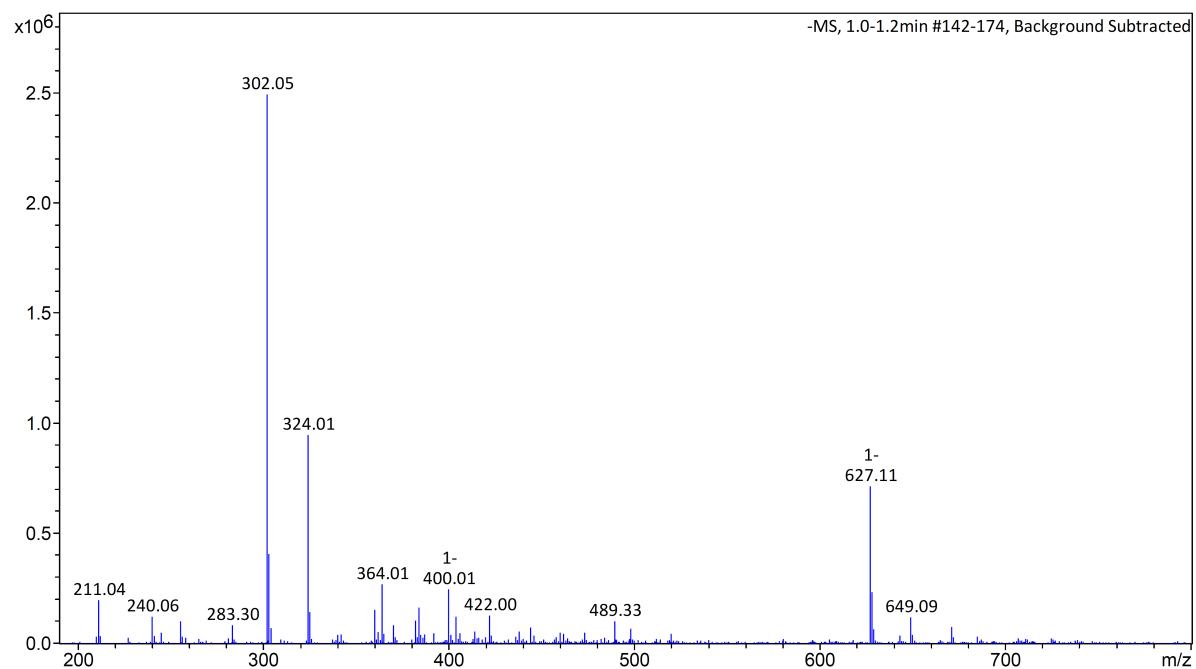
Figure S3. LR-MS (ESI⁻) of 2,2'-Dinitrodiphenylamine-6-carboxylic acid.

1,9-Dinitroacridinone
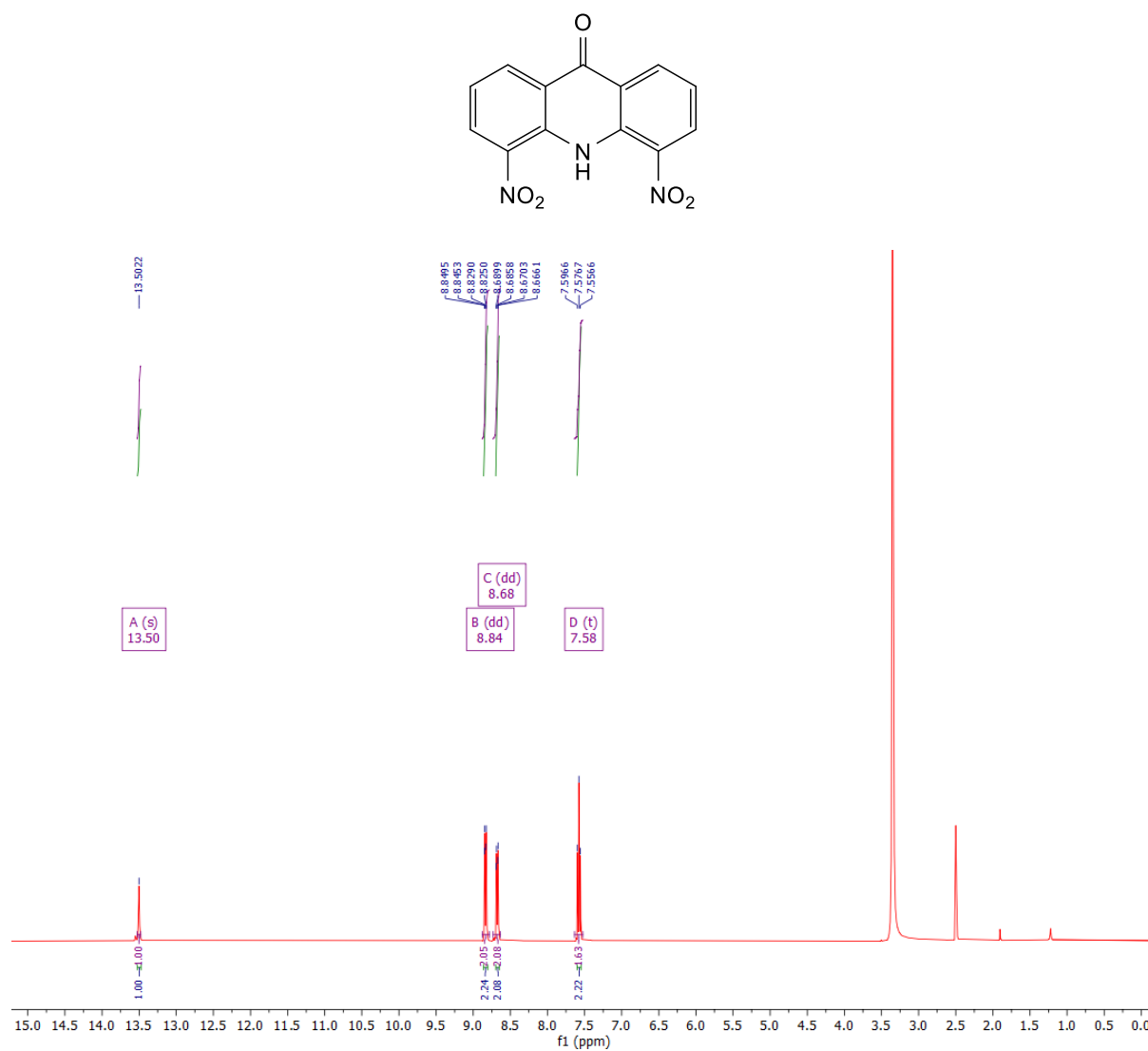
Figure S4. ^{1}H NMR (400 MHz) spectrum of 1,9-Dinitroacridinone in $(CD_3)_2SO_3$ at 298 K.
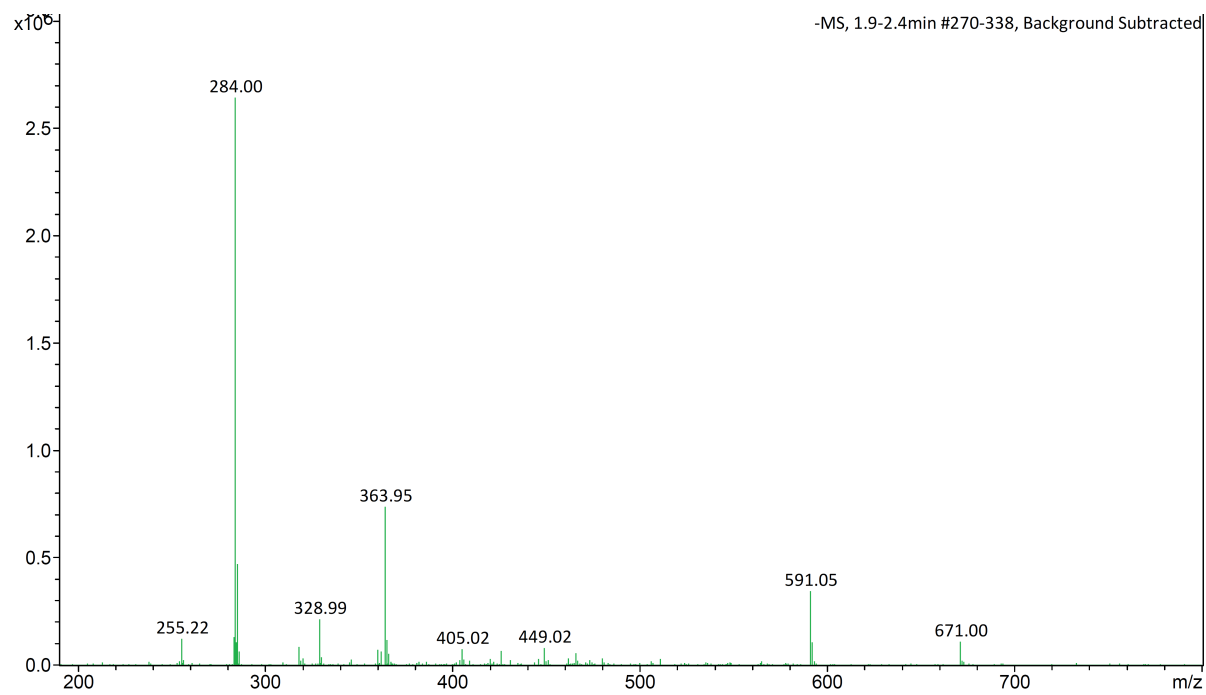
Figure S5. LR-MS (ESI⁻) of 1,9-Dinitroacridinone.

1,9-Diaminoacridinone
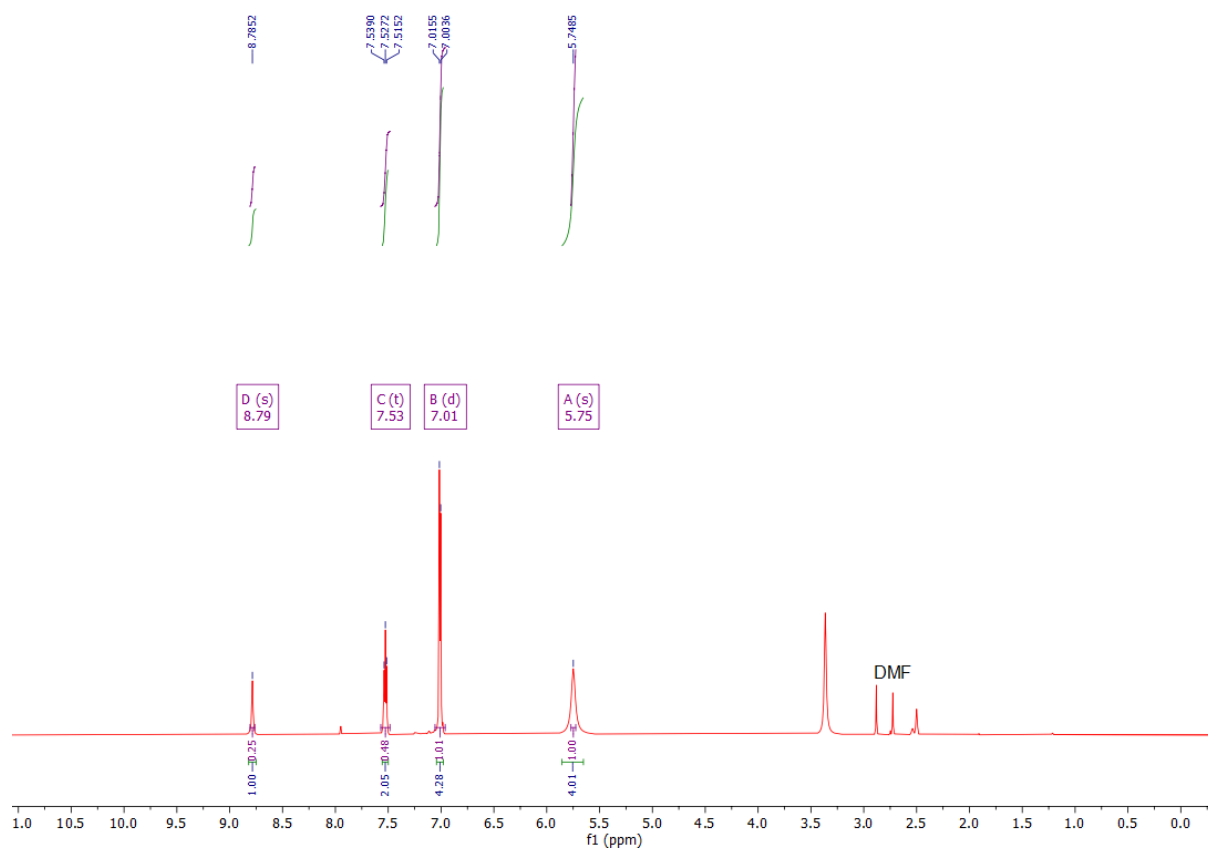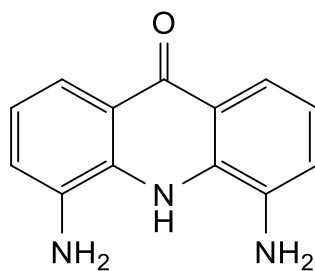
Figure S6. ^{1}H NMR (400 MHz) spectrum of 1,9-diaminoacridinone in $(CD_3)_2SO_3$ at 298 K.
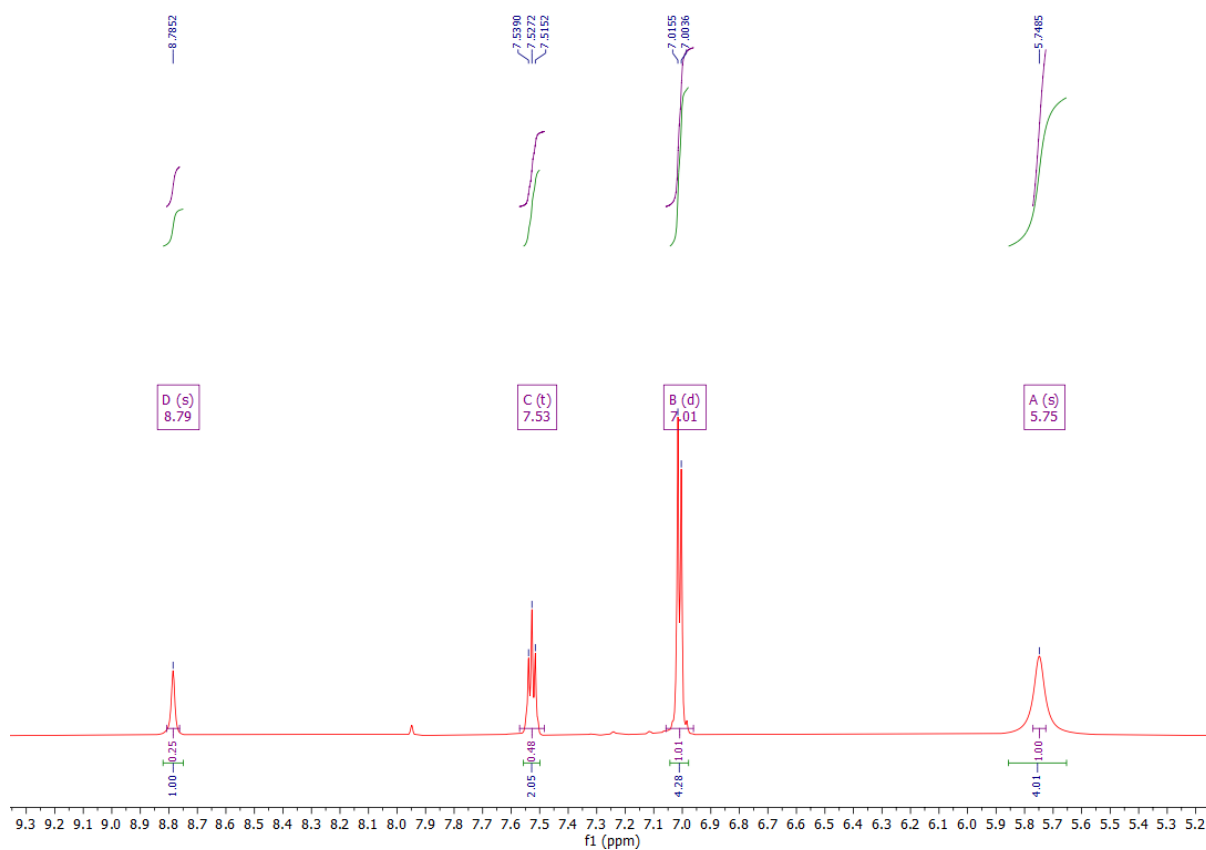
Figure S7. ^{1}H NMR (400 MHz) spectrum of 1,9-diaminoacridinone in $(CD_3)_2SO_3$ at 298 K. Zoomed in for clarity.
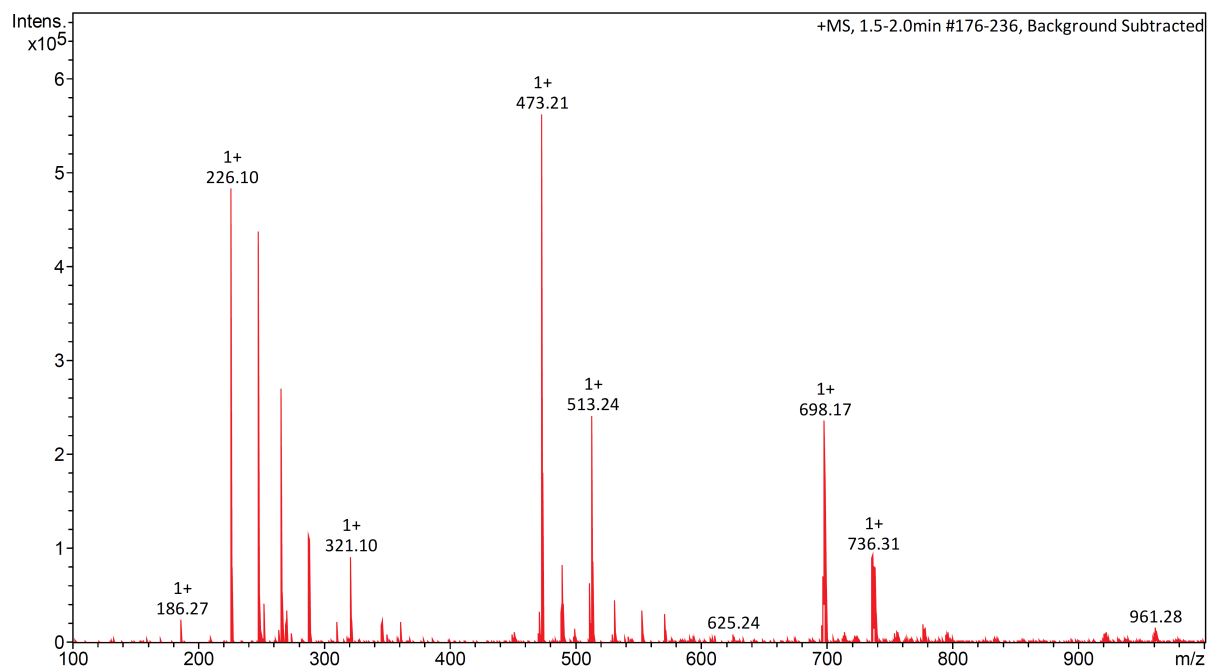
Figure S 8. LR-MS (ESI$^+$) of 1,9-diaminoacridinone.

Compound 1: 1,9-bisphenylurea-9(10H)-acridinone
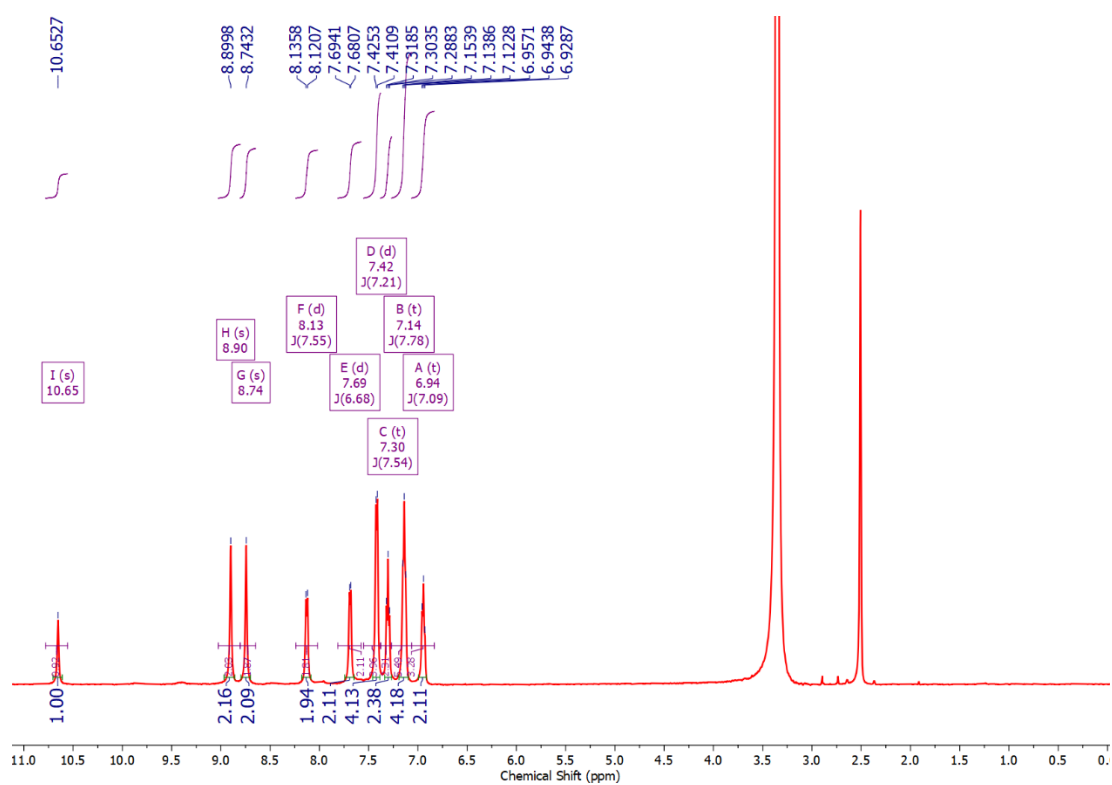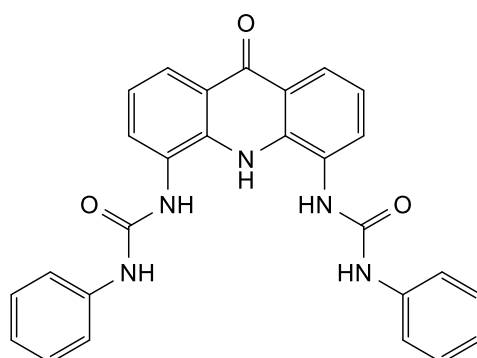
Figure S9. ^{1}H NMR (500 MHz) spectrum of 1,9- bisphenylurea-9(10H)-acridinone in $(CD_3)_2SO_3$ at 298 K.

Figure S10. ^{13}C NMR (101 MHz) spectrum of 1,9-bisphenylurea-9(10H)-acridinone in $(CD_3)_2SO_3$ at 298 K.

Figure S11. ^{13}C NMR (101 MHz) spectrum of 1,9-bisphenylurea-9(10H)-acridinone in $(CD_3)_2SO_3$ at 298 K. Zoomed in for clarity.

Figure S12. LR-MS (ESI⁻) of 1,9-bisphenylurea-9(10H)-acridinone.
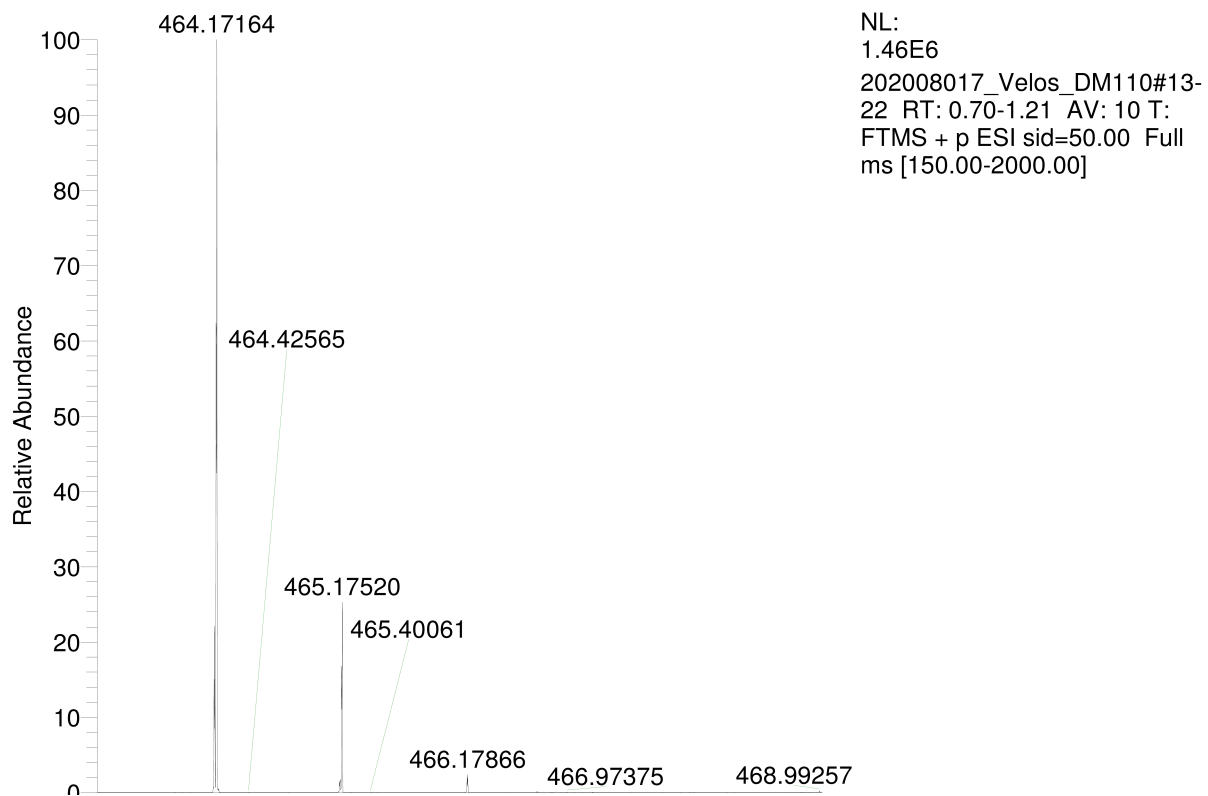
Figure S13. HR-MS (ESI+) of 1,9-bisphenylurea-9(10H)-acridinone.

Compound 2: 1,9-bis(4-(trifluoromethyl)phenyl)urea-9(10H)-acridinone

Figure S14. ^{1}H NMR (600 MHz) spectrum of 1,9-bis(4-(trifluoromethyl)phenyl)urea-9(10H)-acridinone in $(CD_3)_2SO_3$ at 298 K.

Figure S15. ^{13}C NMR (101 MHz) spectrum of 1,9-bis(4-(trifluoromethyl)phenyl)urea-9(10H)-acridinone in $(CD_3)_2SO_3$ at 298 K.
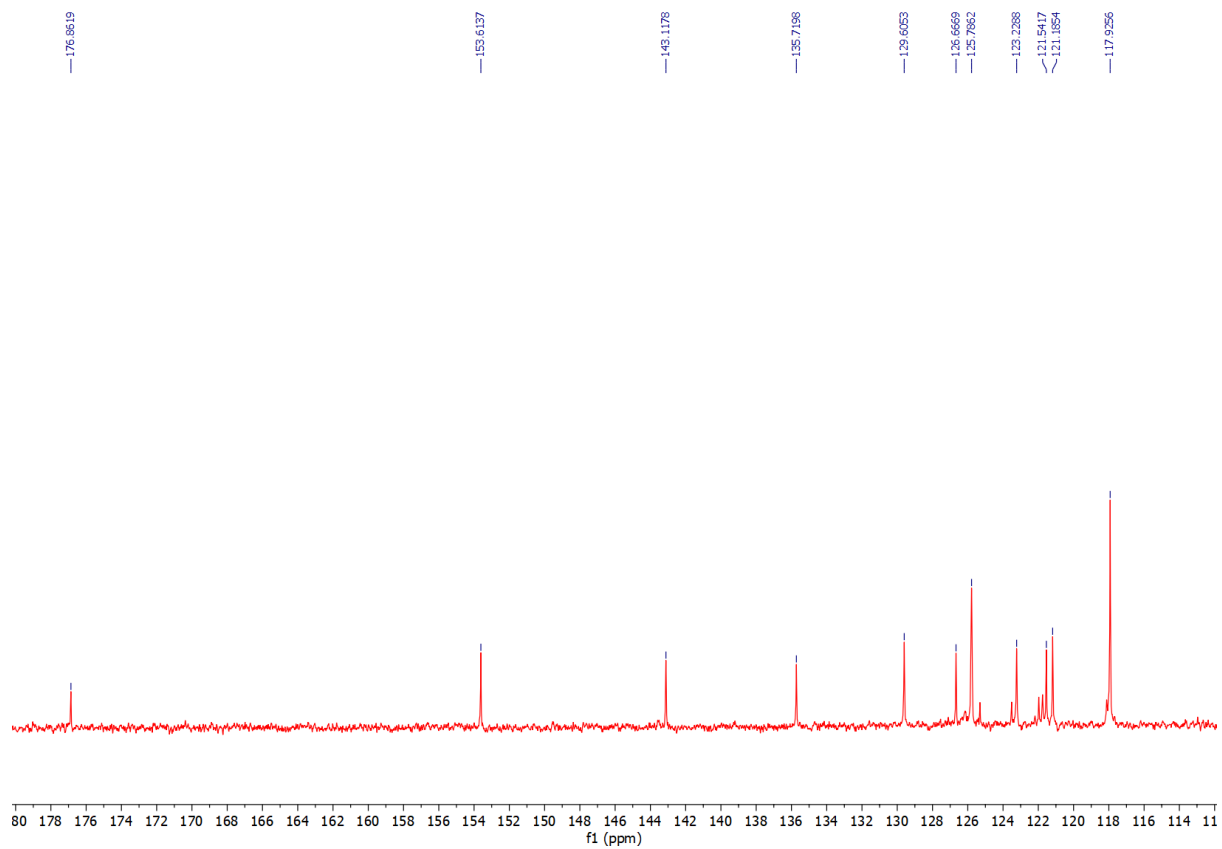
Figure S16. ^{13}C NMR (101 MHz) spectrum of 1,9-bis(4-(trifluoromethyl)phenyl)urea-9(10H)-acridinone in $(CD_3)_2SO_3$ at 298 K. Zoomed in for clarity.

Figure S17. ^{13}C NMR (101 MHz) spectrum of 1,9-bis(4-(trifluoromethyl)phenyl)urea-9(10H)-acridinone in $(CD_3)_2SO_3$ at 298 K. Zoomed in for clarity with splitting of CF_3 β-carbon and CF_3 α-carbon displayed. Full resolution of quartet splitting could not be attained.

Figure S18. LR-MS (ESI⁻) spectrum of 1,9-bis(4-(trifluoromethyl)phenyl)urea-9(10H)-acridinone.

S16

Figure S19.HR-MS (ESI⁺) spectrum of 1,9-bis(4-(trifluoromethyl)phenyl)urea-9(10H)-acridinone.

Compound 3: 1,9-bis(4-nitrophenyl)urea-9(10H)-acridinone

Figure S20. ¹H NMR (600 MHz) spectrum of 1,9-bis(4-nitrophenyl)urea-9(10H)-acridinone in (CD₃)₂SO₃ at 298 K.
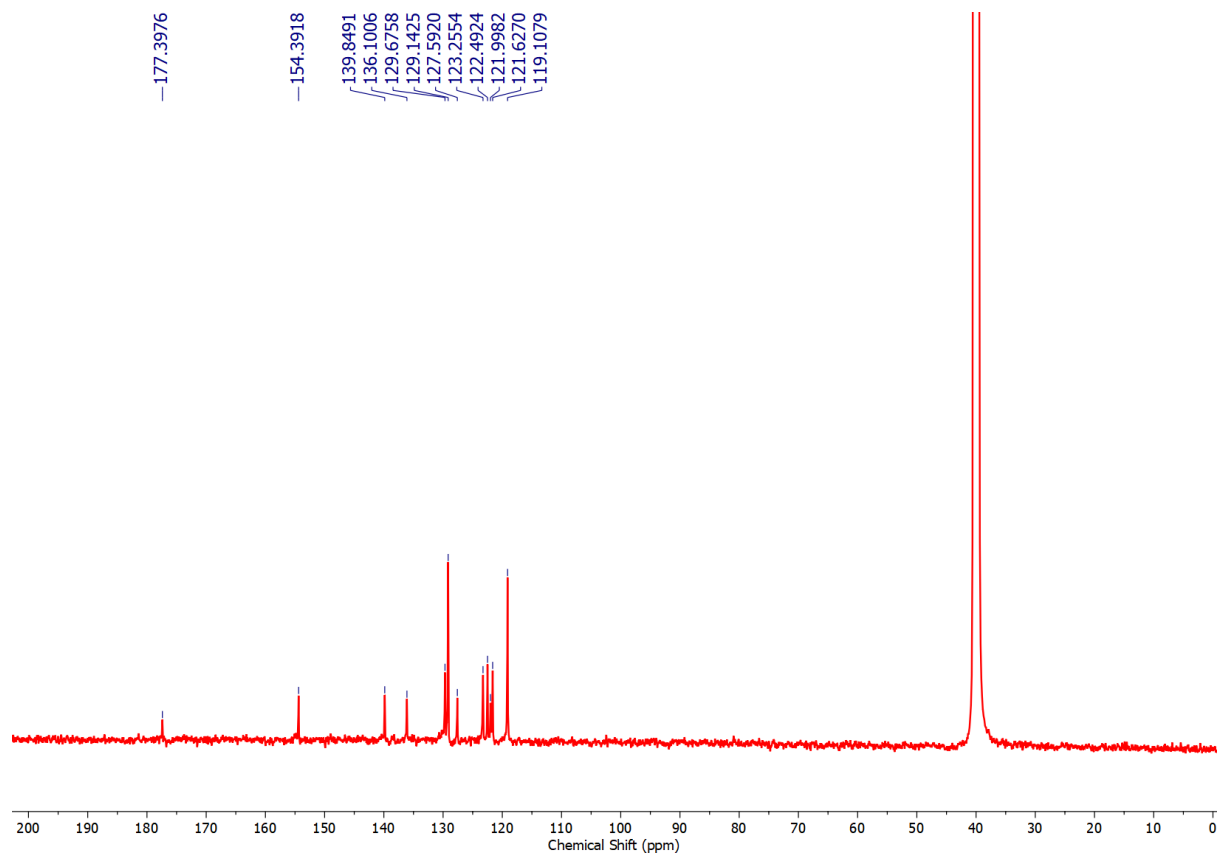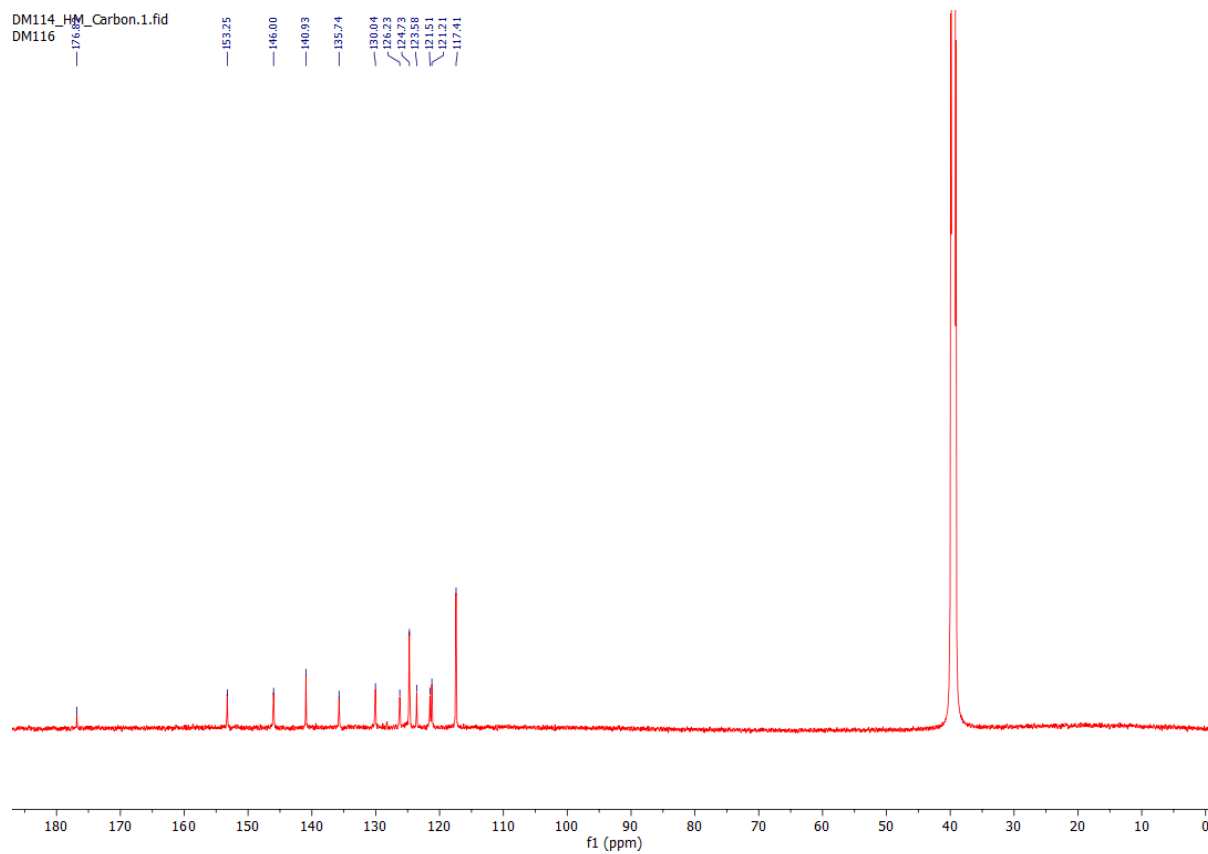
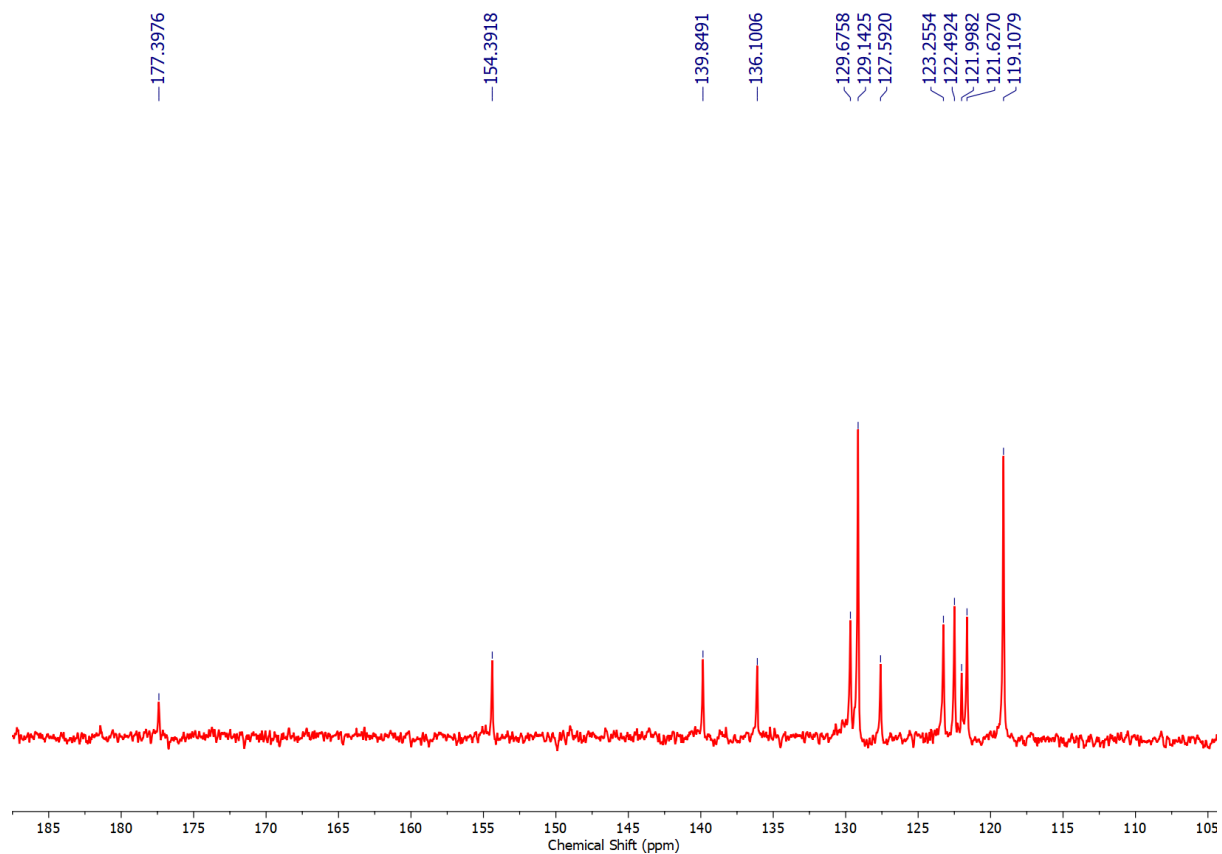Figure S21. ^{13}C NMR (101 MHz) spectrum of 1,9-bis(4-nitrophenyl)urea-9(10H)-acridinone in $(CD_3)_2SO_3$ at 298 K.
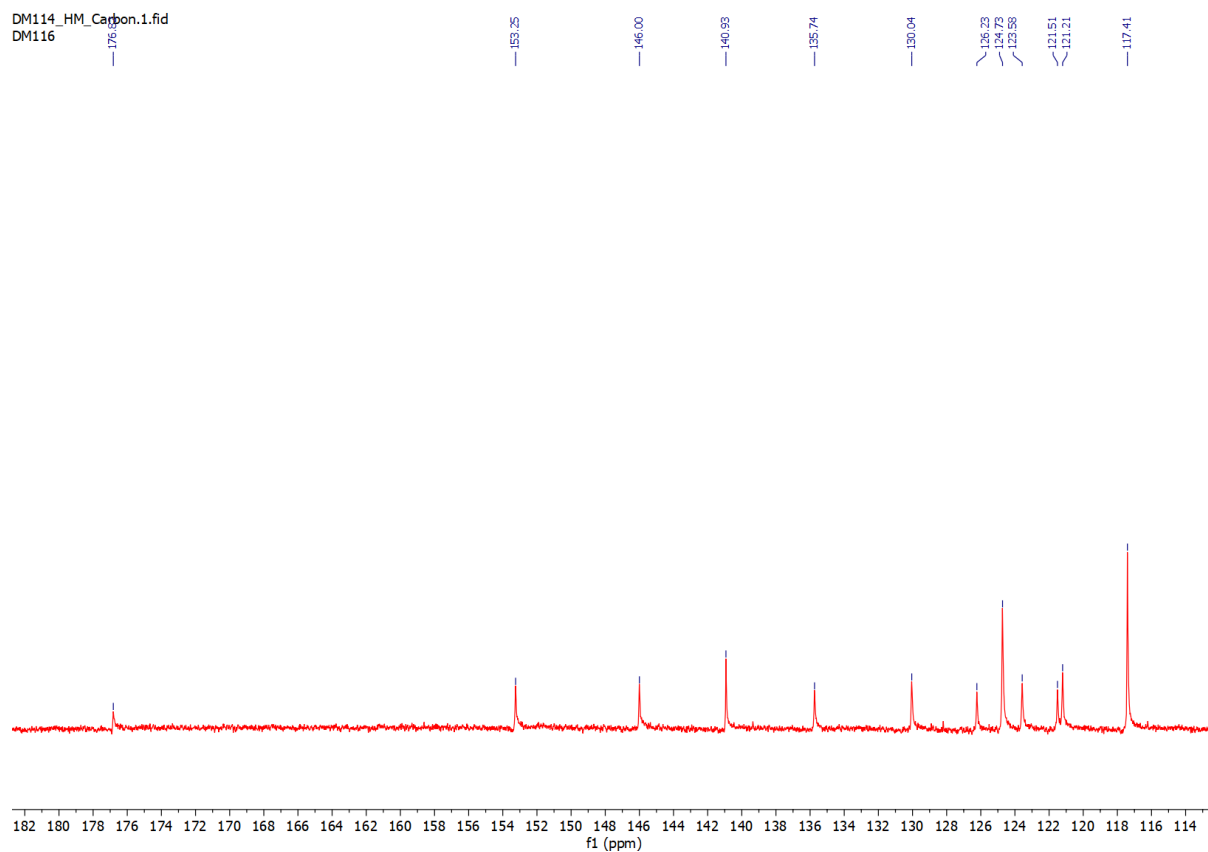
Figure S22. ^{13}C NMR (101 MHz) spectrum of 1,9-bis(4-nitrophenyl)urea-9(10H)-acridinone in (CD$_3$)$_2$SO$_3$ at 298 K. Zoomed in for clarity.
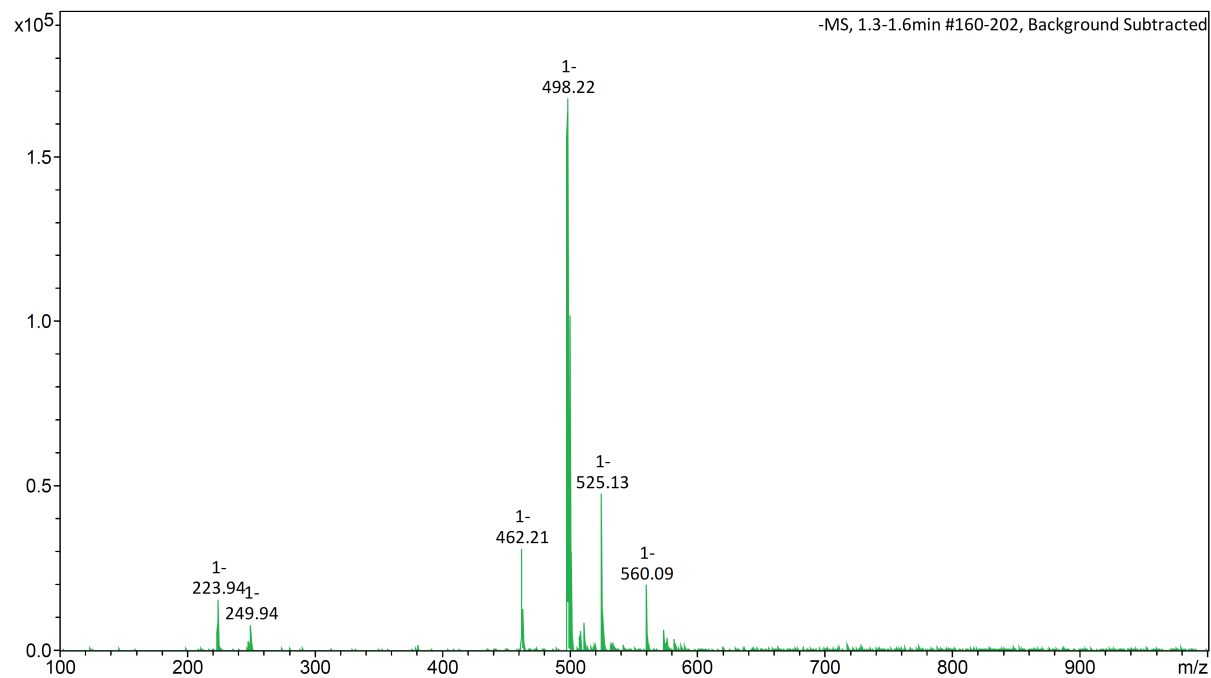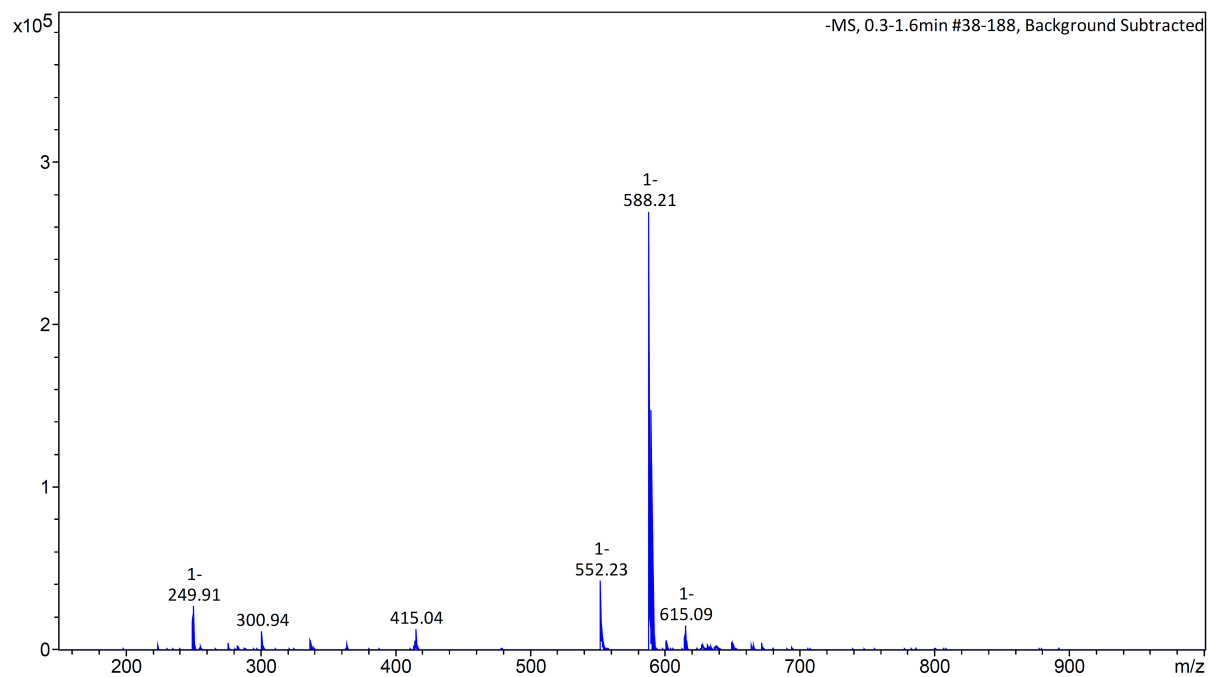

Figure S23. LR-MS (ESI$^-$) spectrum of 1,9-bis(4-nitrophenyl)urea-9(10H)-acridinone.
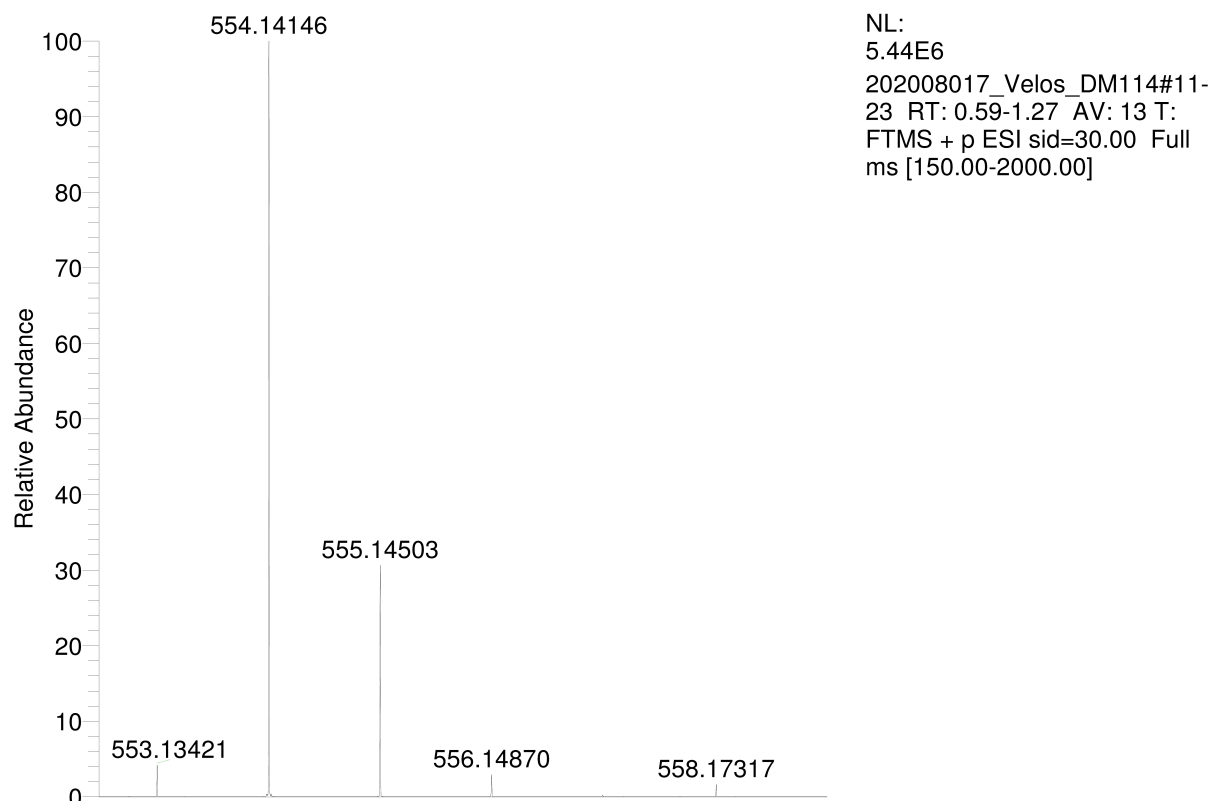
Figure S24. HR-MS (ESI$^+$) spectrum of 1,9-bis(4-nitrophenyl)urea-9(10H)-acridinone.

Compound 4: 1,9-bis(3,5-bis-(trifluoromethyl)phenyl)urea-9(10H)-acridinone
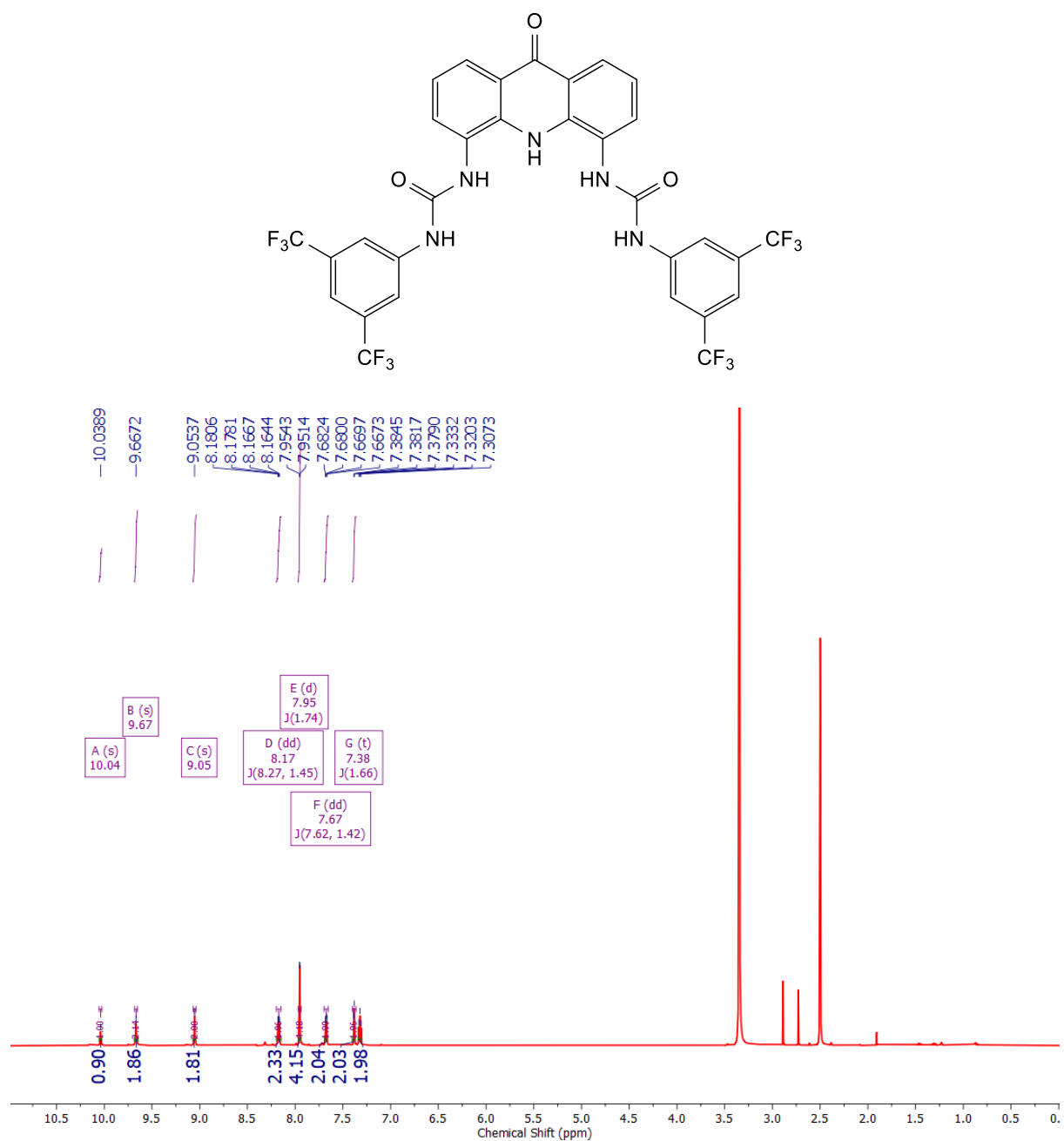
Figure S25. ¹H NMR (600 MHz) spectrum of 1,9-bis(3,5-bis(trifluoromethyl)phenyl)urea-9(10H)-acridinone in $(CD_3)_2SO_3$ at 298 K.

Figure S26. ^{13}C NMR (101 MHz) spectrum of 1,9-bis(3,5-bis-(trifluoromethyl)phenyl)urea-9(10H)-acridinone in $(CD_3)_2SO_3$ at 298 K.
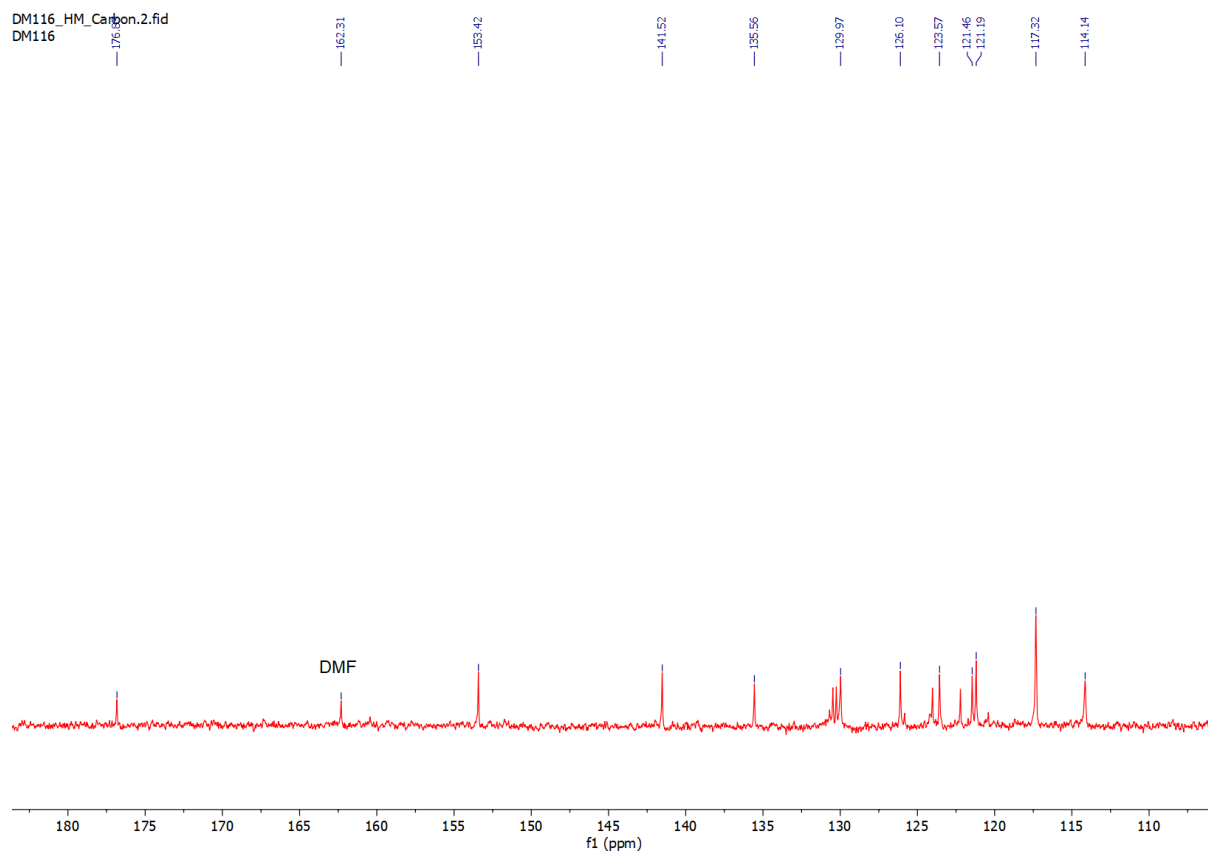
Figure S27. ^{13}C NMR (101 MHz) spectrum of 1,9-bis(3,5-bis-(trifluoromethyl)phenyl)urea-9(10H)-acridinone in $(CD_3)_2SO_3$ at 298 K. Zoomed in for clarity.
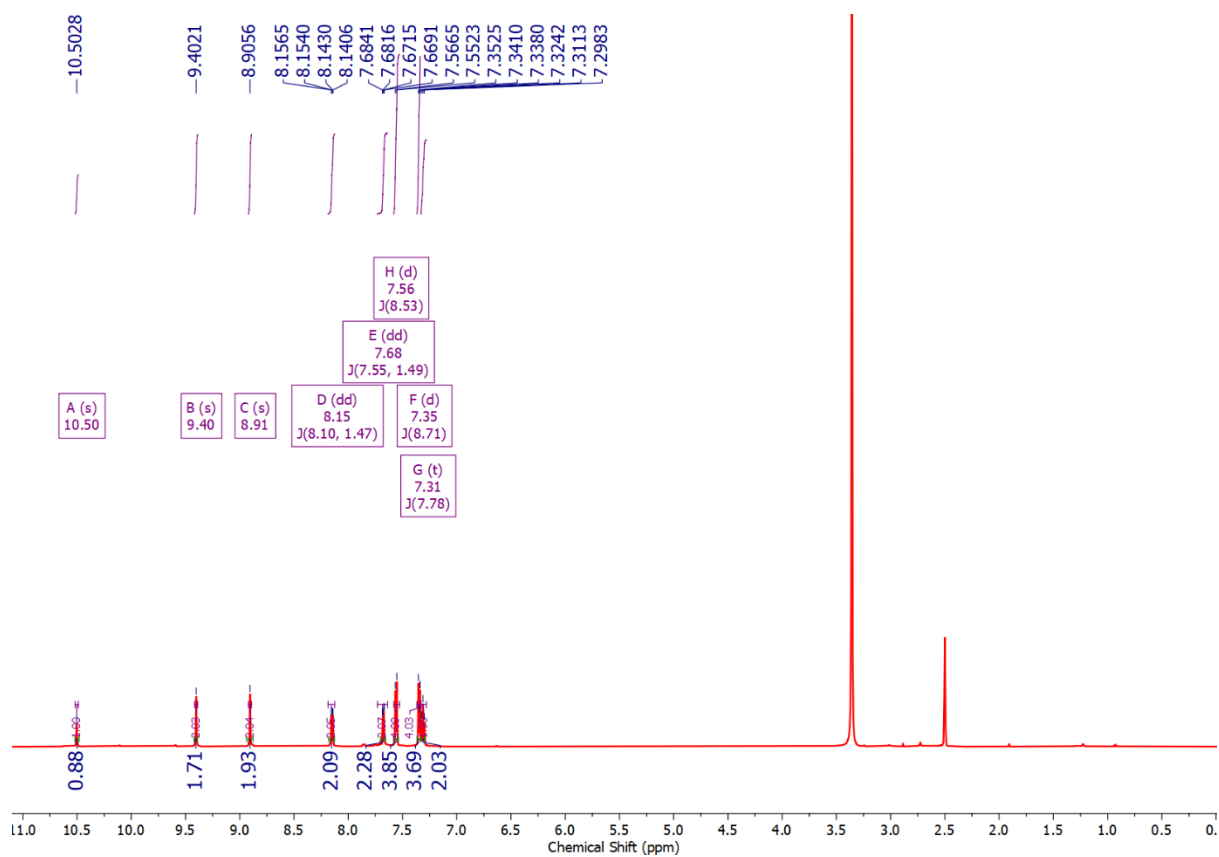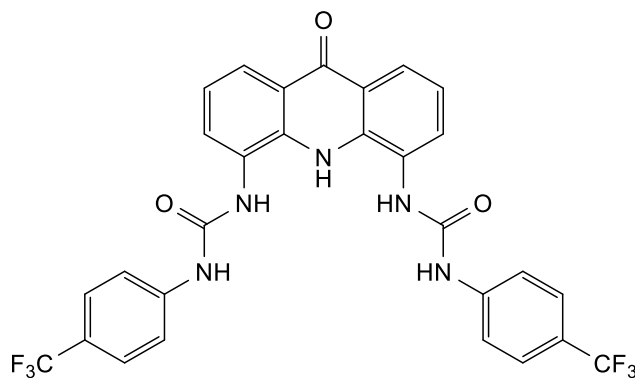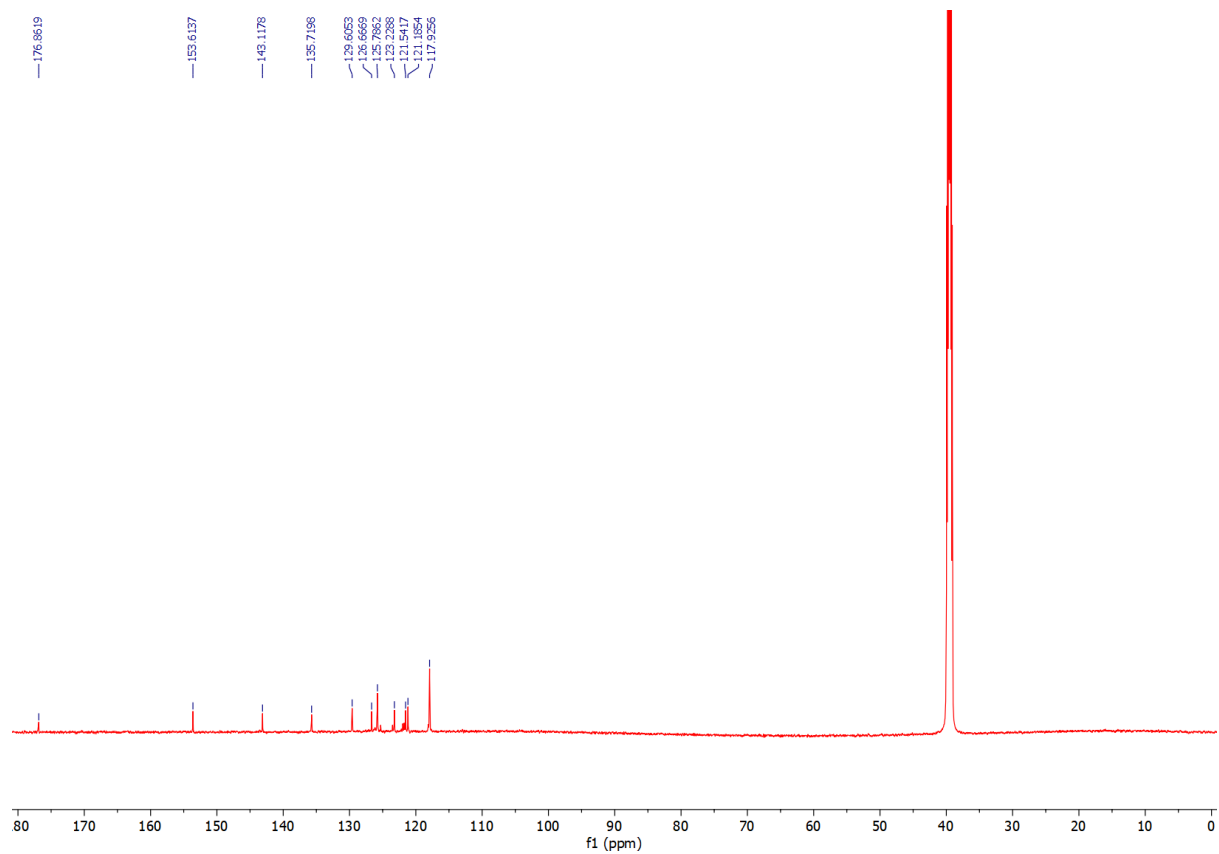
Figure S28. ^{13}C NMR (101 MHz) spectrum of 1,9-bis(3,5-bis-(trifluoromethyl)phenyl) urea-9(10H)-acridinone in $(CD_3)_2SO_3$ at 298 K. Zoomed in for clarity, showing α-carbon splitting (130.4 ppm) and β-carbon splitting (123.1 ppm).
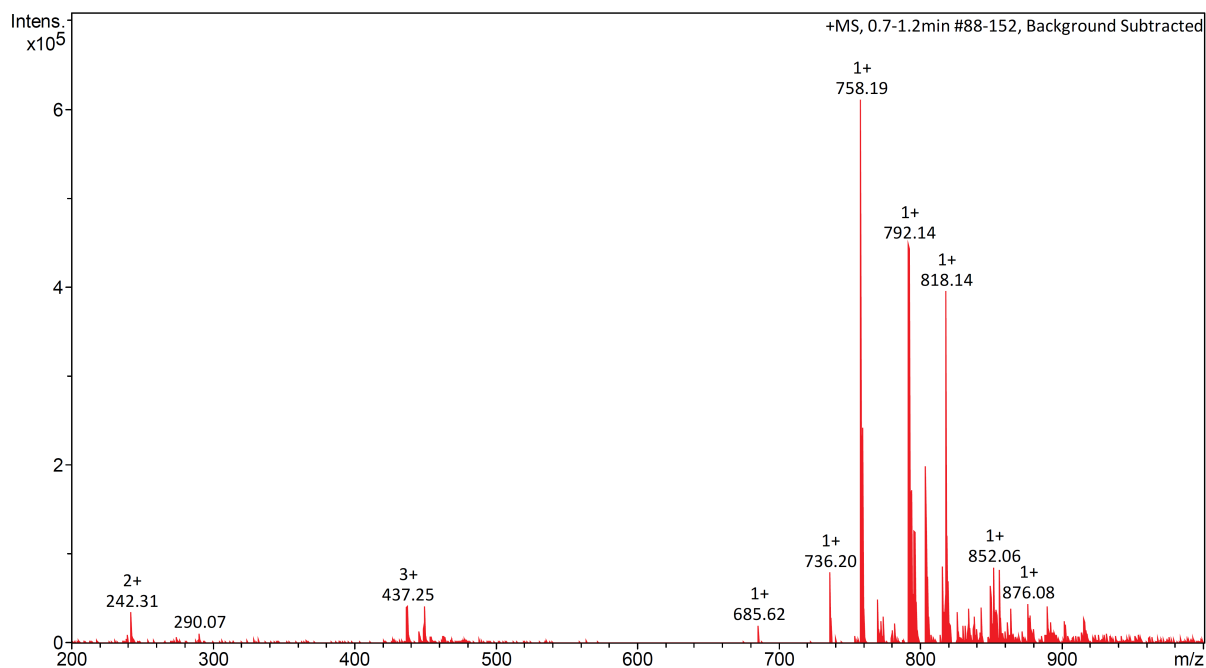
Figure S29. LR-MS (ESI$^+$) spectrum of 1,9-bis(3,5-bis-(trifluoromethyl)phenyl)urea-9(10H)-acridinone.

Figure S30. HR-MS (ESI⁺) spectrum of 1,9-bis(3,5-bis-(trifluoromethyl)phenyl)urea-9(10H)-acridinone.

Compound 5: 1,9-bis(4-(pentafluorosulfanyl)phenyl)urea-9(10H)-acridinone
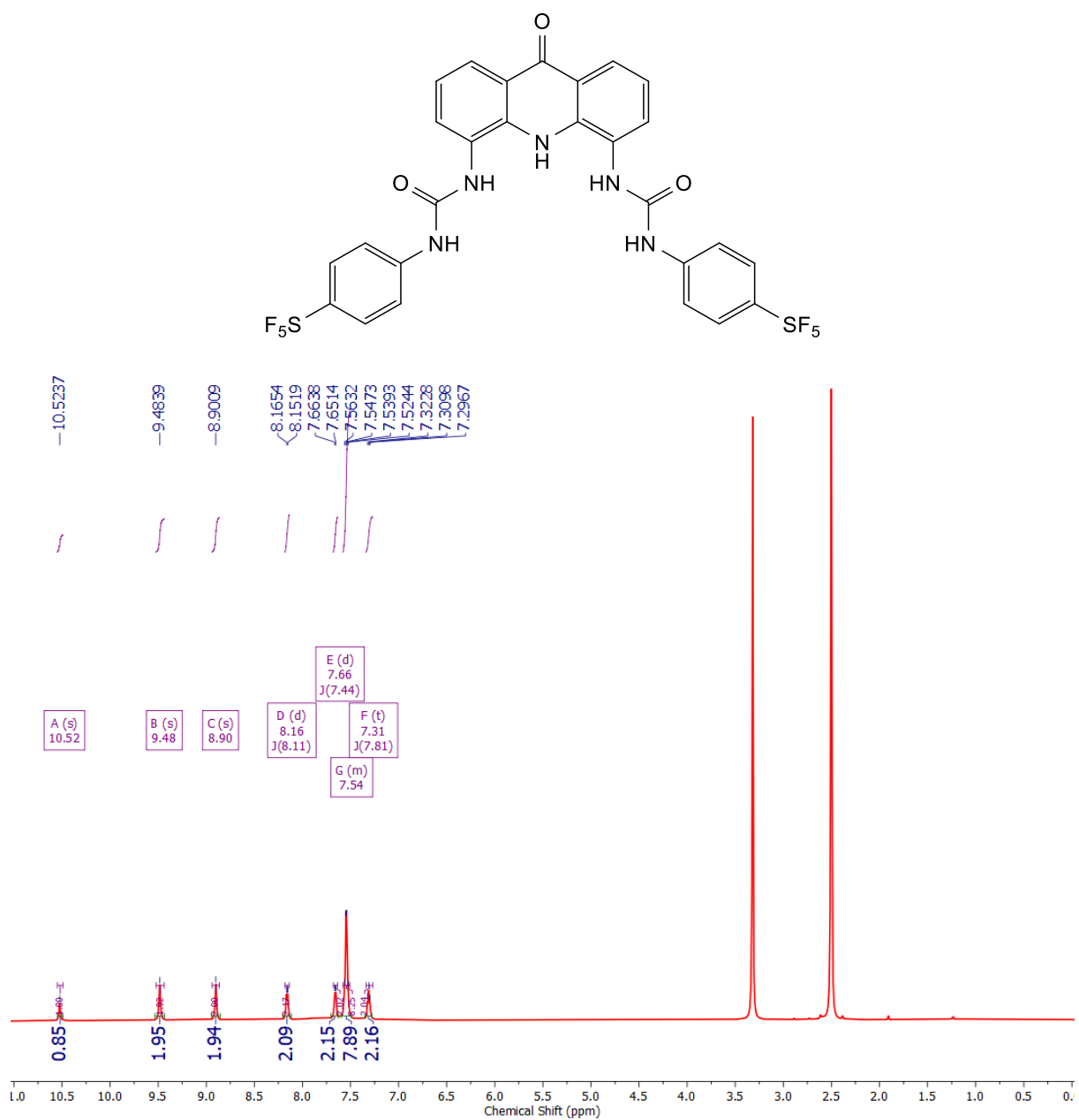
Figure S31. ^{1}H NMR (500 MHz) spectrum of 1,9-bis(4-(pentafluorosulfanyl)phenyl)urea-9(10H)-acridinone in $(CD_3)_2SO_3$ at 298 K.
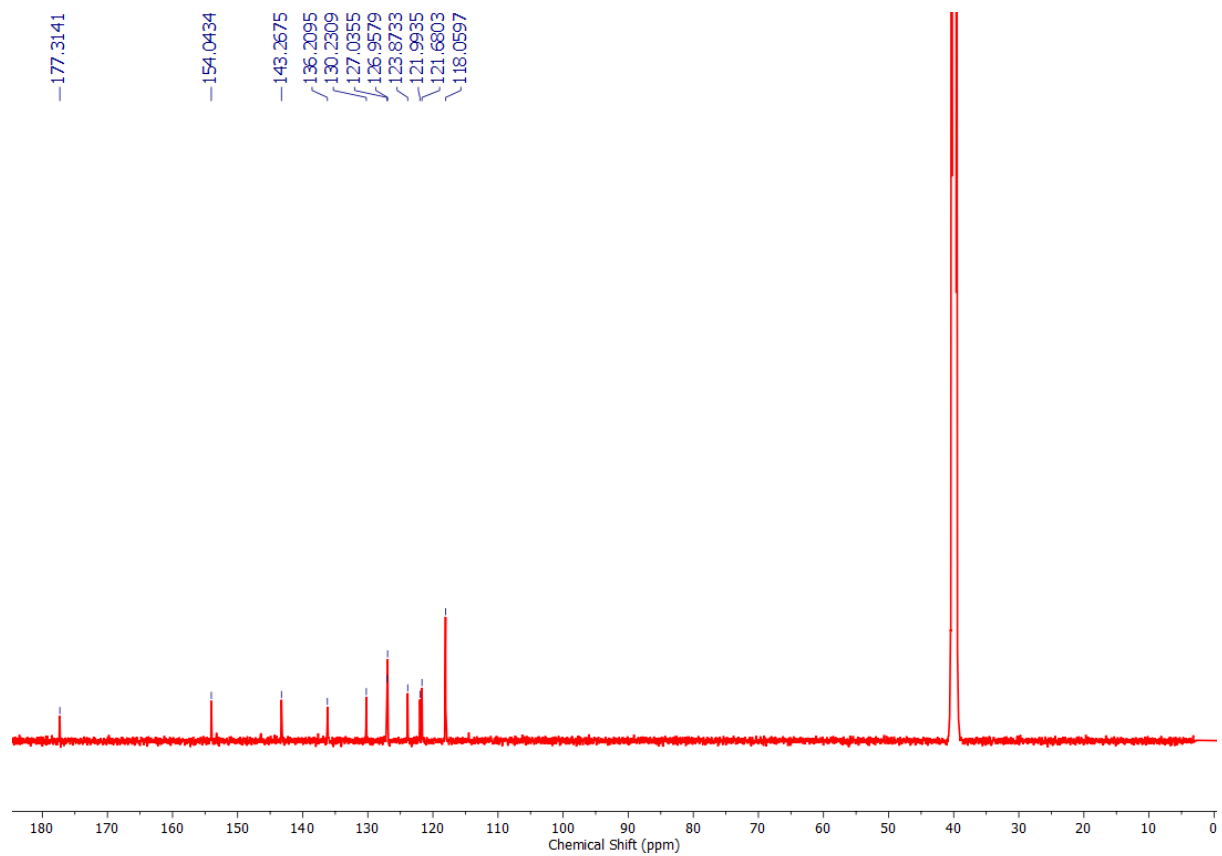
Figure S32. ^{13}C NMR (101 MHz) spectrum of 1,9-bis(4-(pentafluorosulfanyl)phenyl)urea-9(10H)-acridinone in $(CD_3)_2SO_3$ at 298 K.
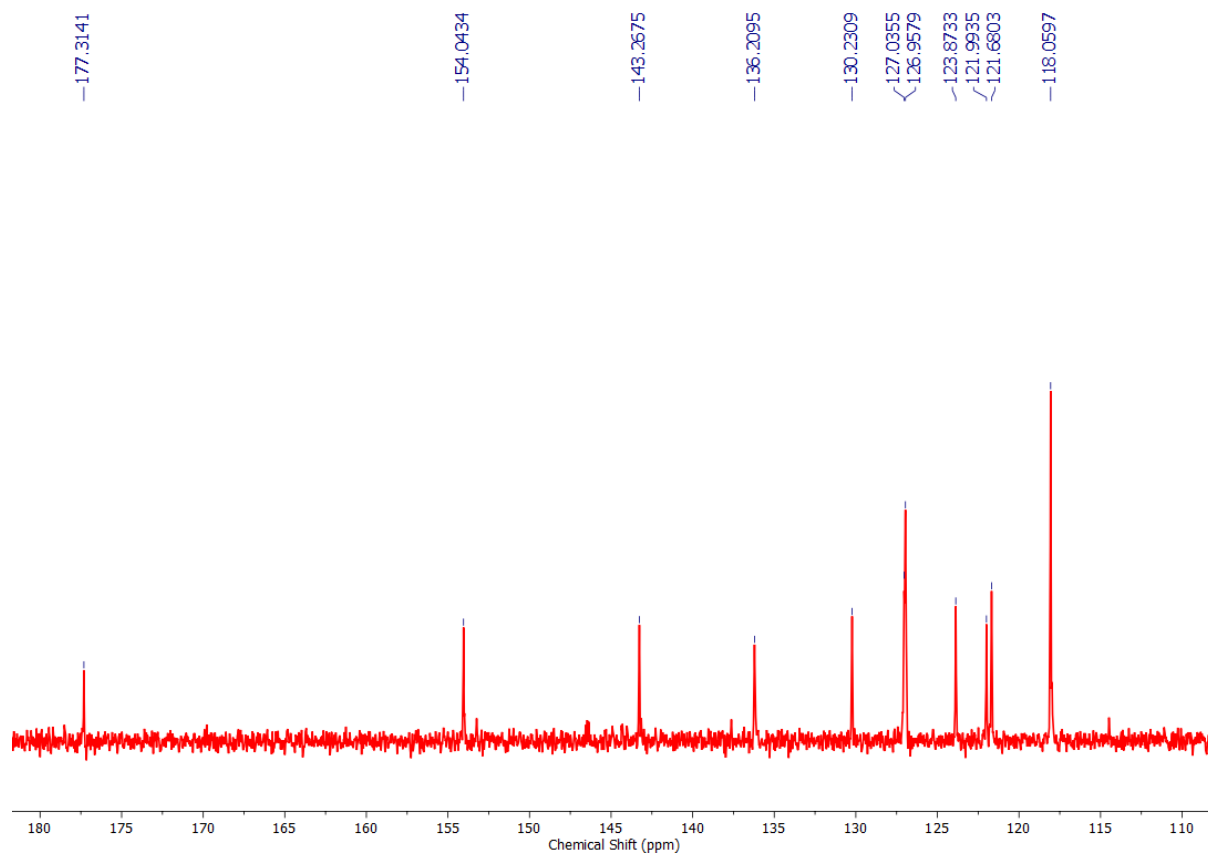
Figure S33. ^{13}C NMR (101 MHz) spectrum of 1,9-bis(4-(pentafluorosulfanyl)phenyl)urea-9(10H)-acridinone in $(CD_3)_2SO_3$ at 298 K. Zoomed in for clarity.
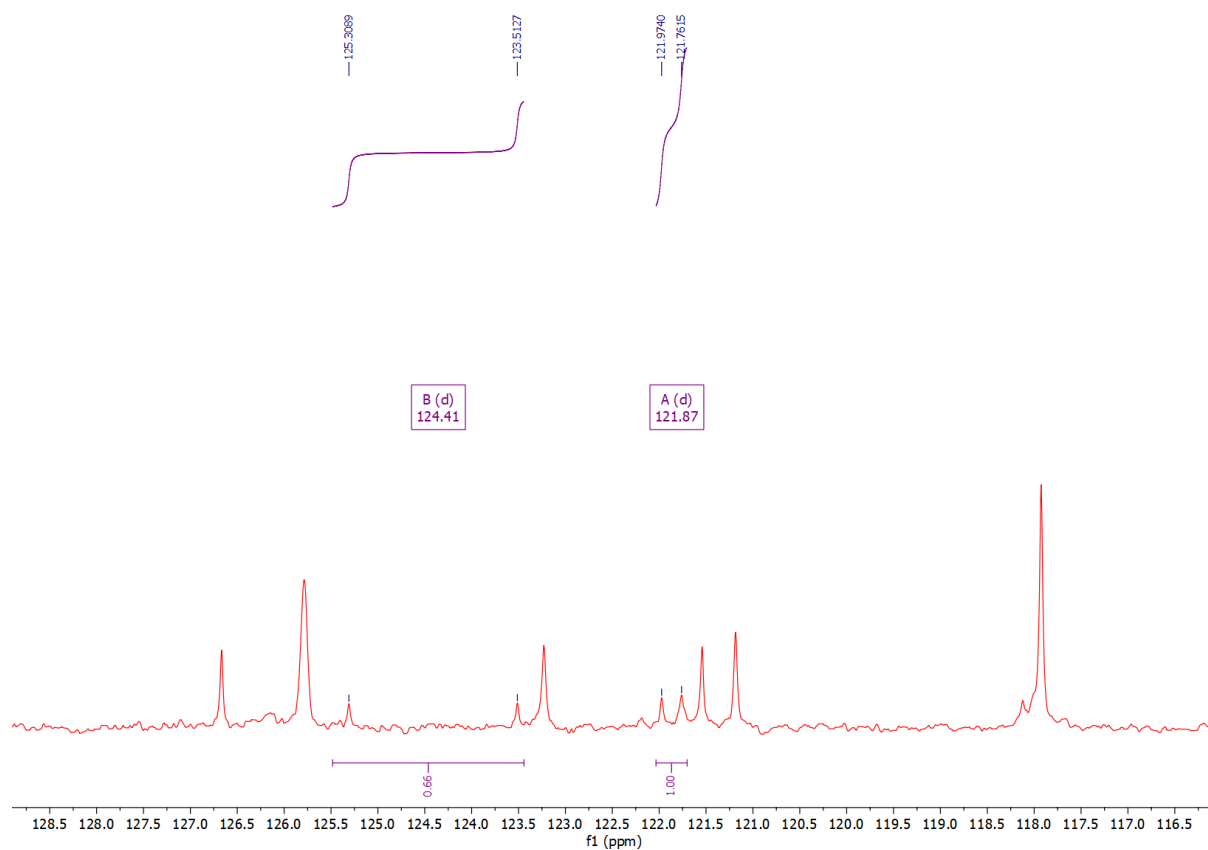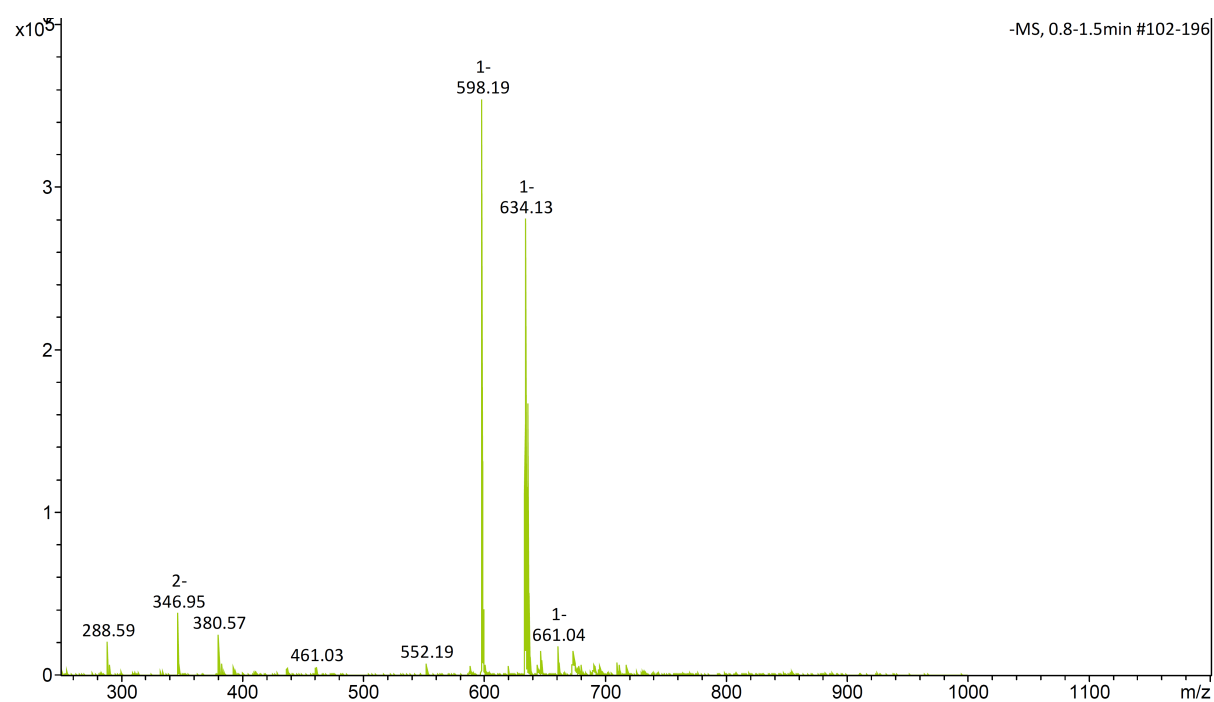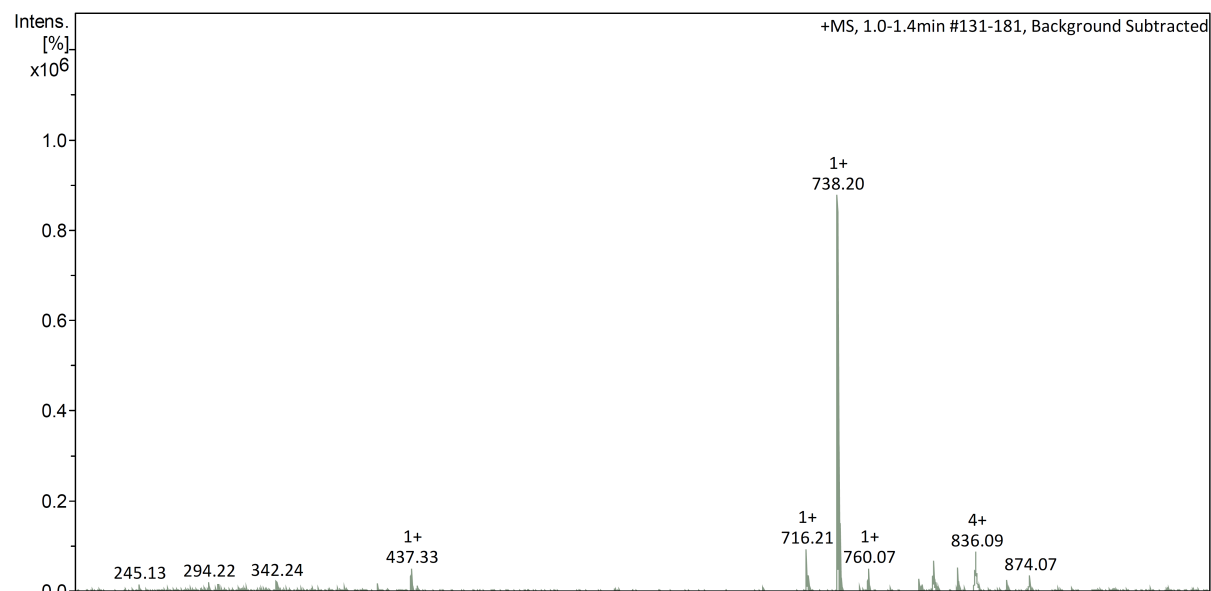

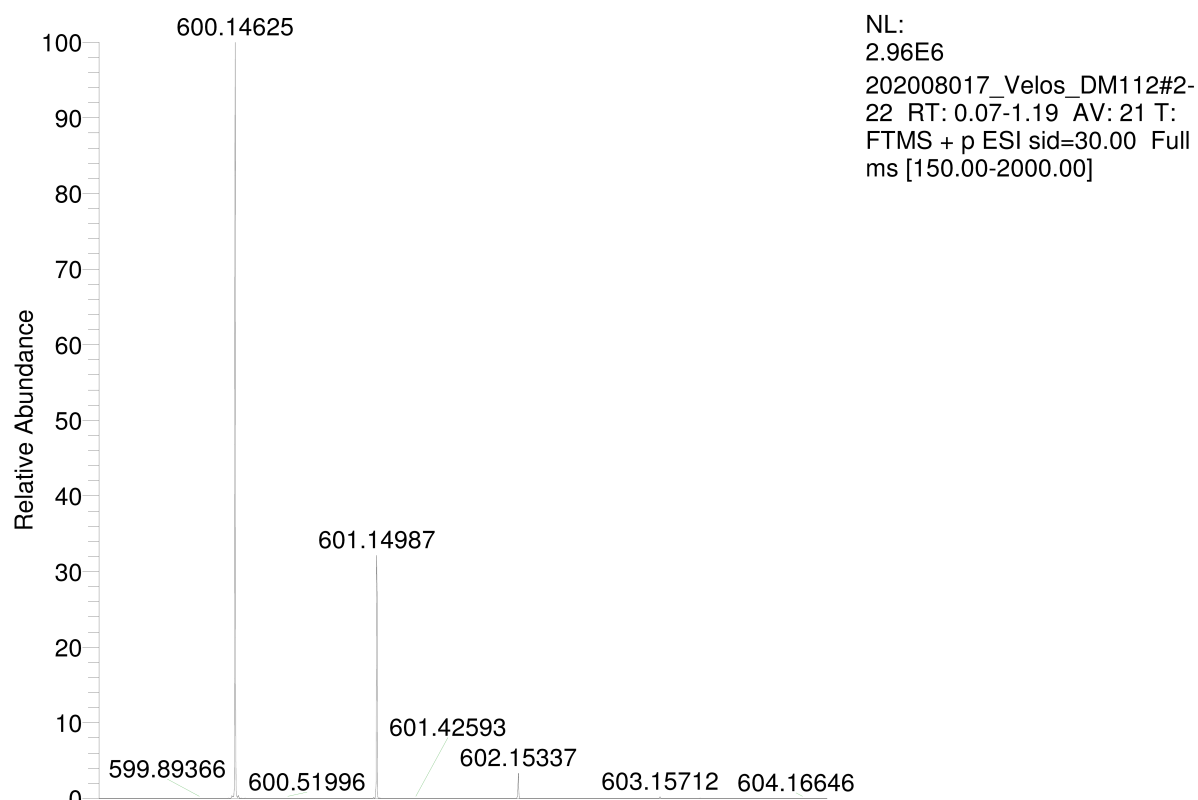Figure S34. LR-MS (ESI$^+$) spectrum of 1,9-bis(4-(pentafluorosulfanyl)phenyl)urea-9(10H)-acridinone.
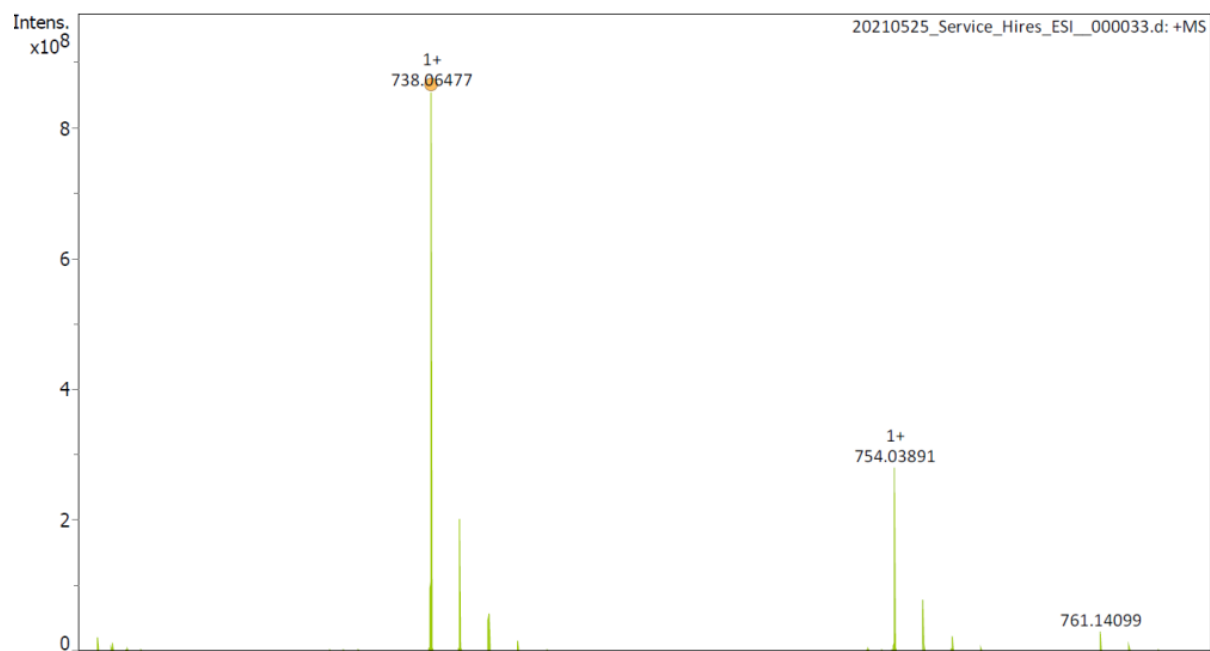
Figure S35. HR-MS (ESI⁻) spectrum of 1,9-bis(4-(pentafluorosulfanyl)phenyl)urea-9(10H)-acridinone.
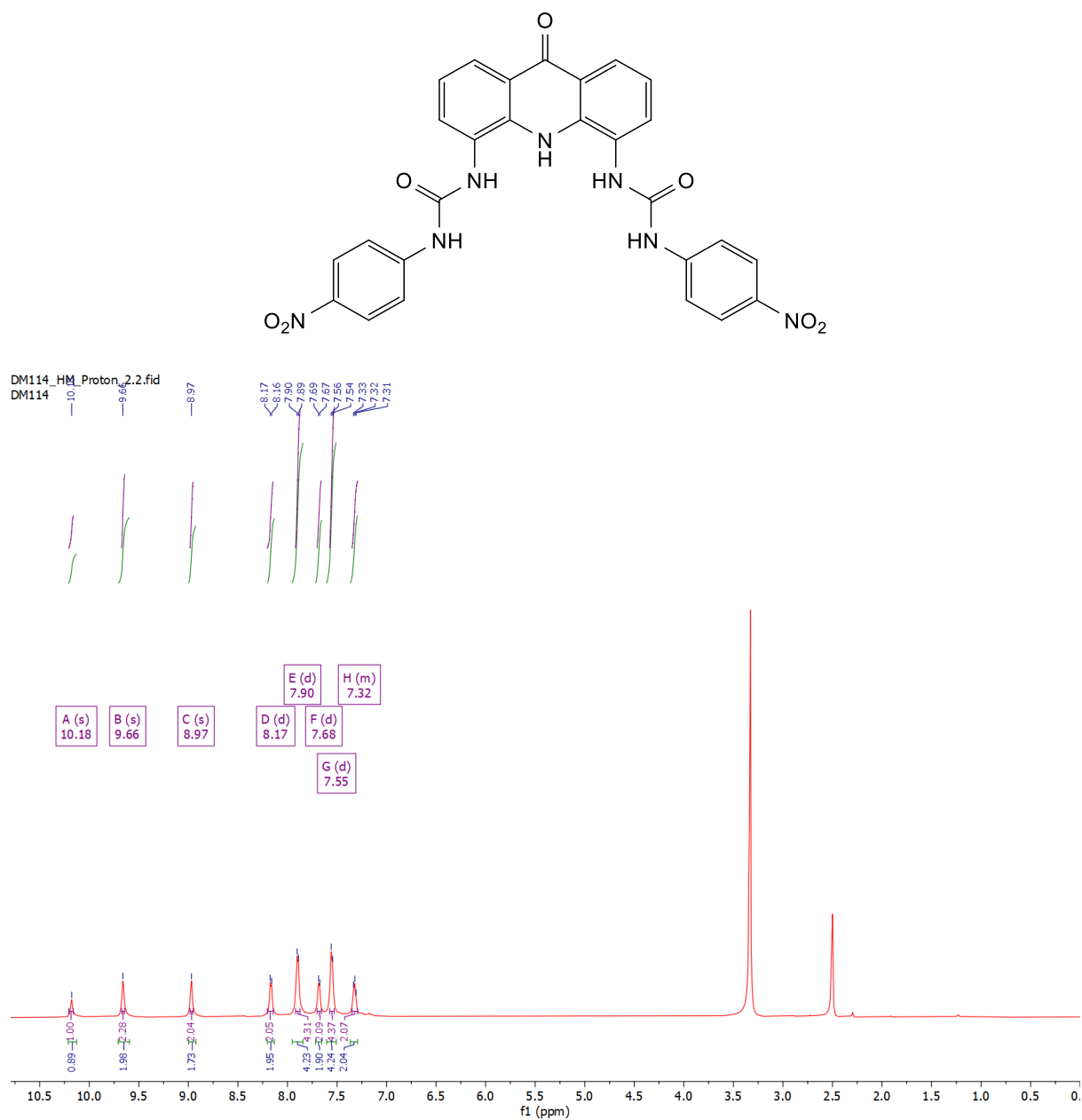
Compound 6: 1,9-bisphenylthiourea-9(10H)-acridinone
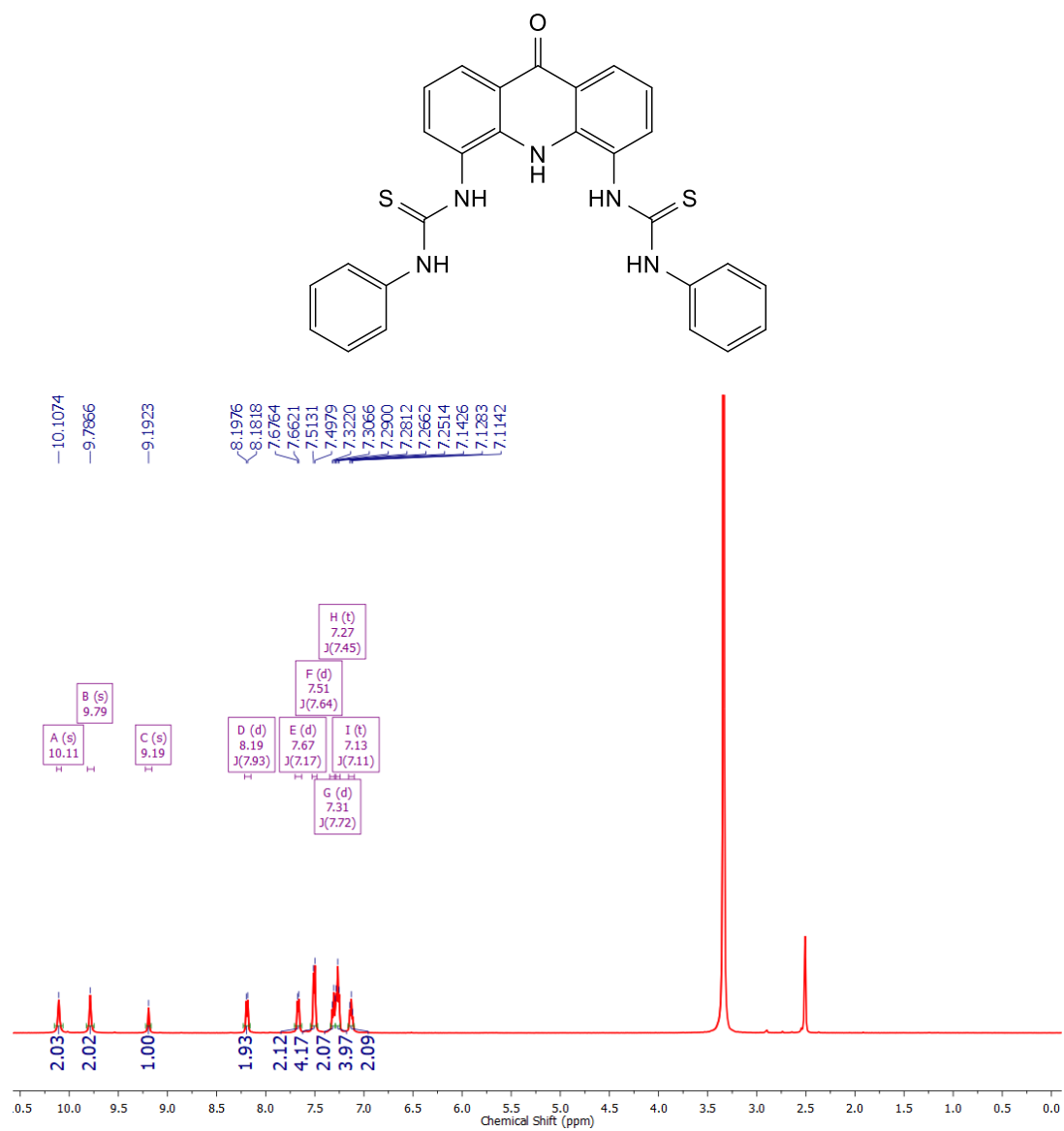
Figure S36. ^{1}H NMR (500 MHz) spectrum of 1,9- bisphenylthiourea-9(10H)-acridinone in $(CD_3)_2SO_3$ at 298 K.
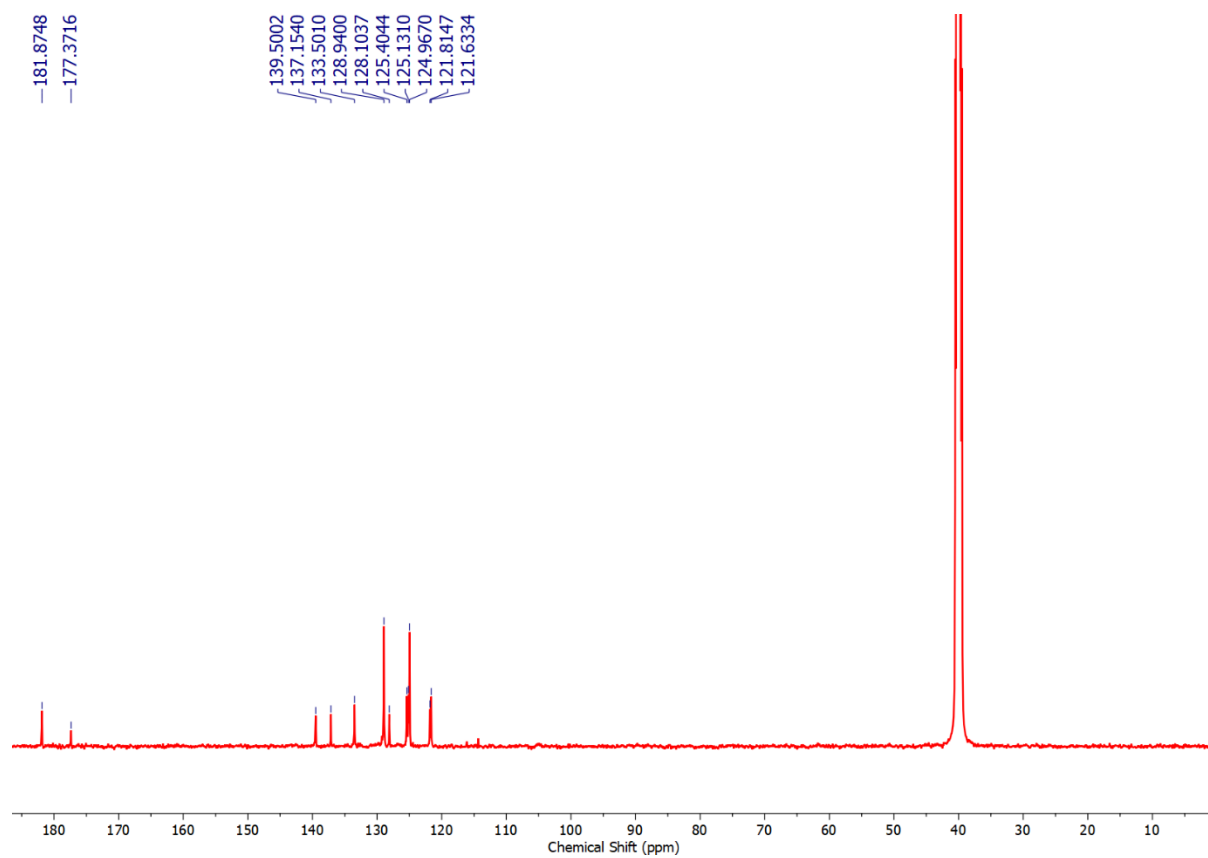
Figure S37. ^{13}C NMR (101 MHz) spectrum of 1,9-bisphenylthiourea-9(10H)-acridinone in $(CD_3)_2SO_3$ at 298 K.
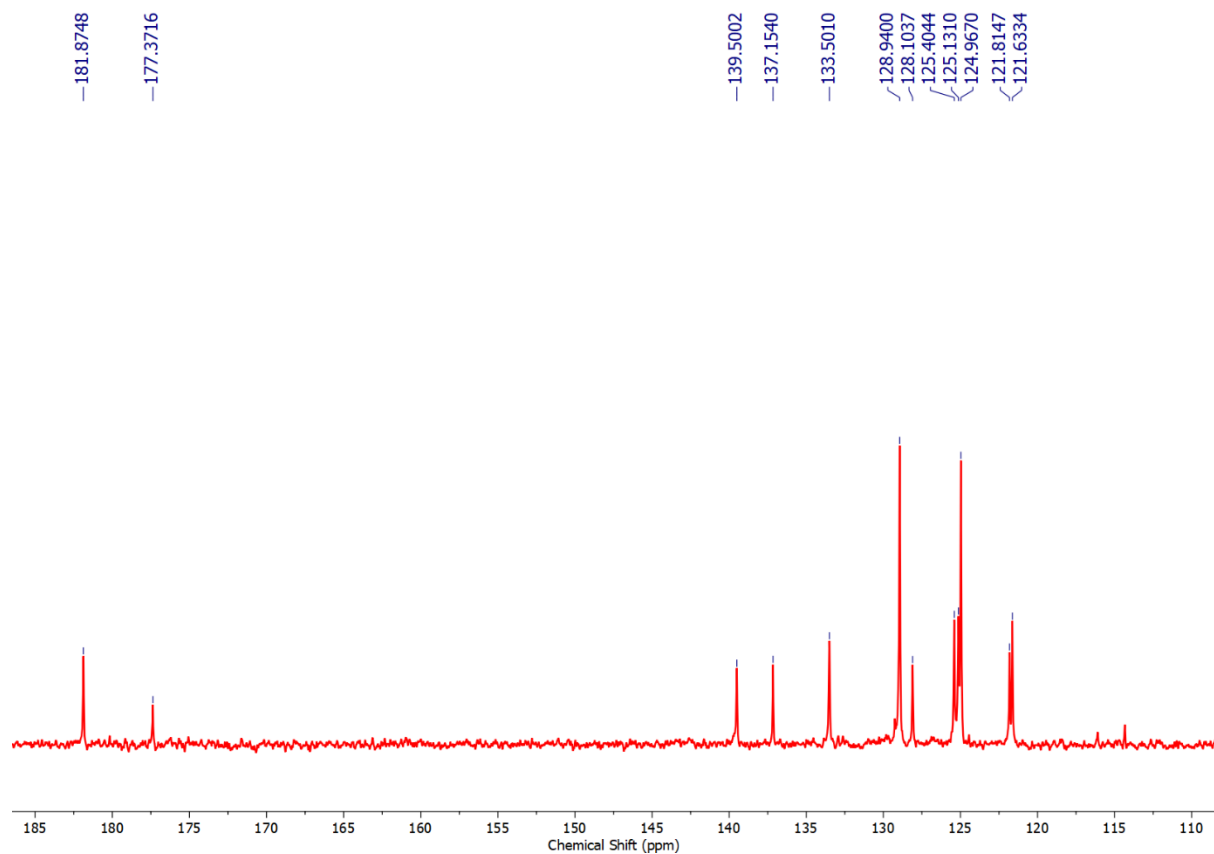
Figure S38. ^{13}C NMR (101 MHz) spectrum of 1,9-bisphenylthiourea-9(10H)-acridinone in $(CD_3)_2SO_3$ at 298 K. Zoomed in for clarity.
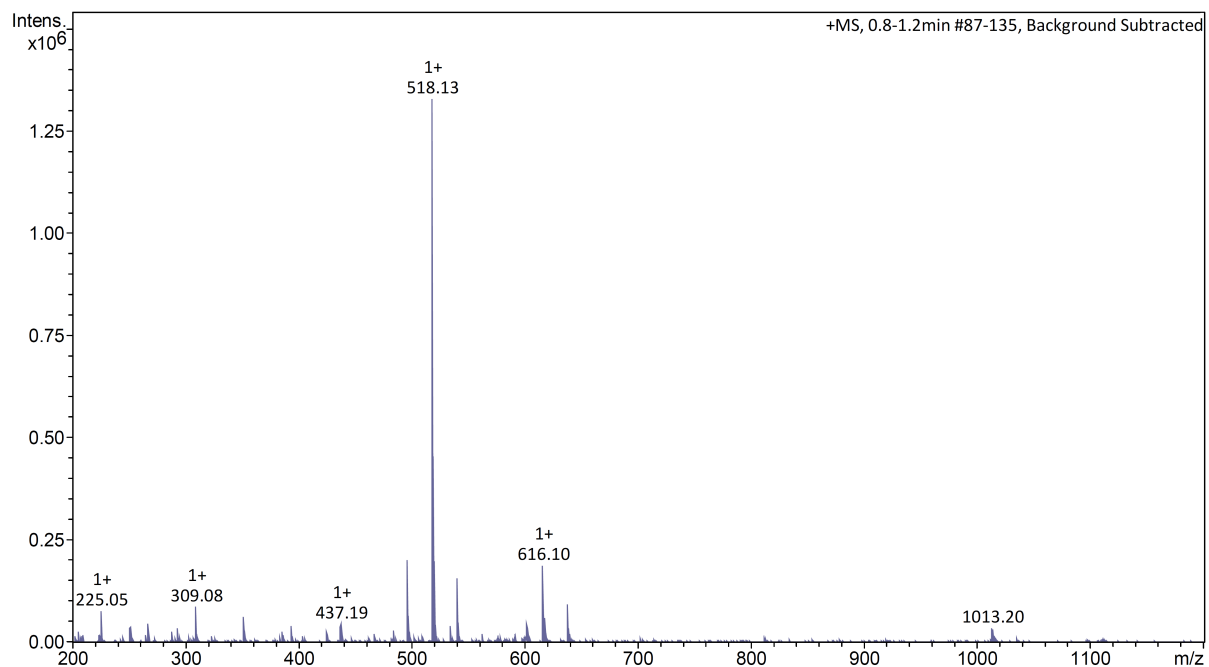
Figure S39. LR-MS (ESI$^+$) spectrum of 1,9-bisphenylthiourea-9(10H)-acridinone.
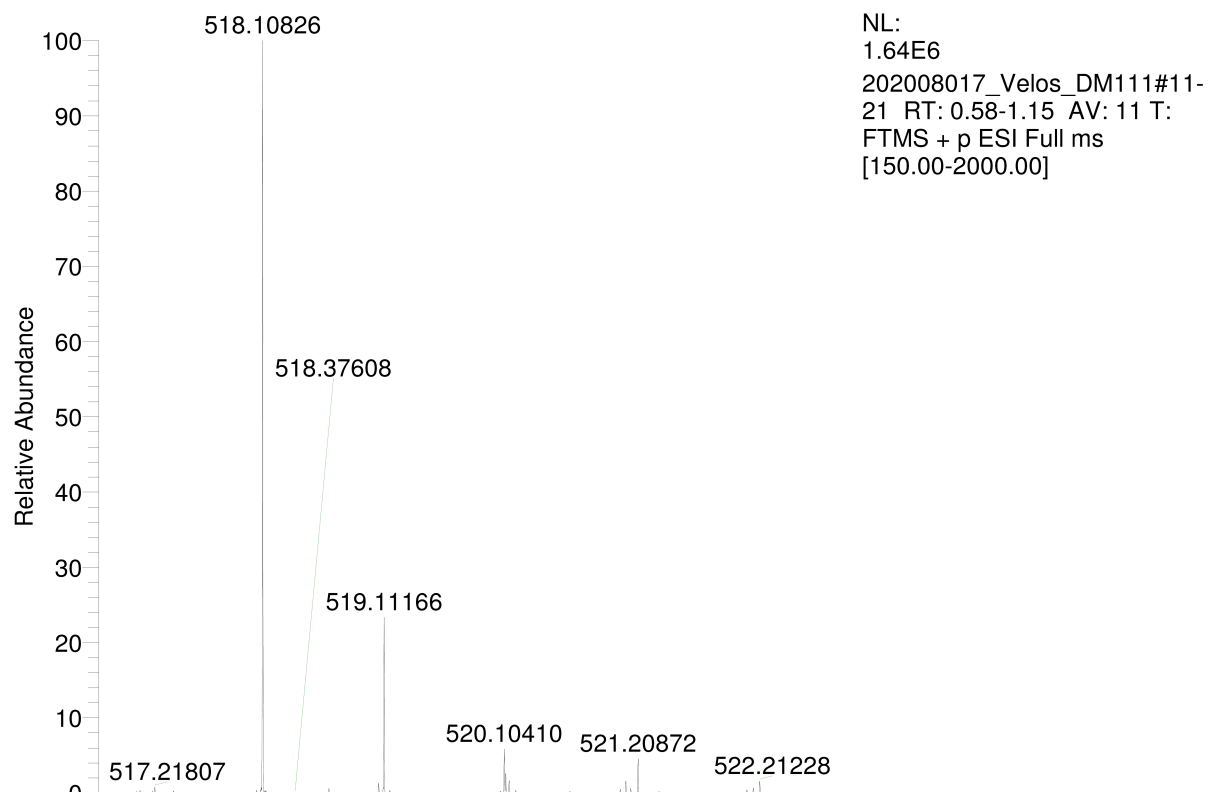
Figure S40. HR-MS (ESI$^+$) spectrum of 1,9-bisphenylthiourea-9(10H)-acridinone.

Compound 7: 1,9-bis(4-(trifluoromethyl)phenyl)thiourea-9(10H)-acridinone
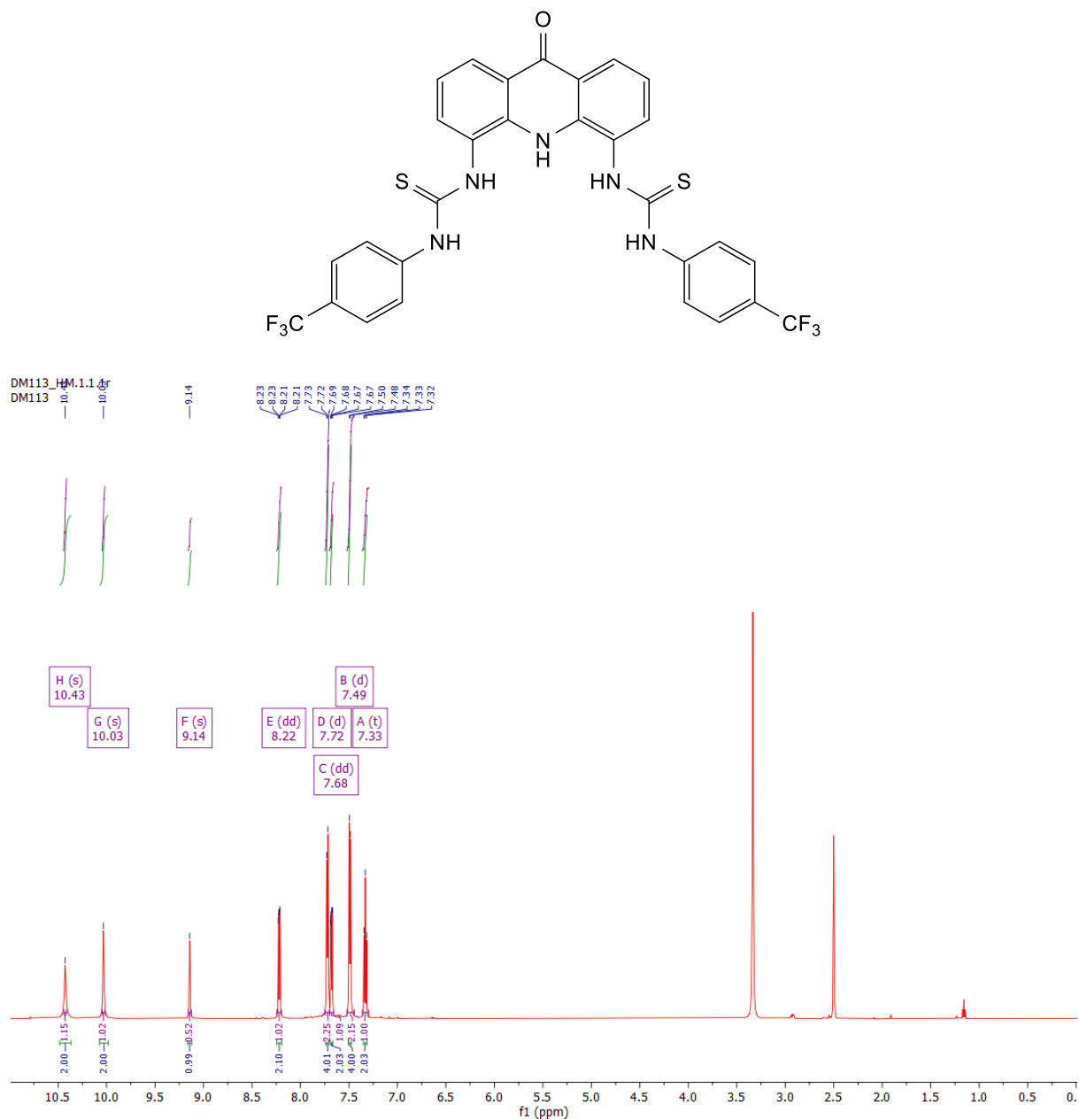
Figure S41. ^{1}H NMR (600 MHz) spectrum of 1,9-bis(4-(trifluoromethyl)phenyl)thiourea-9(10H)-acridinone in $(CD_3)_2SO_3$ at 298 K.
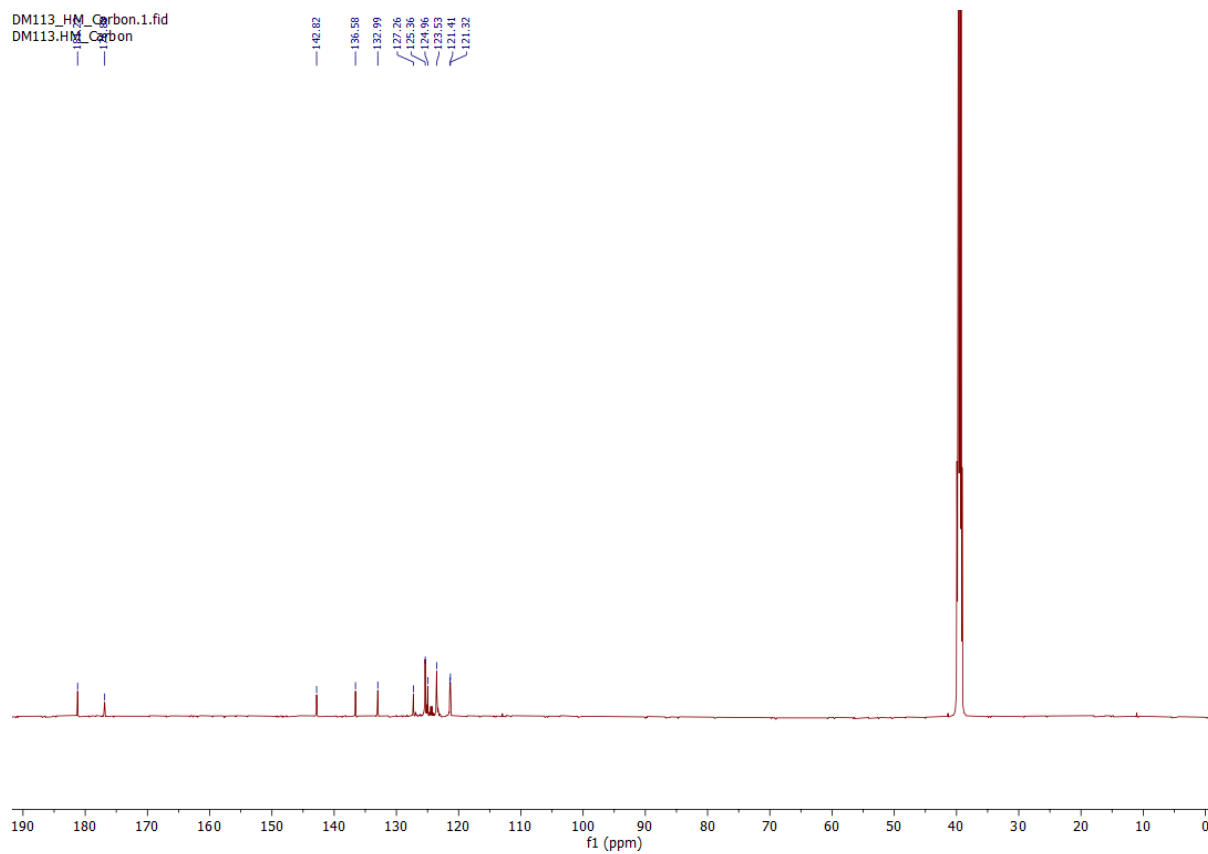
Figure S42. ^{13}C NMR (101 MHz) spectrum of 1,9-bis(4-(trifluoromethyl)phenyl)thiourea-9(10H)-acridinone in $(CD_3)_2SO_3$ at 298 K.
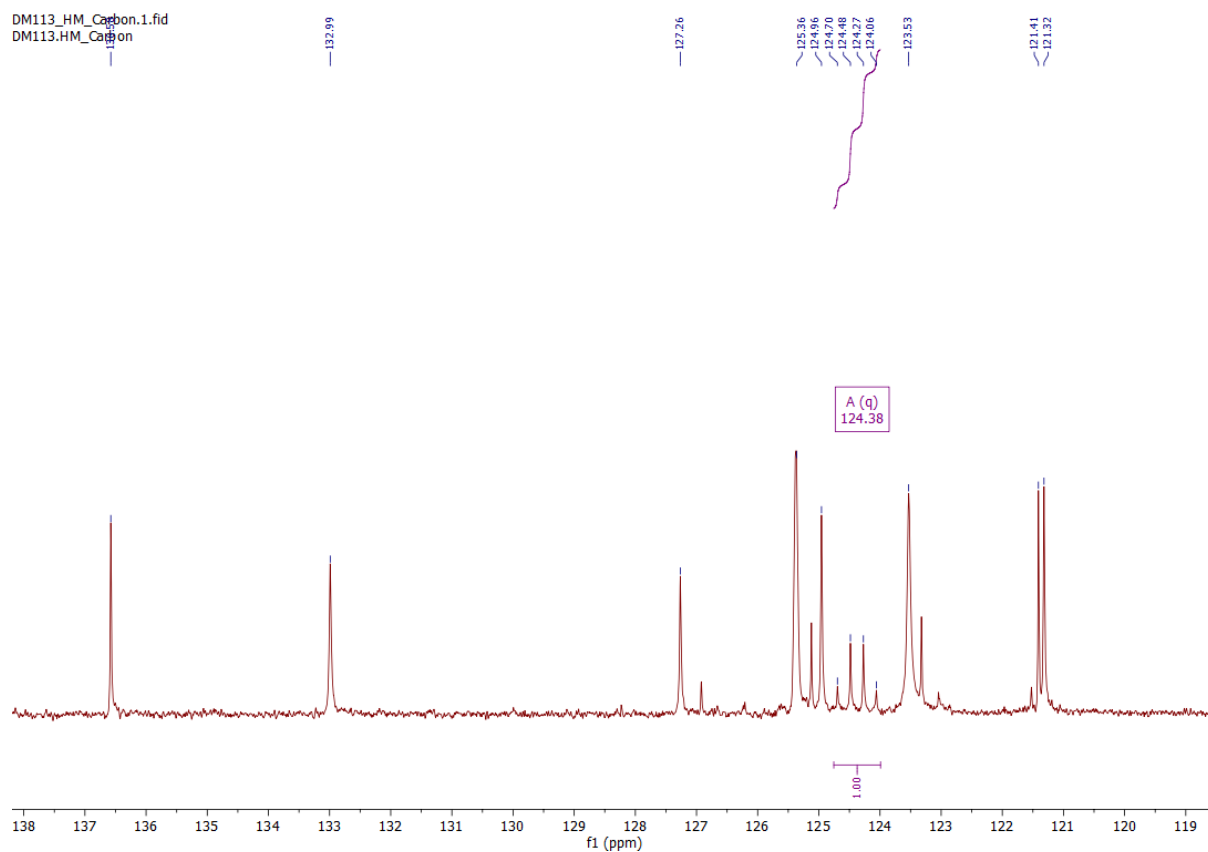
Figure S43. ^{13}C NMR (101 MHz) spectrum of 1,9-bis(4-(trifluoromethyl)phenyl)thiourea-9(10H)-acridinone in $(CD_3)_2SO_3$ at 298 K. Zoomed in for clarity with quartet splitting of CF_3 β-carbon displayed.
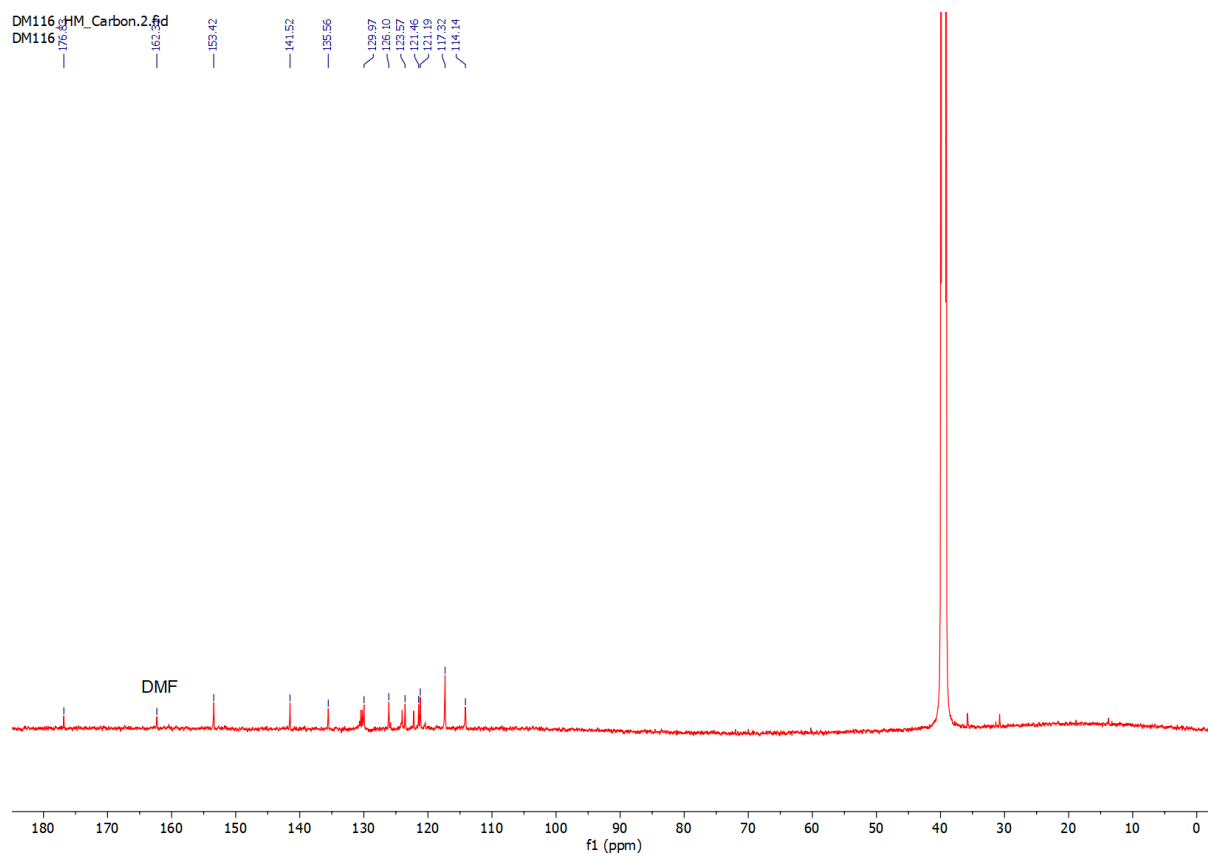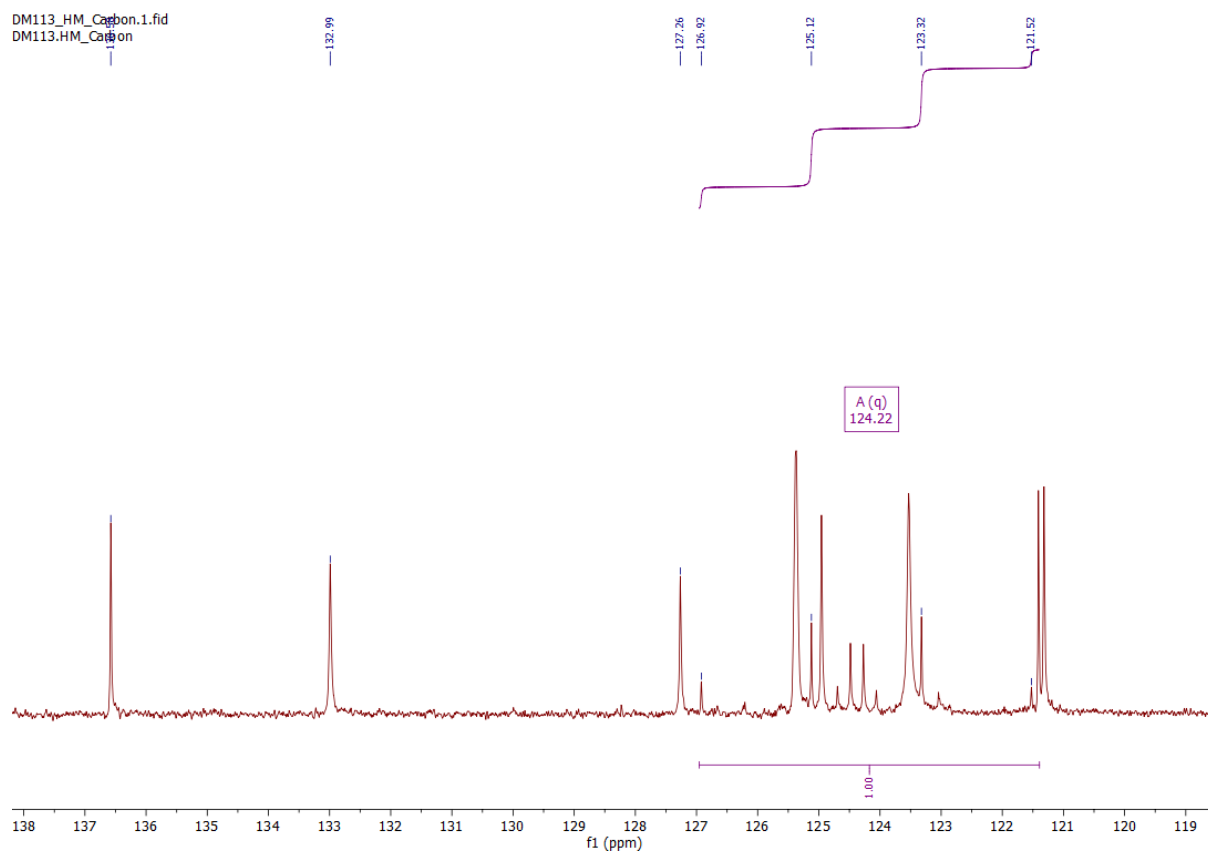
Figure S44. ^{13}C NMR (101 MHz) spectrum of 1,9-bis(4-(trifluoromethyl)phenyl)thiourea-9(10H)-acridinone in $(CD_3)_2SO_3$ at 298 K. Zoomed in for clarity with quartet splitting of CF_3 α-carbon displayed.
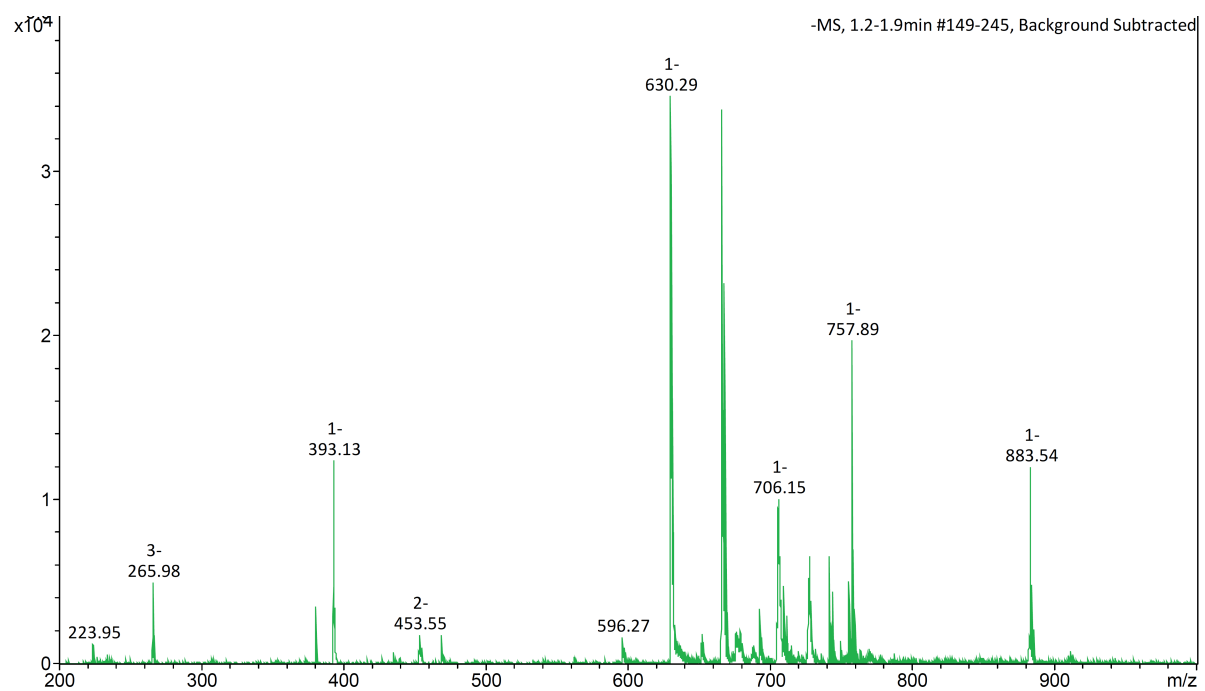
Figure S45. LR-MS (ESI⁻) spectrum of 1,9-bis(4-(trifluoromethyl)phenyl)thiourea-9(10H)-acridinone.
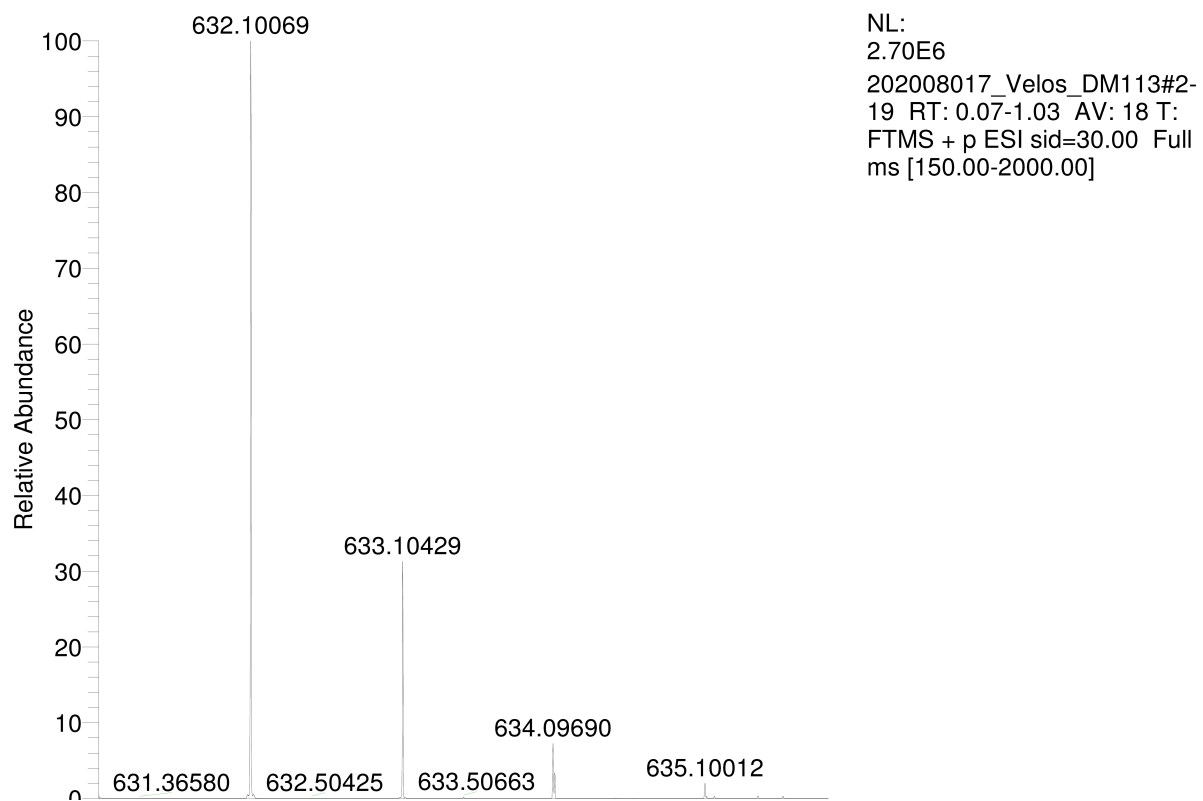
Figure S46. HR-MS (ESI⁻) spectrum of 1,9-bis(4-(trifluoromethyl)phenyl)thiourea-9(10H)-acridinone.

Compound 8: 1,9-bis(4-nitrophenyl)thiourea-9(10H)-acridinone
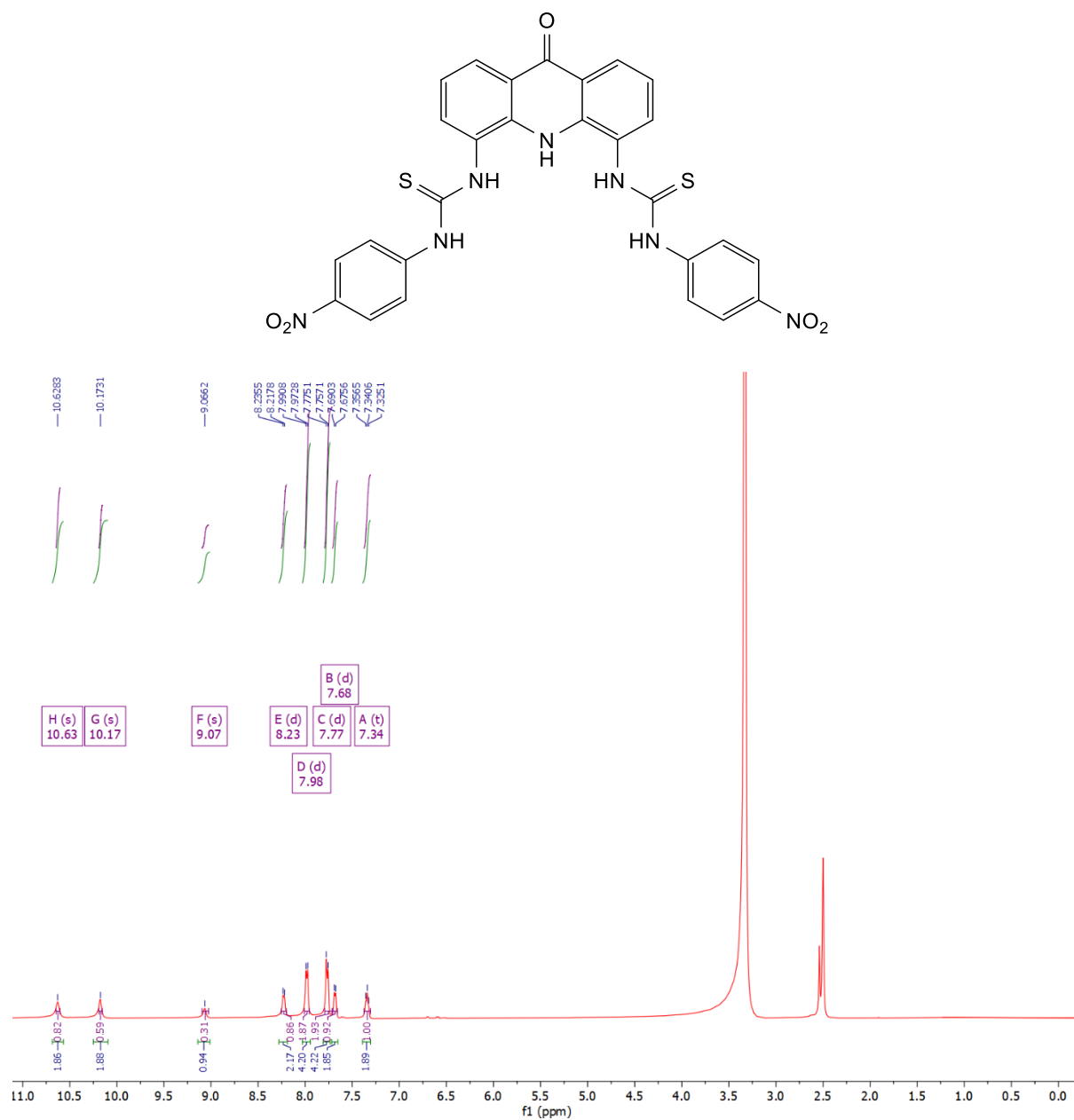
Figure S47. ^{1}H NMR (500 MHz) spectrum of 1,9-bis(4-nitrophenyl)thiourea-9(10H)-acridinone in (CD$_3$)$_2$SO$_3$ at 298 K.
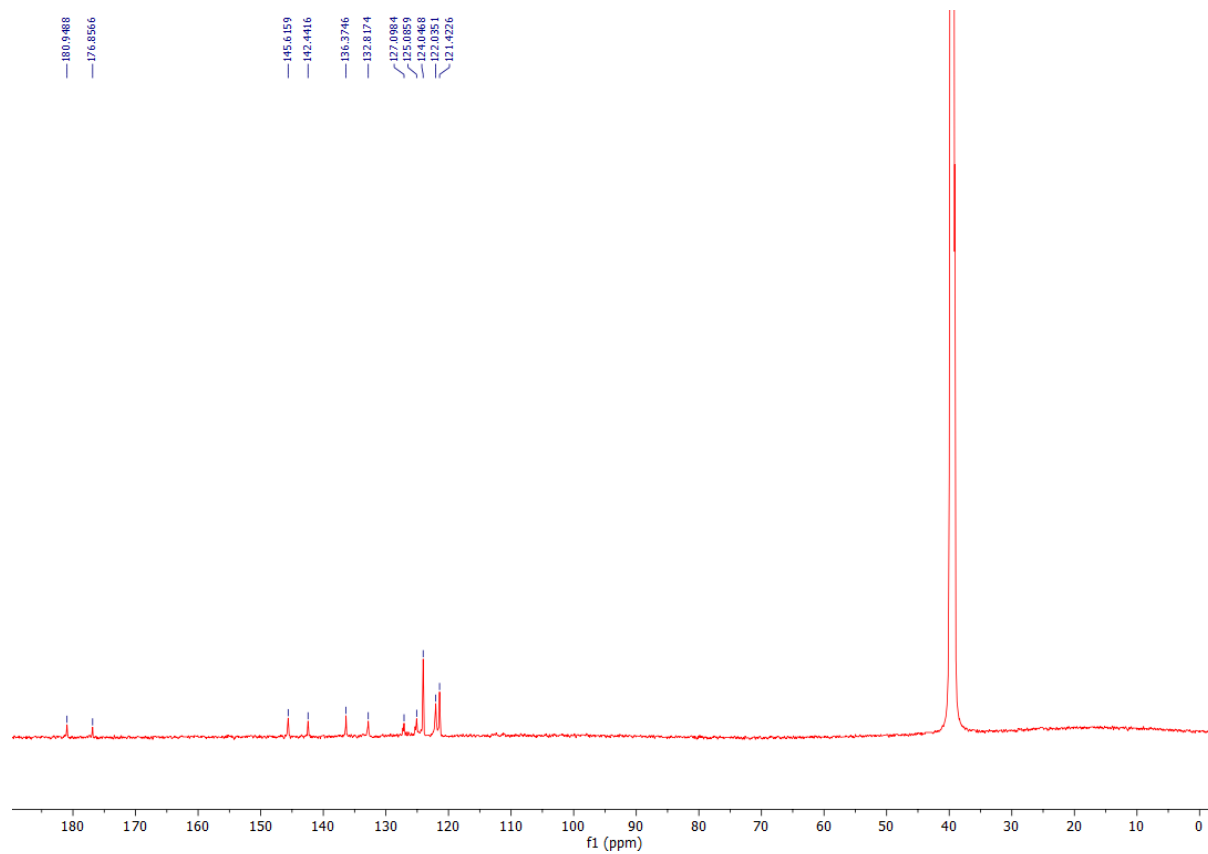
Figure S48. ^{13}C NMR (101 MHz) spectrum of 1,9-bis(4-nitrophenyl)thiourea-9(10H)-acridinone in $(CD_3)_2SO_3$ at 298 K.
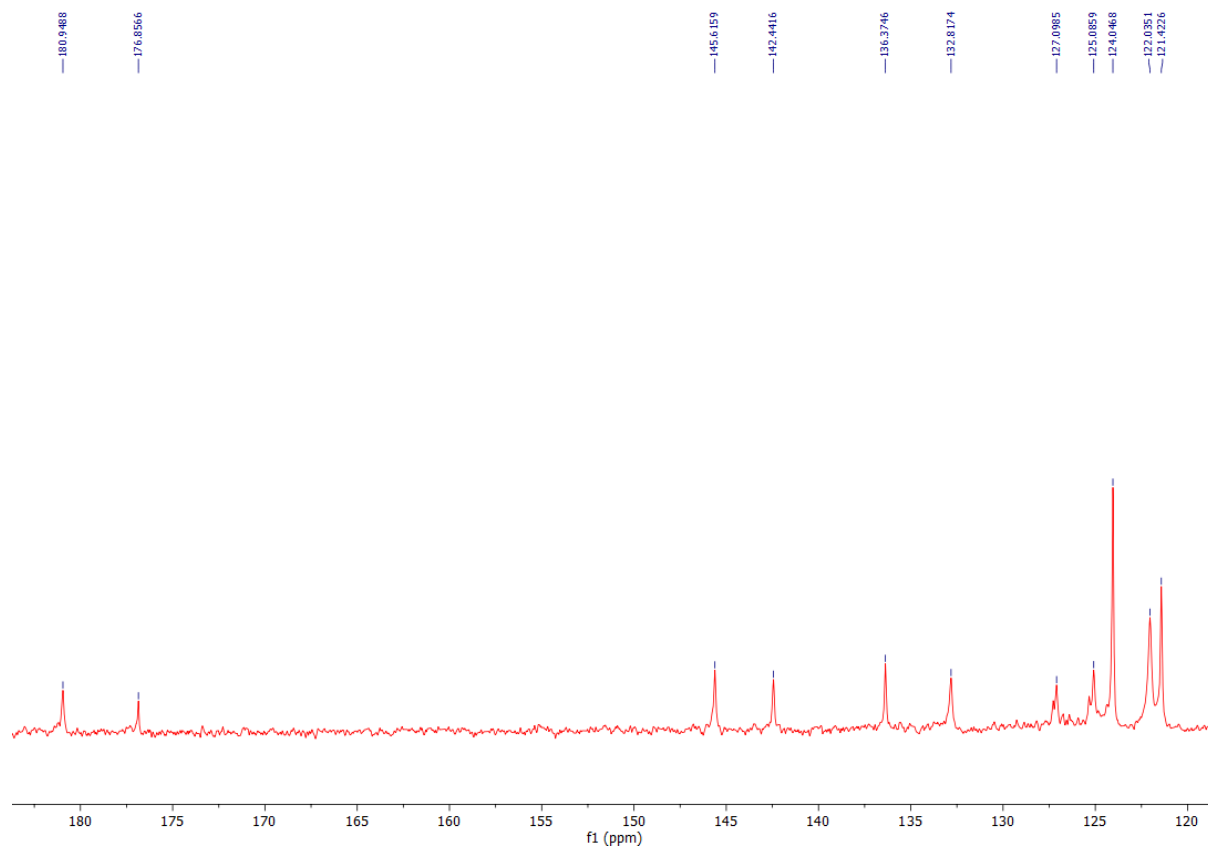
Figure S49. ^{13}C NMR (101 MHz) spectrum of 1,9-bis(4-nitrophenyl)thiourea-9(10H)-acridinone in (CD$_3$)$_2$SO$_3$ at 298 K. Zoomed in for clarity.
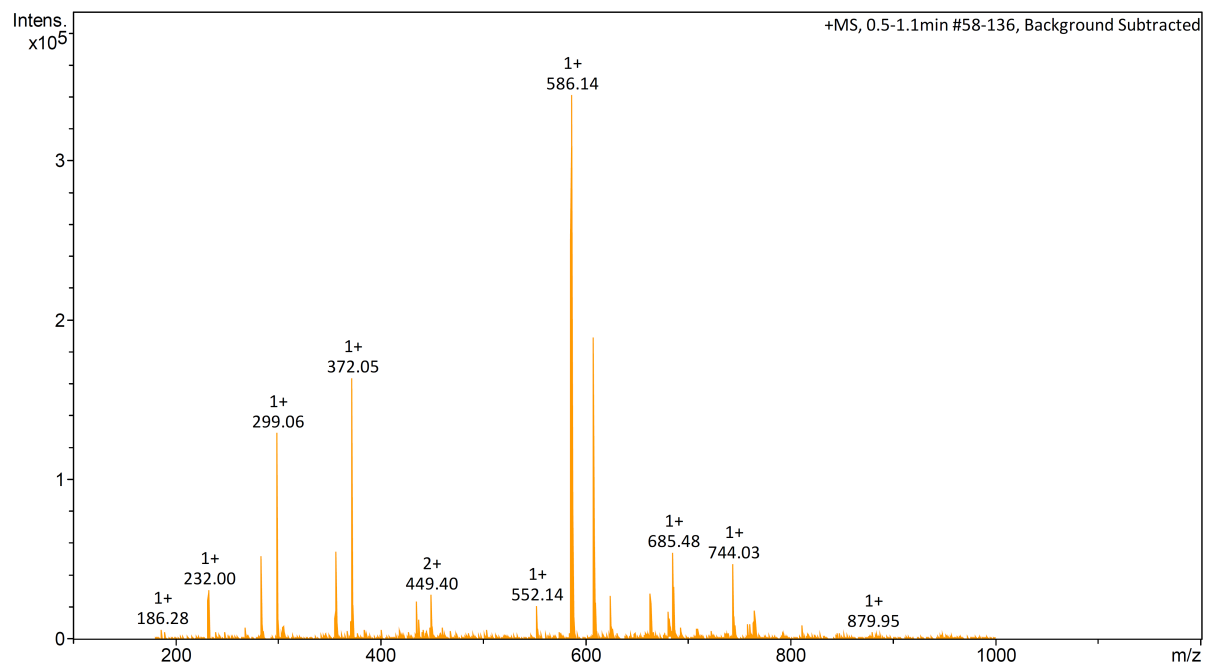
Figure S50. LR-MS (ESI$^+$) spectrum of 1,9-bis(4-nitrophenyl)thiourea-9(10H)-acridinone.
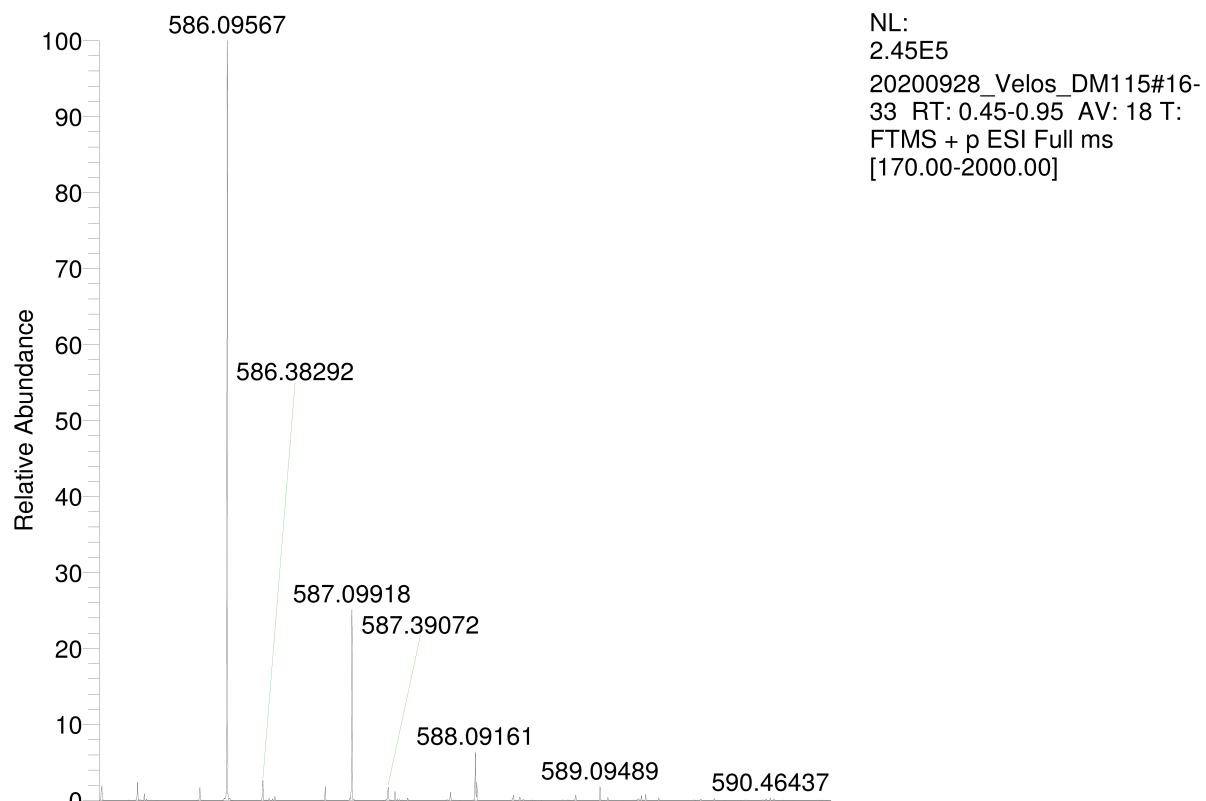
Figure S51. HR-MS (ESI$^+$) spectrum of 1,9-bis(4-nitrophenyl)thiourea-9(10H)-acridinone.

Compound 9: 1,9-bis(3,5-bis-(trifluoromethyl)phenyl)thiourea-9(10H)-acridinone
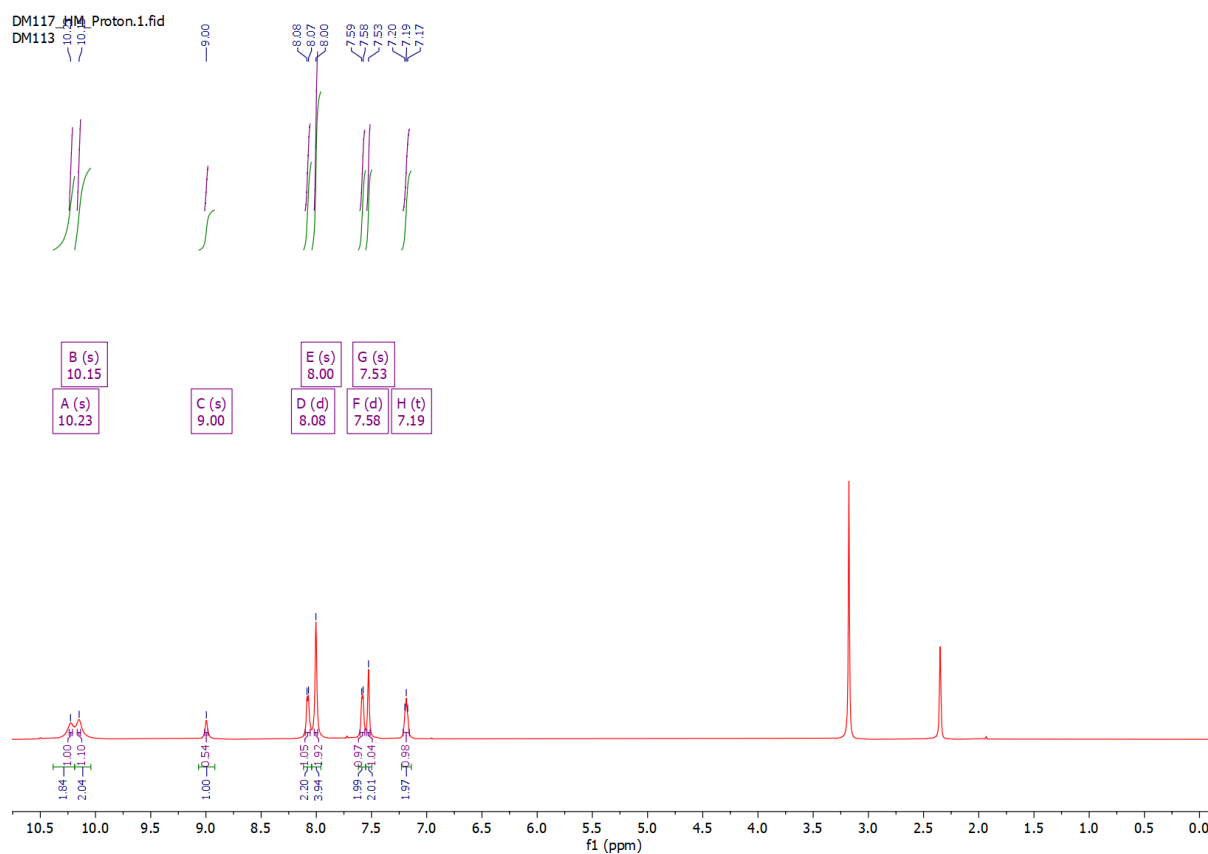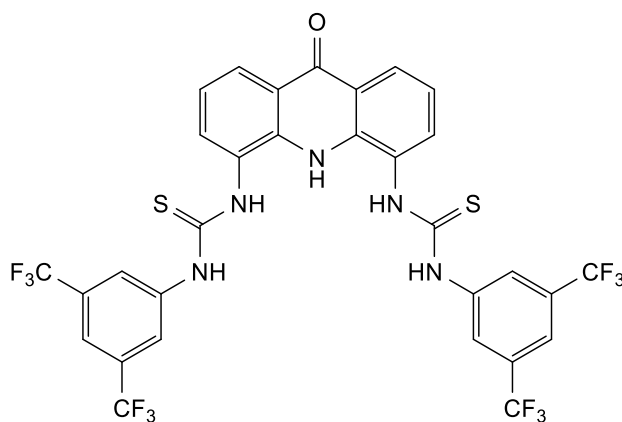
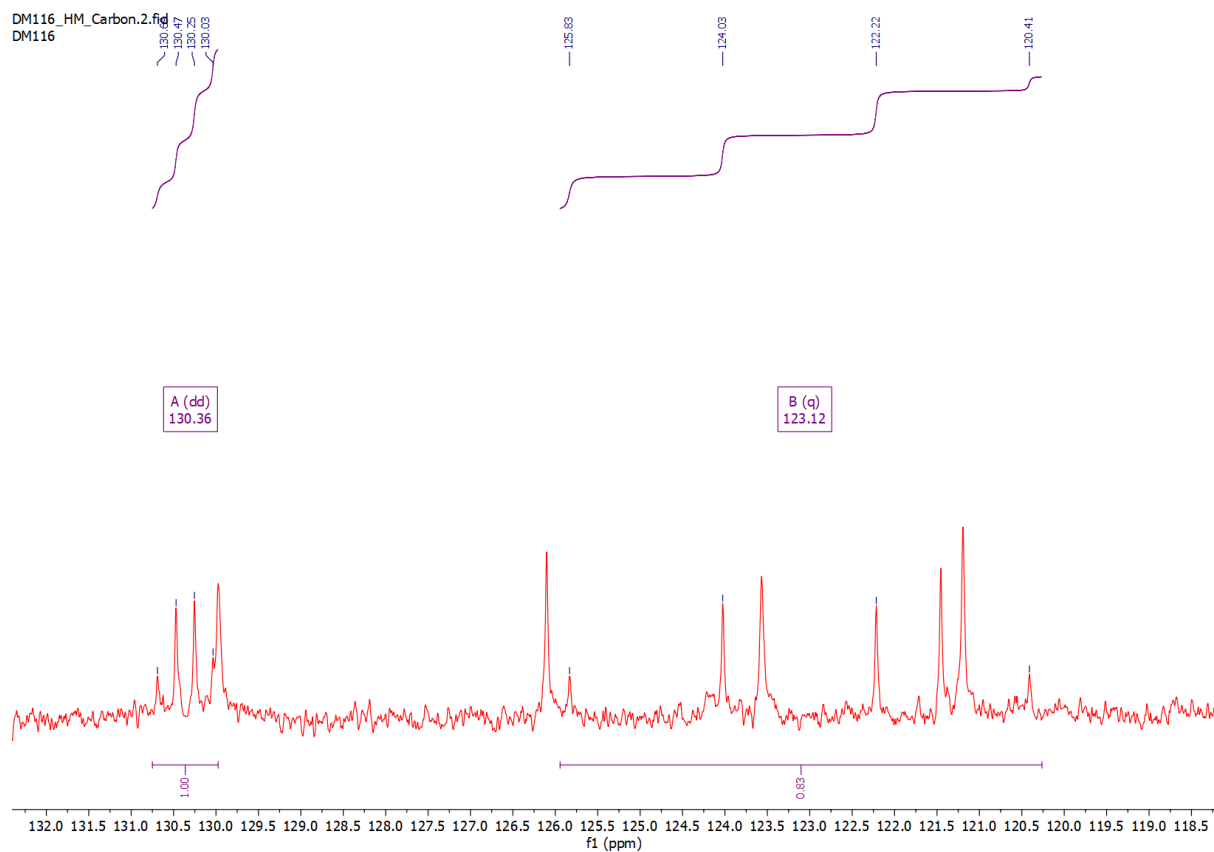Figure S52. ^{1}H NMR (600 MHz) spectrum of 1,9-bis(3,5-bis(trifluoromethyl)phenyl)thiourea-9(10H)-acridinone in $(CD_3)_2SO_3$ at 298 K.
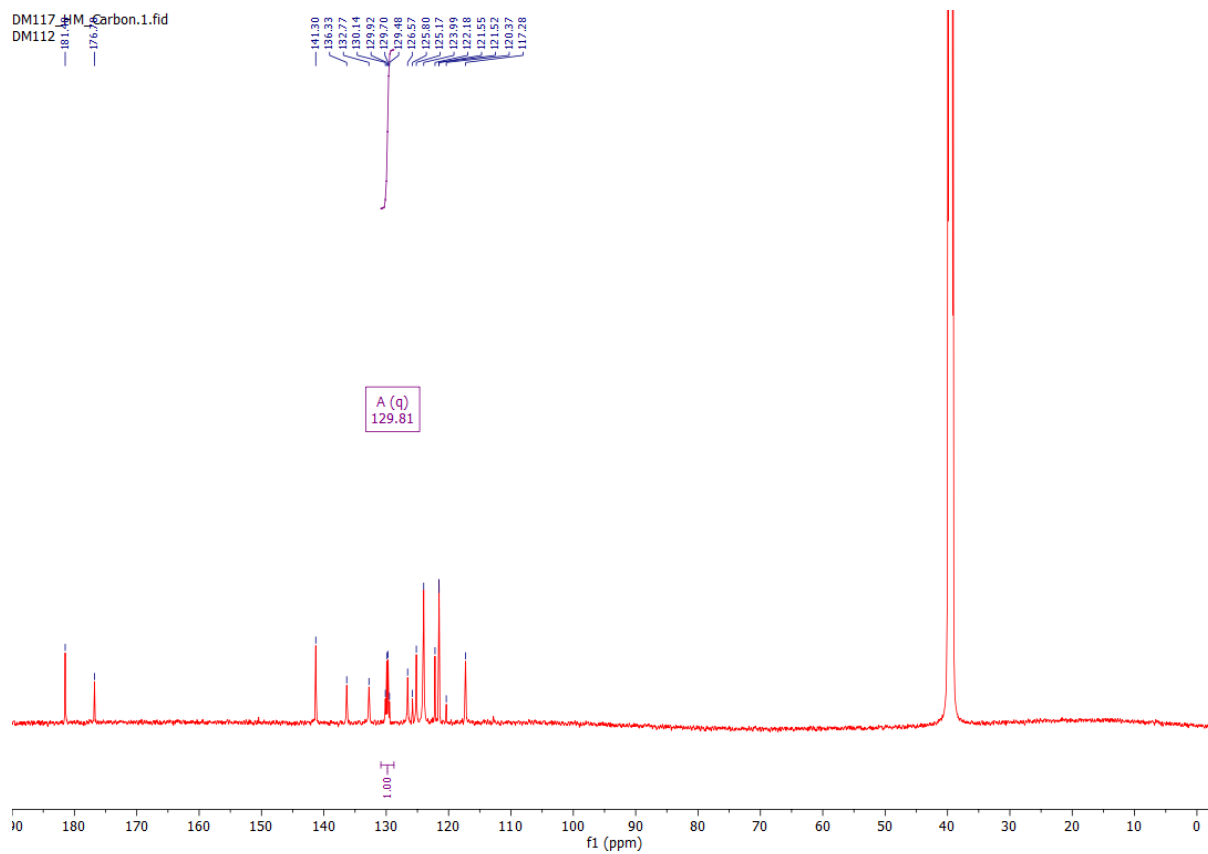
Figure S53. ^{13}C NMR (101 MHz) spectrum of 1,9-bis(3,5-bis-(trifluoromethyl)phenyl)thiourea-9(10H)-acridinone in $(CD_3)_2SO_3$ at 298 K.
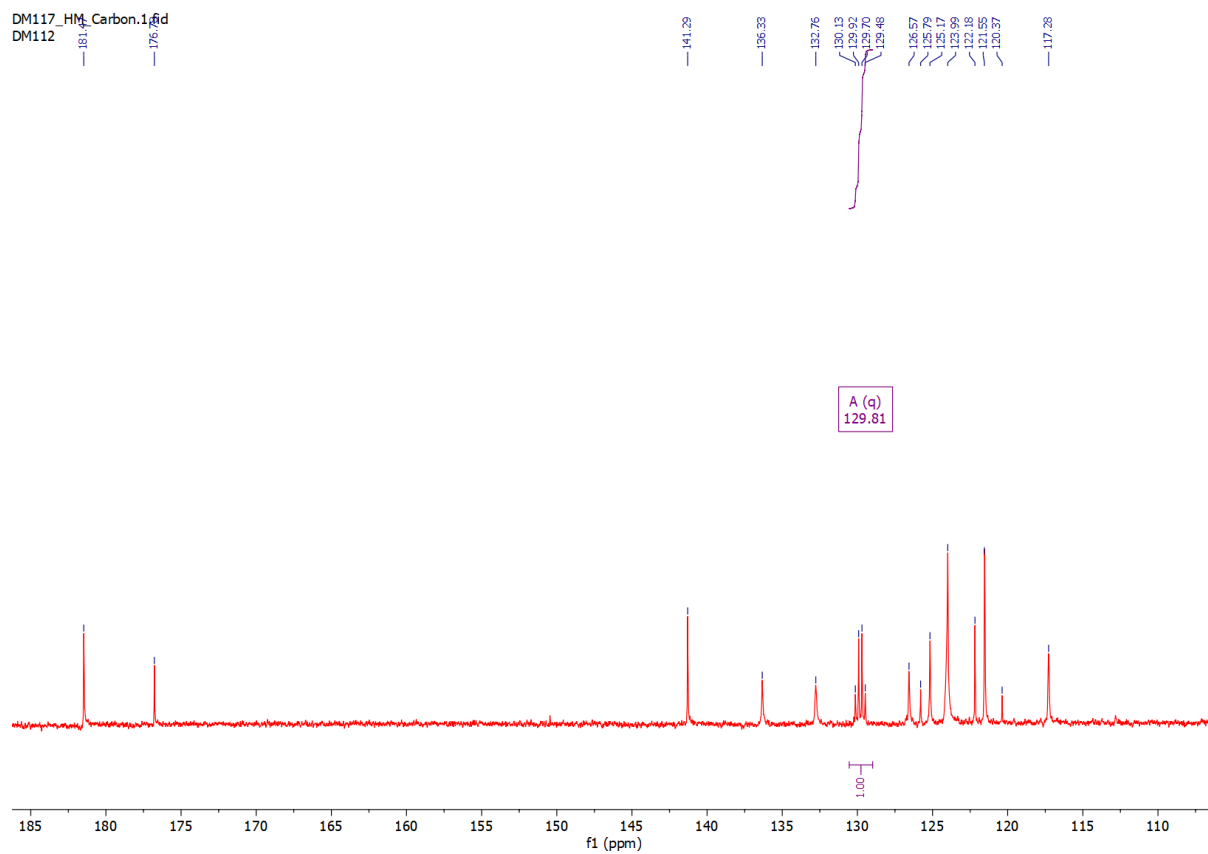
Figure S54. ^{13}C NMR (101 MHz) spectrum of 1,9-bis(3,5-bis-(trifluoromethyl)phenyl)thiourea-9(10H)-acridinone in $(CD_3)_2SO_3$ at 298 K. Zoomed in for clarity.
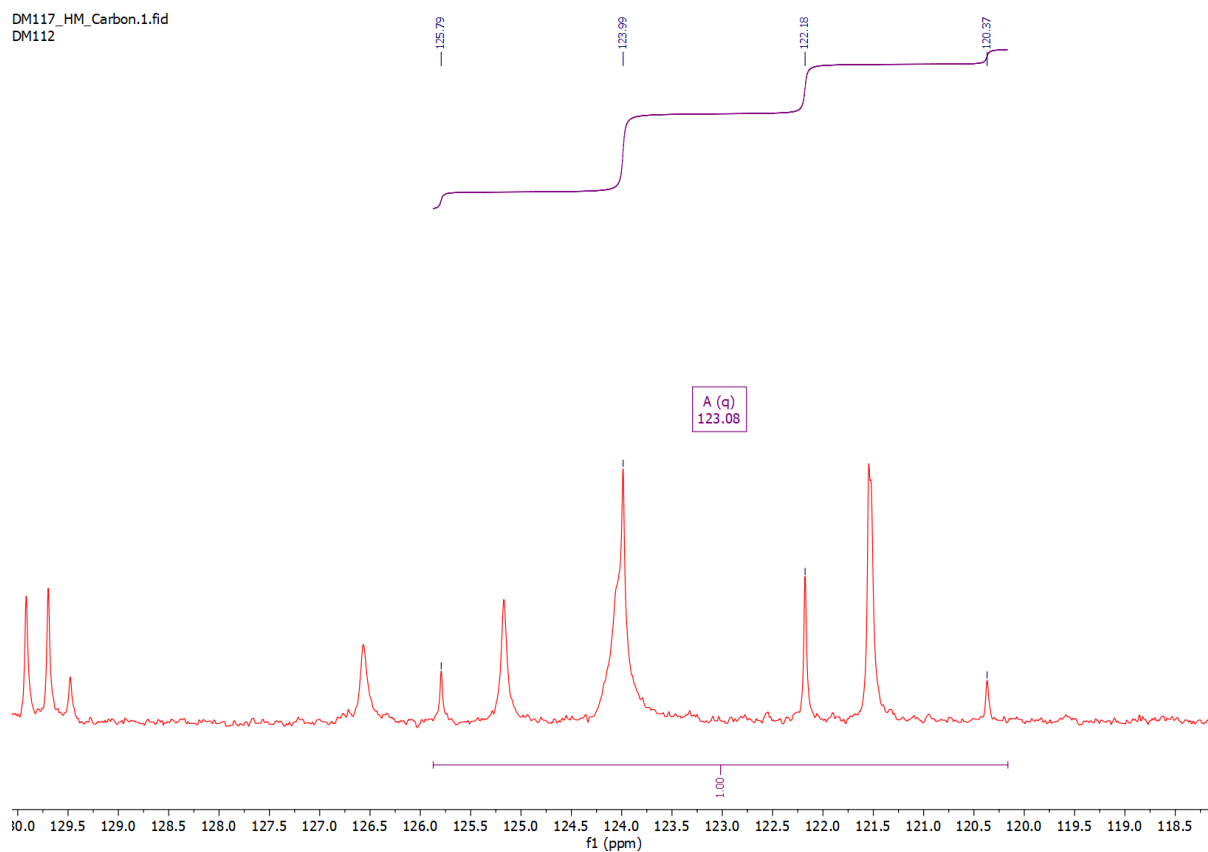
Figure S55. ^{13}C NMR (101 MHz) spectrum of 1,9-bis(3,5-bis-(trifluoromethyl)phenyl)thiourea-9(10H)-acridinone in (CD$_3$)$_2$SO$_3$ at 298 K. Zoomed in for clarity, showing α-carbon splitting.
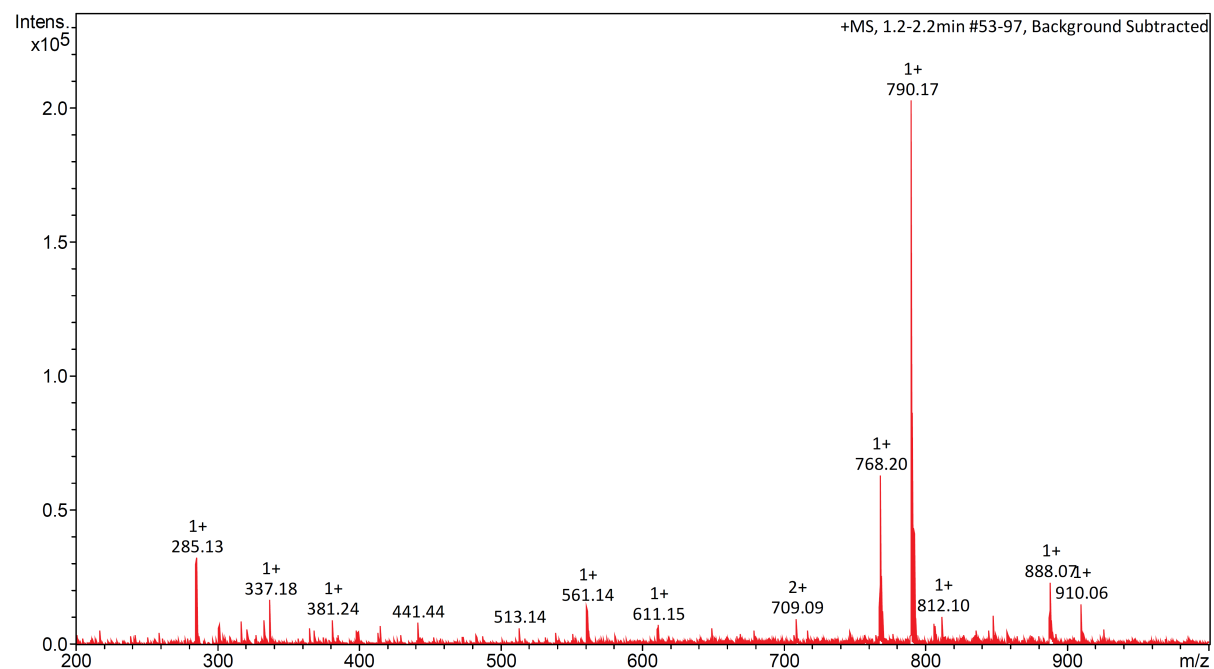
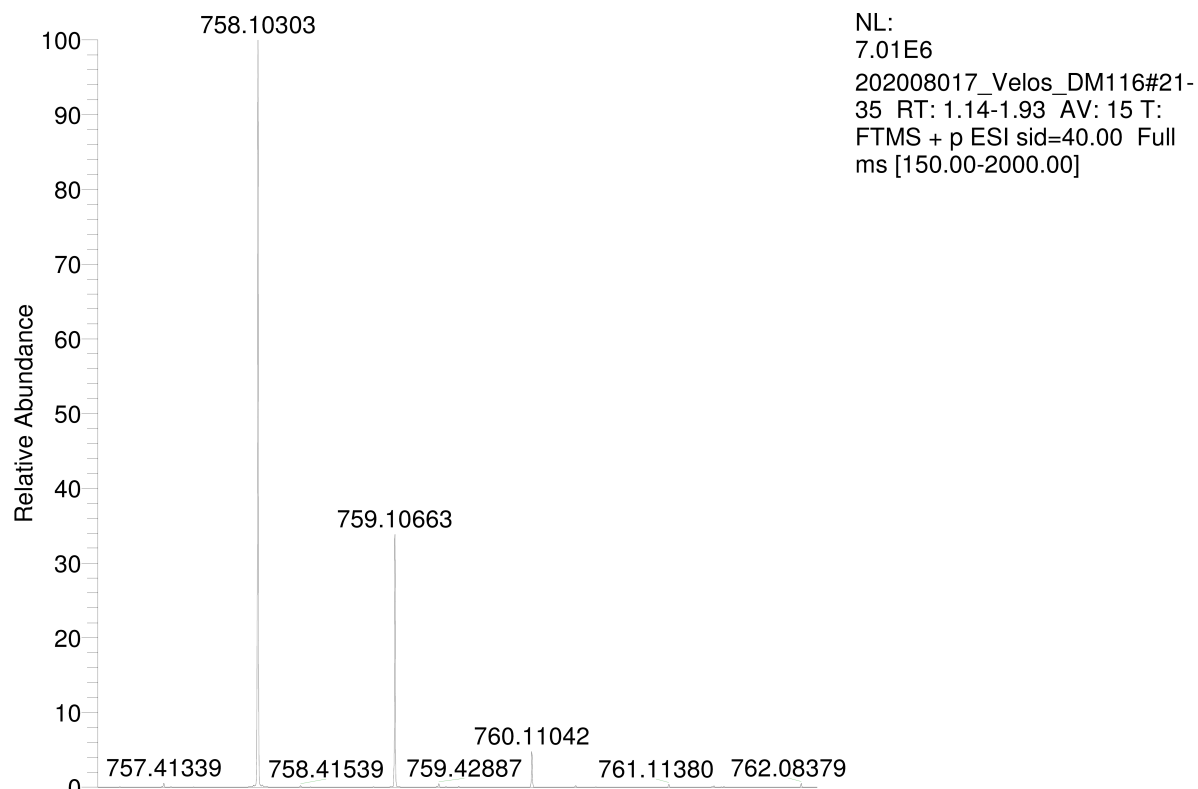Figure S56. LR-MS (ESI$^+$) spectrum of 1,9-bis(3,5-bis-(trifluoromethyl)phenyl)thiourea-9(10H)-acridinone.
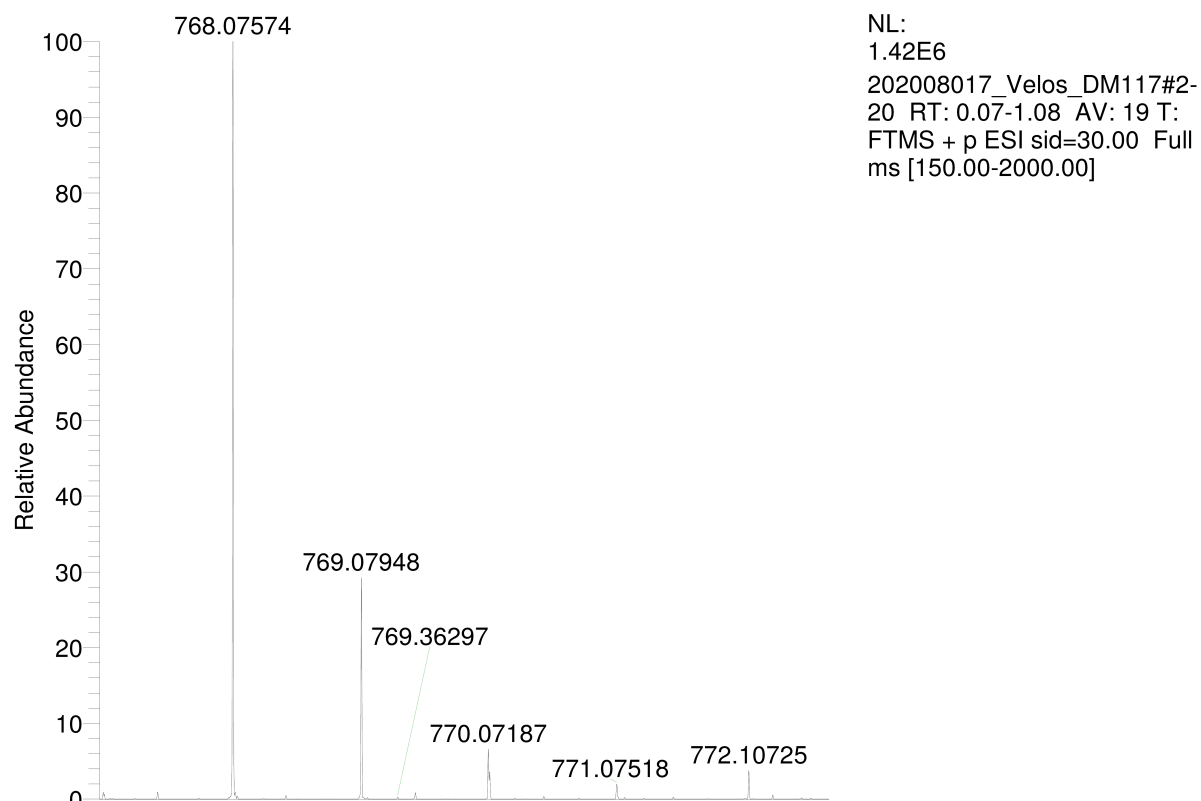
Figure S57. HR-MS (ESI⁺) spectrum of 1,9-bis(3,5-bis-(trifluoromethyl)phenyl)thiourea-9(10H)-acridinone.

4-(pentafluorosulfanyl)phenyl isothiocyanate
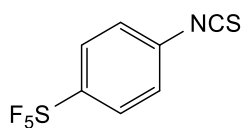
4-pentafluorosulfanyl aniline (410 mg, 1.86 mmol) was dissolved in dichloromethane (15 mL). Thiophosgene (0.16 mL, 2.05 mmol) was added, followed by a layer of saturated aqueous $NaHCO_3$ solution (20 mL) to trap any volatile thiophosgene. The mixed was stirred gently at room temperature for 12 hours. Next, the aqueous layer was removed, and the organic layer dried with magnesium sulfate for 1 hour. The solvent was removed in vacuo and the resultant solid used immediately in the next reaction.

Compound 10: 1,9-bis(4-(pentafluorosulfanyl)phenyl)thiourea-9(10H)-acridinone
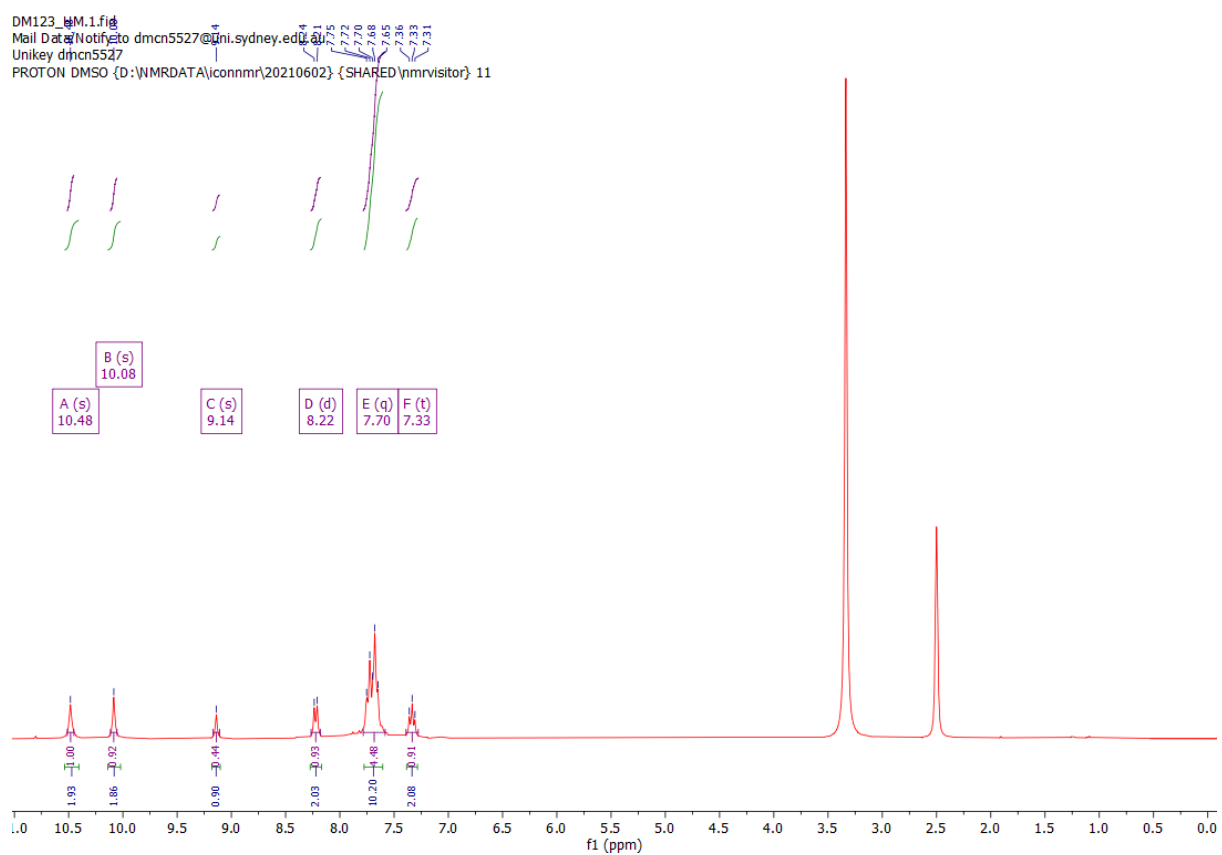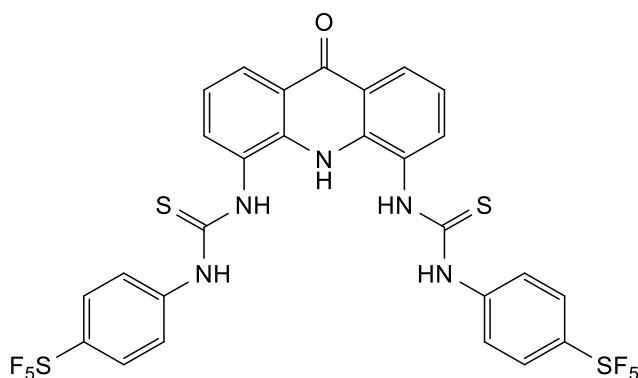
Figure S58. ^{1}H NMR (400 MHz) spectrum of 1,9-bis(4-(pentafluorosulfanyl)phenyl)thiourea-9(10H)-acridinone in $(CD_3)_2SO_3$ at 298 K.
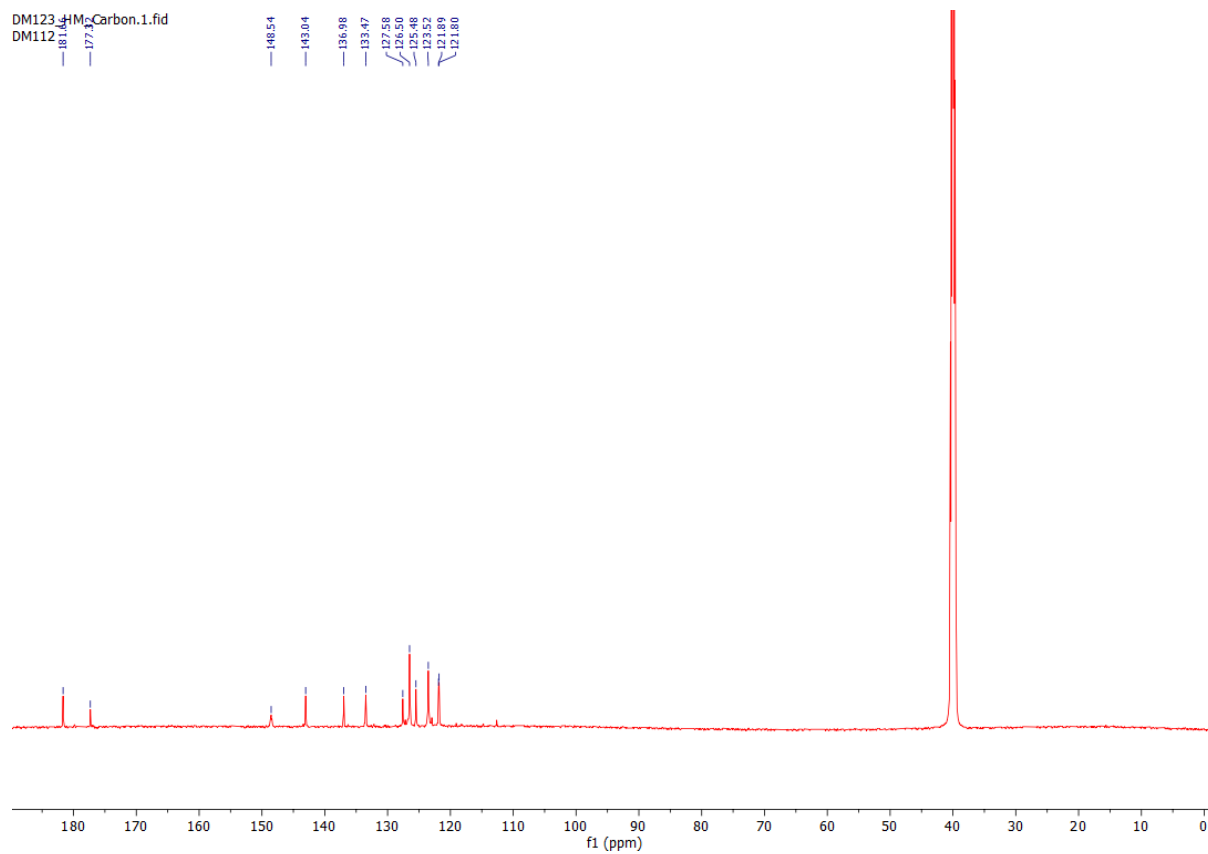
Figure S59. ^{13}C NMR (101 MHz) spectrum of 1,9-bis(4-(pentafluorosulfanyl)phenyl)thiourea-9(10H)-acridinone in $(CD_3)_2SO_3$ at 298 K.

DM123_HM_Carbon_1.fid
DM112

181.47 177.2 148.54 143.04 136.98 133.47 127.58 126.50 125.48 123.52 121.89 121.80
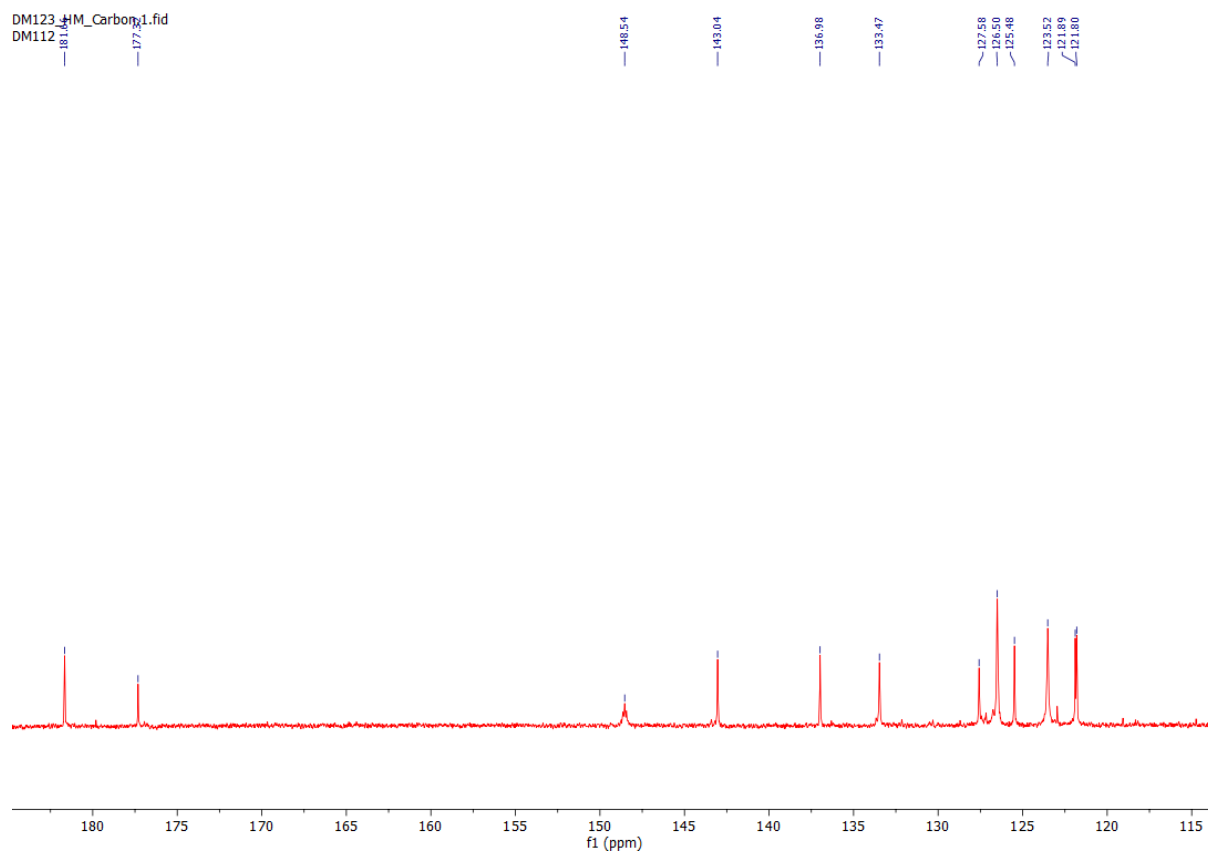
Figure S60. ^{13}C NMR (101 MHz) spectrum of 1,9-bis(4-(pentafluorosulfanyl)phenyl)urea-9(10H)-acridinone in $(CD_3)_2SO_3$ at 298 K. Zoomed in for clarity.
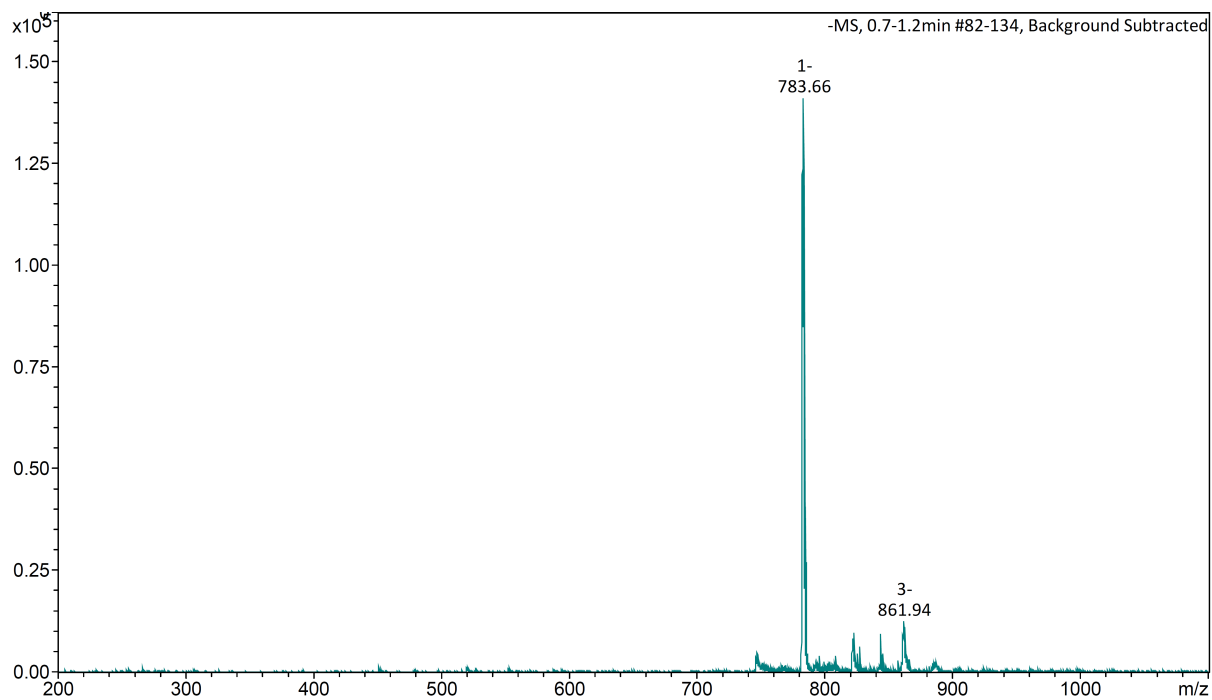
Figure S61. LR-MS (ESI⁻) spectrum of 1,9-bis(4-(pentafluorosulfanyl)phenyl)thiourea-9(10H)-acridinone.
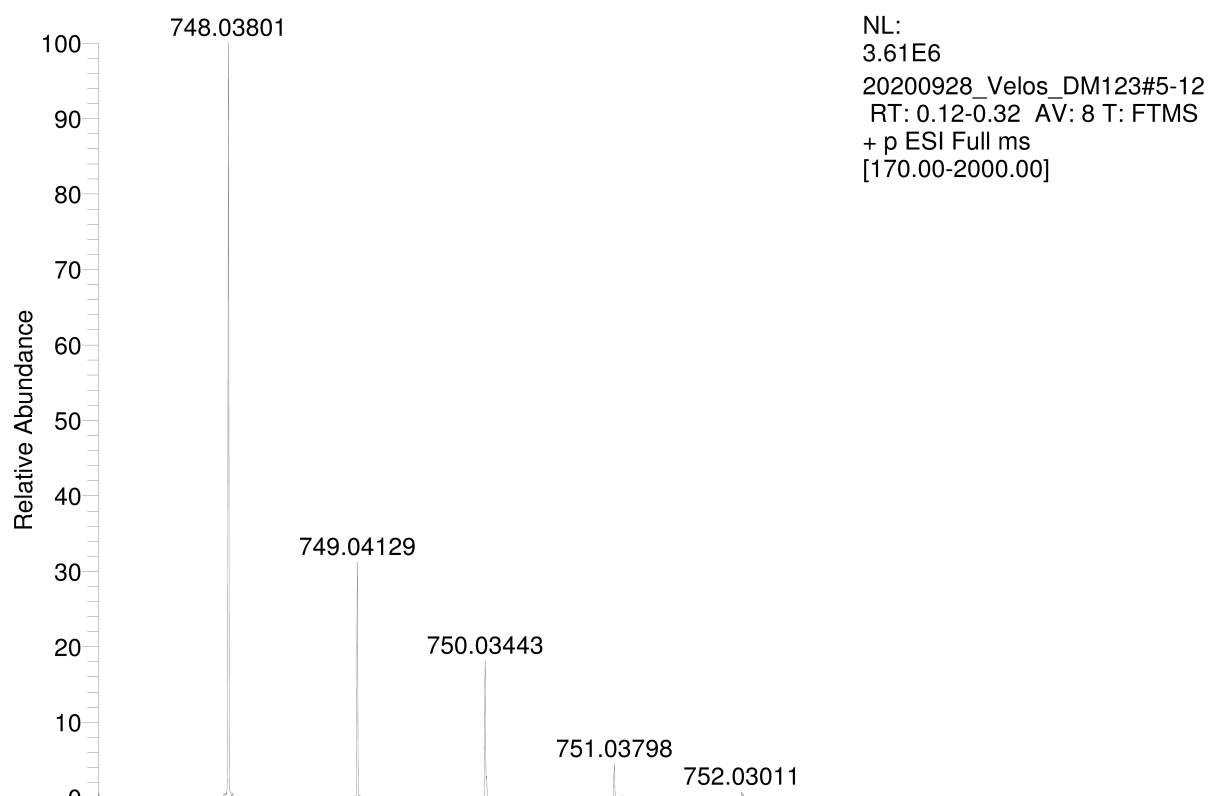
Figure S62. HR-MS (ESI⁻) spectrum of 1,9-bis(4-(pentafluorosulfanyl)phenyl)thiourea-9(10H)-acridinone.

Single Crystal X-ray Diffraction

X-ray diffraction data were collected at 100 K on the MX2 Macromolecular Crystallography beamline at the Australian Synchrotron at a wavelength of 0.71073 Å.[1] The data collection and integration were performed within the Blu-Ice[1] and XDS[2] software programs. The solutions were obtained by direct methods using SHELXT[3] followed by successive refinements using full matrix least squares method against F^2 using SHELXL-2018/3.[4] The program OLEX2[5] was used was used as a graphical SHELX interface.
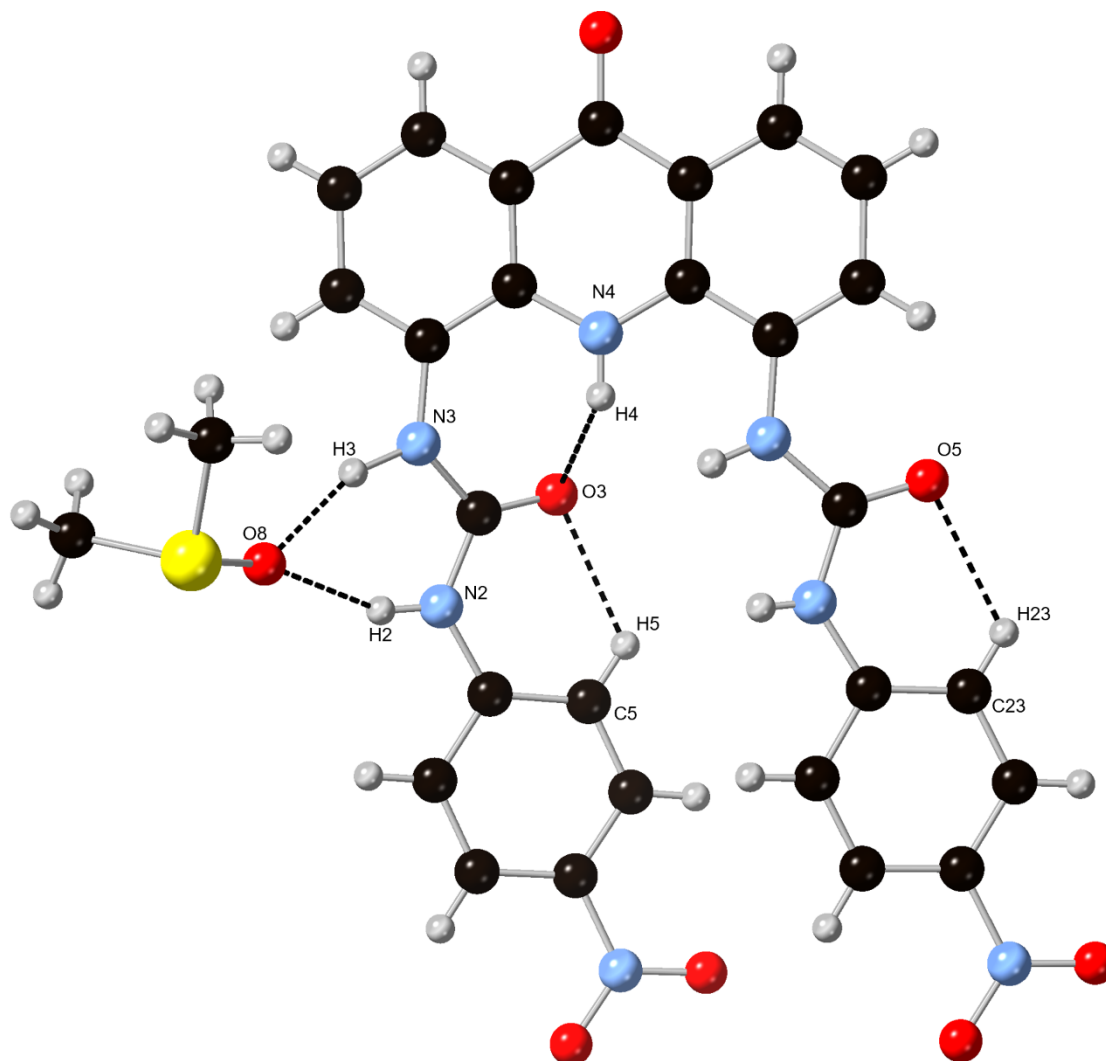
Figure S63. The X-ray crystal structure of the DMSO solvate of receptor **3**.

Table S 1. Crystal and data refinement parameters for the X-ray studies.

	3
CCDC Deposition number	2101004
Formula	C31 H31 N7 O9 S2
Formula weight	709.75
Temperature/K	100(2)
Crystal system	monoclinic
Space group	$P2_1/n$
a (Å)	11.069(2)
b (Å)	19.863(4)
c (Å)	14.418(3)
B (°)	93.29(3)
Volume (Å^3)	3164.8(11)
Z	4
ρ_{calc} /g cm^{-3}	1.490
μ (mm^{-1})	0.236
F (000)	1480
Reflections collected	9277
Independent reflections	[R_{int} = 0.0338, R_{sigma} = 0.0208]
Data/restraints/parameters	9277/2/484
GooF	1.034
Final R indexes [I>=2σ (I)]	R_1 = 0.1079, wR_2 = 0.3095
Final R indexes [all data]	R_1 = 0.1187, wR_2 = 0.3192
Largest diff. peak/hole / e Å^{-3}	1.239/−0.697

Table S 2. Hydrogen-bonding parameters from the X-ray study of 3.

Interaction	H⋯A [A°][B]	D⋯A [A°][B]	D–H⋯A [°][B]
N(2)⋯O(8)[1]	2.01	2.796(4)	151.1
N(4)⋯O(3)	2.16	2.736(4)	123.8
C(5)⋯O(3)	2.27	2.867(4)	121.6
C(23)⋯O(5)	2.30	2.896(4)	121.2
N(3)⋯O(8)[1]	1.78(5)	2.800(4)	159(4)

[1] - ½ +X, ½ - Y, ½ + Z

^{1}H NMR Titration Anion Binding Studies

Equipment and Sample Preparation

^{1}H NMR titrations were performed on a Bruker Avance DPX 400 spectrometer. For NMR titrations with chloride, a constant host concentration was maintained ($\sim$ 1.0 mM) using a prepared host solution to dissolve the guest (as TBACl) to make the guest stock solution. Over the course of the titration, Hamiltonian Microlitre syringes were used to add aliquots of the guest stock solution to the NMR sample of the host solution.

Chloride was added as the tetrabutylammonium (TBA) salt after being dried under high vacuum (< 1.0 mmHg) for 24 h. Stock solutions of the host were prepared in a DMSO-d_6 / 0.5% H_2O solution. The host stock solutions (600 μL) were transferred to an air-tight screw-cap NMR sample tube (5 mm ID), and the same host stock solution was used to prepare the standard guest titrant solutions containing either 0.1 M or 1 M of TBACl. This ensured a constant concentration of the host for the duration of the titration experiment.

Titration Procedure

Over the course of the titration, small aliquots (2–200 μL) of the standard guest solution were added to the host solution ($\sim$ 600 μL) in the NMR tube. For each titration, 16–20 data points were collected, and at the end of the titration, approximately 300 equivalents of the guest anion were present. Before collecting each data point, an aliquot of the standard guest solution was added, and the sample was thoroughly mixed in the NMR tube. The system was allowed to equilibrate for up to 2 min inside the NMR probe before the spectra was collected. Throughout each titration experiment, all parameters of the NMR spectrometer remained constant.

Titration Data Fitting

In all cases, the proton resonances were monitored for changes in chemical shift. When possible, two or more resonances were followed, allowing several data sets to determine the association constant (K_a). Global fitting takes into account all data sets at the same time and improves the quality of the non-linear curve fitting. The supramolecular.org web applet was used to fit the titration data to a 1:1 or 1:2 host:guest binding model. A 1:2 model was preferred when the covariance of fit (cov_{fit}) was 5 times better than the covariance of fit for the 1:1 model. The fitting of the same data to both models has been included for comparison.

Figure S64. ^{1}H NMR titration spectra as a stack plot for 1,9-bisphenylurea-9(10H)-acridinone (1 mM) + TBACl in DMSO-d_6 /0.5% D$_2$O at 298 K.
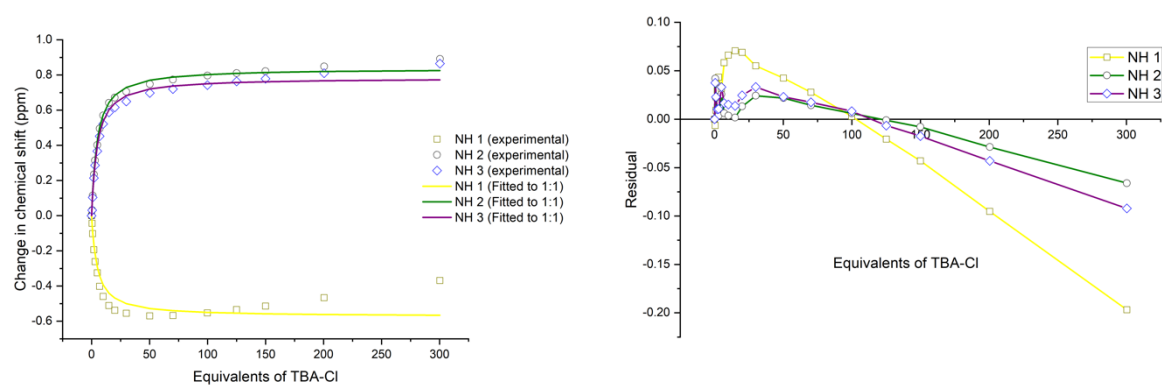
Figure S65. Fitted binding isotherm of 1,9-bisphenylurea-9(10H)-acridinone + TBACl showing the change in chemical shift of the NH protons fitted to the 1:1 binding model (left). K_a = 244.65 M^{-1}. Residual plot showing the random error obtained from the binding isotherm fitting (right). Covariance of fit (cov$_{fit}$) = 7.53×10^{-3}. Link to Bindfit fitting: http://app.supramolecular.org/bindfit/view/95a73490-ce71-4386-a8f1-8b437860a77e.

Figure S66. Fitted binding isotherm of 1,9-bisphenylurea-9(10H)-acridinone + TBACl showing the change in chemical shift of the NH protons fitted to the 1:2 binding model (left) K_{11} = 246.59 M^{-1}, K_{12} = 2.4 x 10^{-8} M^{-1}. Residual plot showing the random error obtained from the binding isotherm fitting (right). Covariance of fit (cov$_{fit}$) = 5.80×10^{-4}. Link to Bindfit fitting: http://app.supramolecular.org/bindfit/view/173fdeaf-717a-411a-8e8f-56f30a8db3ef.

Figure S67. ^{1}H NMR titration spectra as a stack plot for 1,9-bisphenylthiourea-9(10H)-acridinone (1 mM) + TBACl in DMSO-d_6 /0.5% D$_2$O at 298 K.

Figure S68. Fitted binding isotherm of 1,9-bisphenylthiourea-9(10H)-acridinone + TBACl showing the change in chemical shift of the NH protons fitted to the 1:1 binding model (left). K_a = 54.19 M^{-1}. Residual plot showing the random error obtained from the binding isotherm fitting (right). Covariance of fit (cov$_{fit}$) = 1.40×10^{-2}. Link to Bindfit fitting: http://app.supramolecular.org/bindfit/view/e1d98591-b4fc-4fad-8aa5-9964b6271803.

Figure S69. Fitted binding isotherm of 1,9-bisphenylthiourea-9(10H)-acridinone + TBACl showing the change in chemical shift of the NH protons fitted to the 1:2 binding model (left) K_{11} = 115.01 M^{-1}, K_{12} = 2.36 M^{-1}. Residual plot showing the random error obtained from the binding isotherm fitting (right). Covariance of fit (cov$_{fit}$) = 1.85 x 10^{-3}. Link to Bindfit fitting: http://app.supramolecular.org/bindfit/view/f92f7b59-0946-46e0-8c85-8c204cd84409

Figure S70. ^{1}H NMR titration spectra as a stack plot for 1,9-bis(4-(trifluoromethyl)phenyl)urea-9(10H)-acridinone (1 mM) + TBACl in DMSO-d_6 /0.5% D$_2$O at 298 K.

Figure S71. Fitted binding isotherm of 1,9-bis(4-(trifluoromethyl)phenyl)urea-9(10H)-acridinone + TBACl showing the change in chemical shift of the NH protons fitted to the 1:1 binding model (left). K_a = 139.85 M^{-1}. Residual plot showing the random error obtained from the binding isotherm fitting (right). Covariance of fit (cov$_{fit}$) = 5.21×10^{-2}. Link to Bindfit fitting: http://app.supramolecular.org/bindfit/view/2c7da4b1-5599-4ff1-acd6-616be2295eea.

Figure S72. Fitted binding isotherm of 1,9-bis(4-(trifluoromethyl)phenyl)urea-9(10H)-acridinone + TBACl showing the change in chemical shift of the NH protons fitted to the 1:2 binding model (left) K_{11} = 264.07 M^{-1}, K_{12} = 1.26 M^{-1}. Residual plot showing the random error obtained from the binding isotherm fitting (right). Covariance of fit (cov$_{fit}$) = 5.80×10^{-4}. Link to Bindfit fitting: http://app.supramolecular.org/bindfit/view/6de308b8-bb70-4dd2-a859-657d56cb6948.

Figure S73. ^{1}H NMR titration spectra as a stack plot for 1,9-bis(4-(trifluoromethyl)phenyl)thiourea-9(10H)-acridinone (1 mM) + TBACl in DMSO-d_6 /0.5% D$_2$O at 298 K.

Figure S74. Fitted binding isotherm of 1,9-bis(4-(trifluoromethyl)phenyl)thiourea-9(10H)-acridinone + TBACl showing the change in chemical shift of the NH protons fitted to the 1:1 binding model (left). K_a = 49.06 M^{-1}. Residual plot showing the random error obtained from the binding isotherm fitting (right). Covariance of fit (cov$_{fit}$) = 1.86×10^{-2}. Link to Bindfit fitting: http://app.supramolecular.org/bindfit/view/3cee3ef4-1f9e-4306-be2c-5e95cde33d76.

Figure S75. Fitted binding isotherm of 1,9-bis(4-(trifluoromethyl)phenyl)thiourea-9(10H)-acridinone + TBACl showing the change in chemical shift of the NH protons fitted to the 1:2 binding model (left) K_{11} = 121.26 M^{-1}, K_{12} = 2.00 M^{-1}. Residual plot showing the random error obtained from the binding isotherm fitting (right). Covariance of fit (cov$_{fit}$) = 3.49×10^{-4}. Link to Bindfit fitting: http://app.supramolecular.org/bindfit/view/e8aab5d8-78a8-4016-b2ad-a74c26a959eb.

Figure S76. ^{1}H NMR titration spectra as a stack plot for 1,9-bis(4-nitrophenyl)urea-9(10H)-acridinone (1 mM) + TBACl in DMSO-d_6 /0.5% D_2O at 298 K.

Figure S77. Fitted binding isotherm of 1,9-bis(4-nitrophenyl)urea-9(10H)-acridinone + TBACl showing the change in chemical shift of the NH protons fitted to the 1:1 binding model (left). K_a = 167.63 M^{-1}. Residual plot showing the random error obtained from the binding isotherm fitting (right). Covariance of fit (cov$_{fit}$) = 5.98×10^{-2}. Link to Bindfit fitting: http://app.supramolecular.org/bindfit/view/7160eae2-4bd6-4972-8bcc-7fcbc5d674c4.
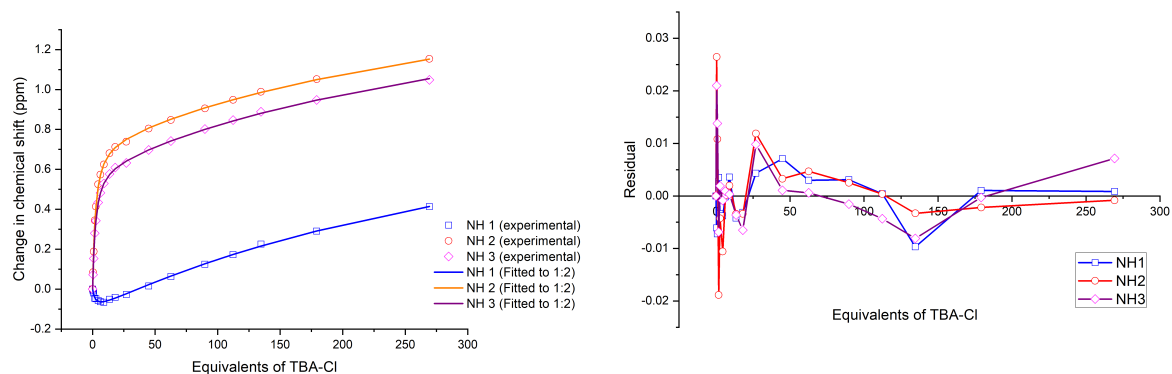
Figure S78. Fitted binding isotherm of 1,9-bis(4-nitrophenyl)urea-9(10H)-acridinone + TBACl showing the change in chemical shift of the NH protons fitted to the 1:2 binding model (left) K_{11} = 500.33 M^{-1}, K_{12} = 2.00 M^{-1}. Residual plot showing the random error obtained from the binding isotherm fitting (right). Covariance of fit (cov$_{fit}$) = 3.78×10^{-4}. Link to Bindfit fitting: http://app.supramolecular.org/bindfit/view/934a87c6-73a5-43d0-84d8-a871685c658b.
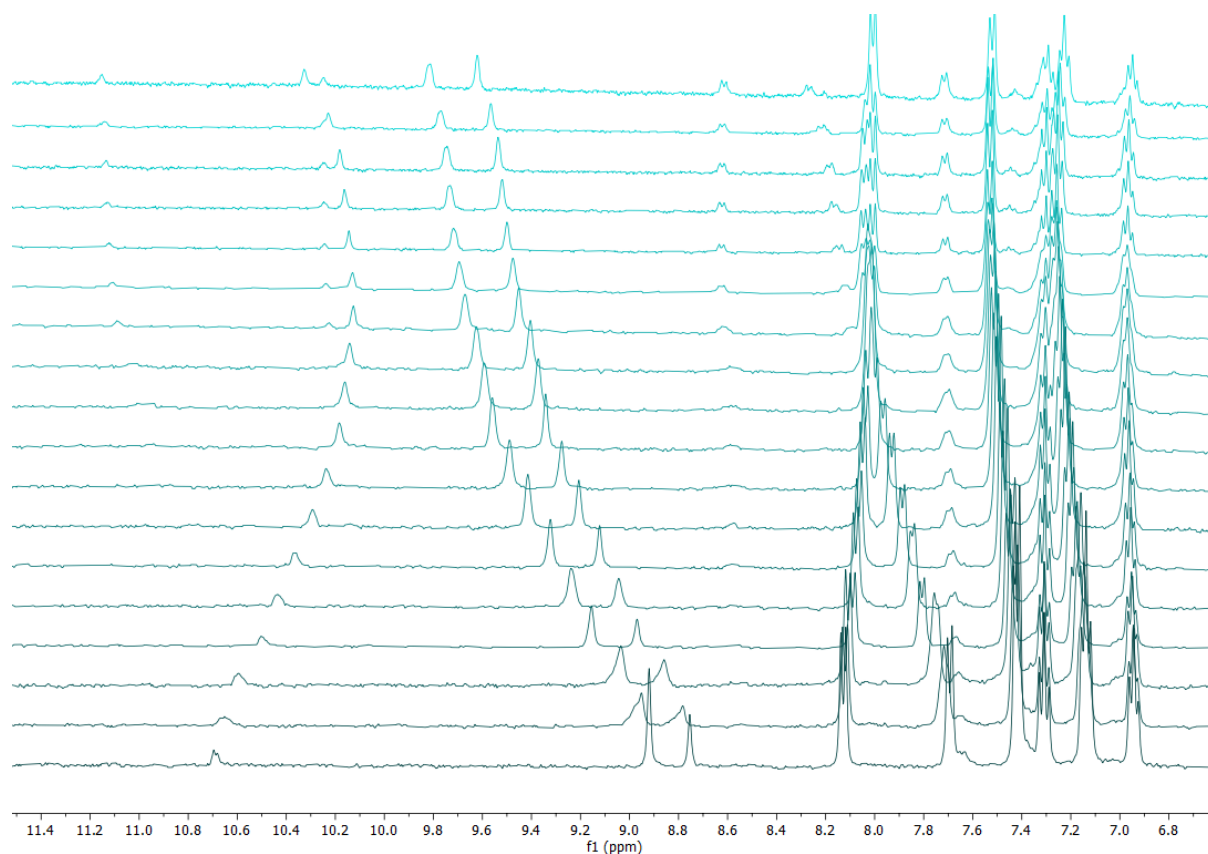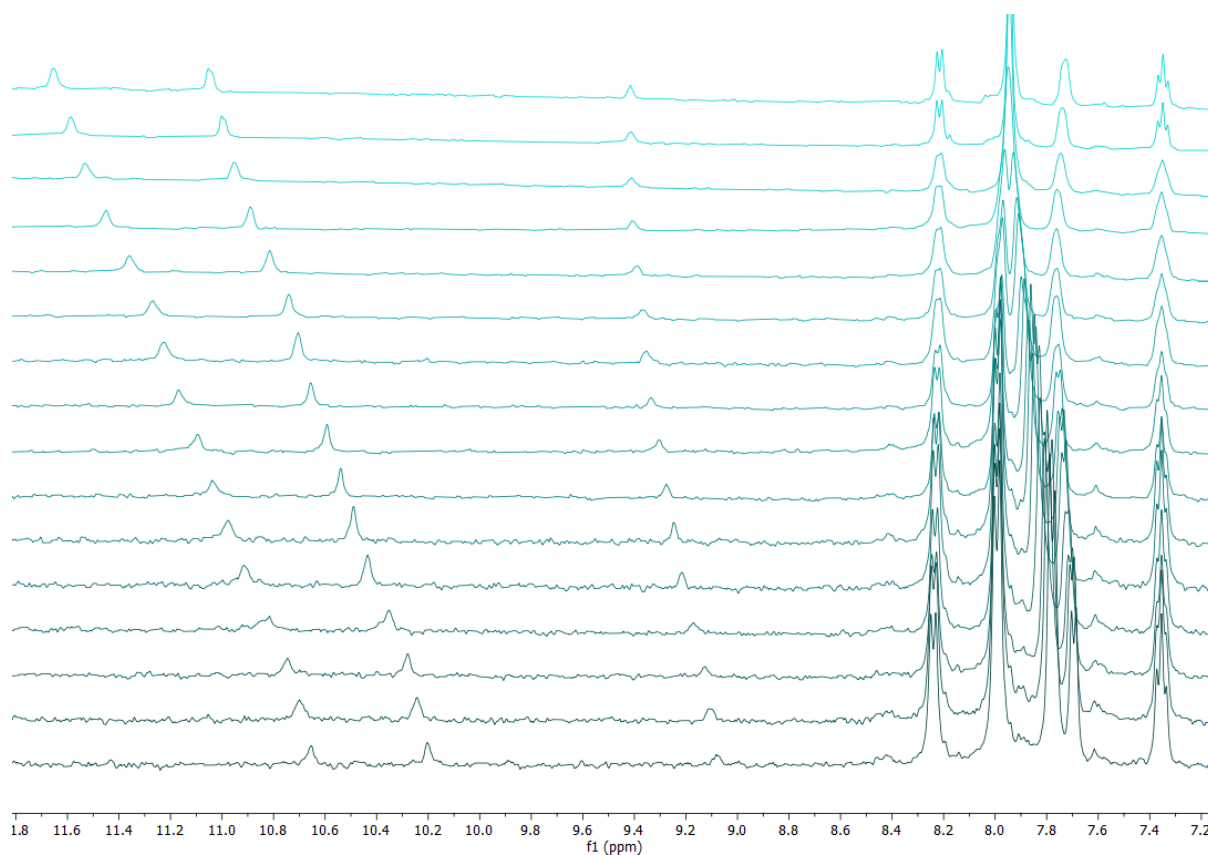

Figure S79. ^{1}H NMR titration spectra as a stack plot for 1,9-bis(4-nitrophenyl)thiourea-9(10H)-acridinone (1 mM) + TBACl in DMSO-d_6 /0.5% D$_2$O at 298 K.
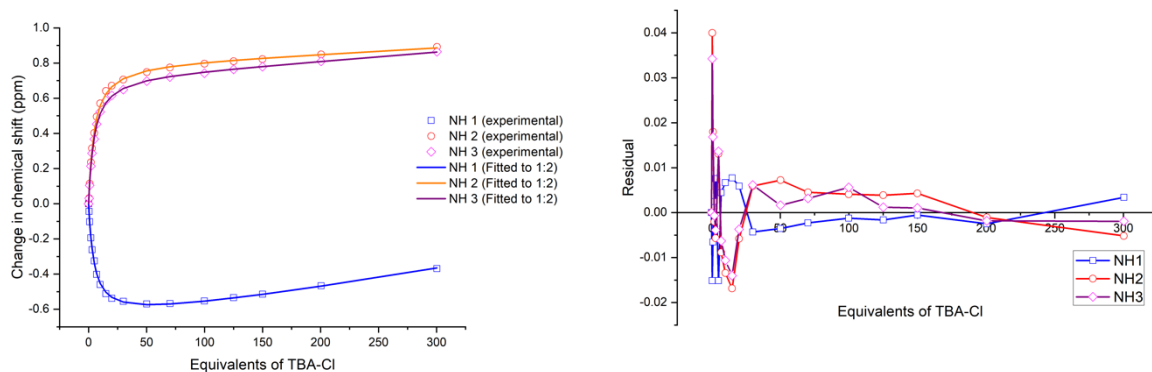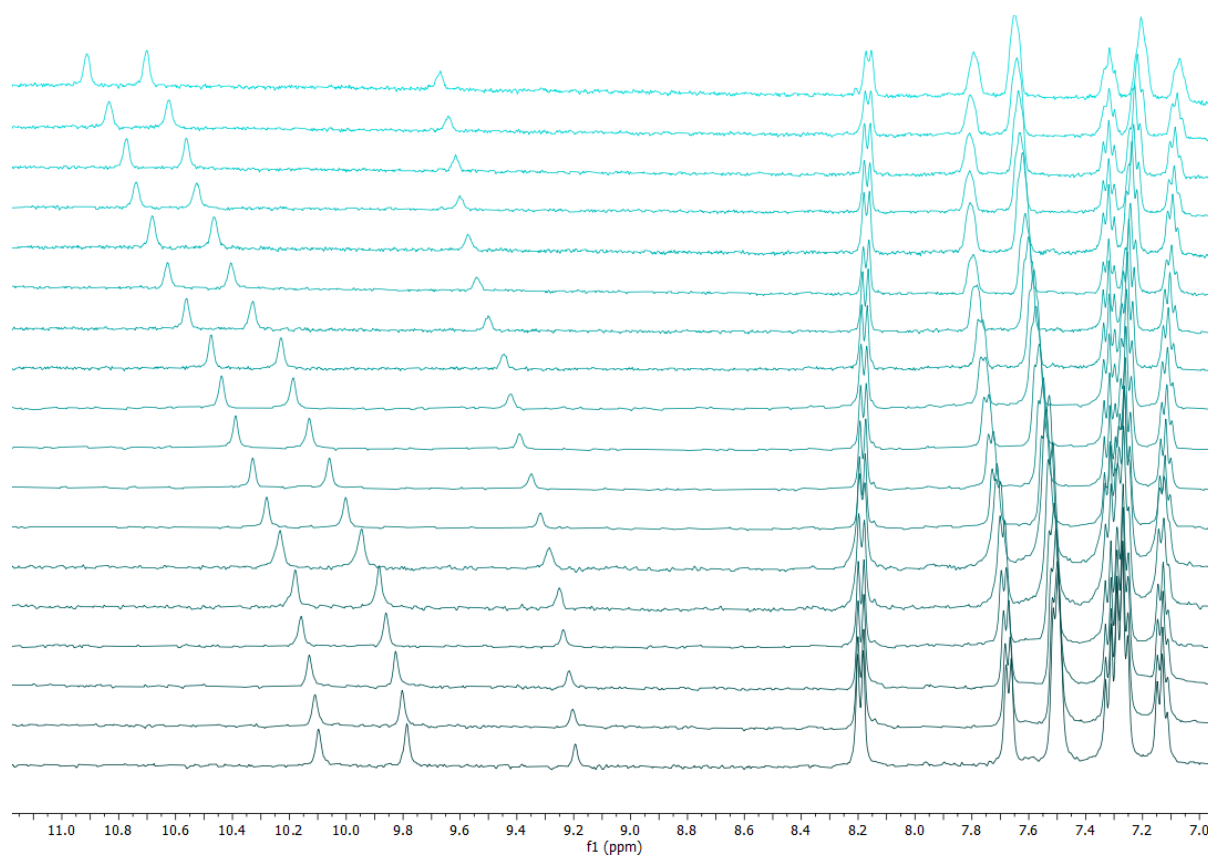
S64

Figure S80. Fitted binding isotherm of 1,9-bis(4-nitrophenyl)thiourea-9(10H)-acridinone + TBACl showing the change in chemical shift of the NH protons fitted to the 1:1 binding model (left). K_a = 66.73 M^{-1}. Residual plot showing the random error obtained from the binding isotherm fitting (right). Covariance of fit (cov$_{fit}$) = 3.29×10^{-2}. Link to Bindfit fitting: http://app.supramolecular.org/bindfit/view/bd10986b-2075-482e-9873-ca1a3ecb108a.
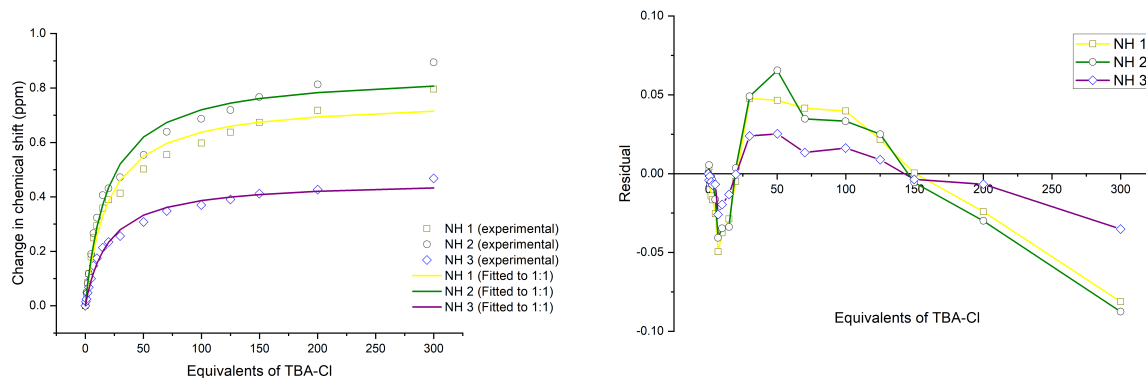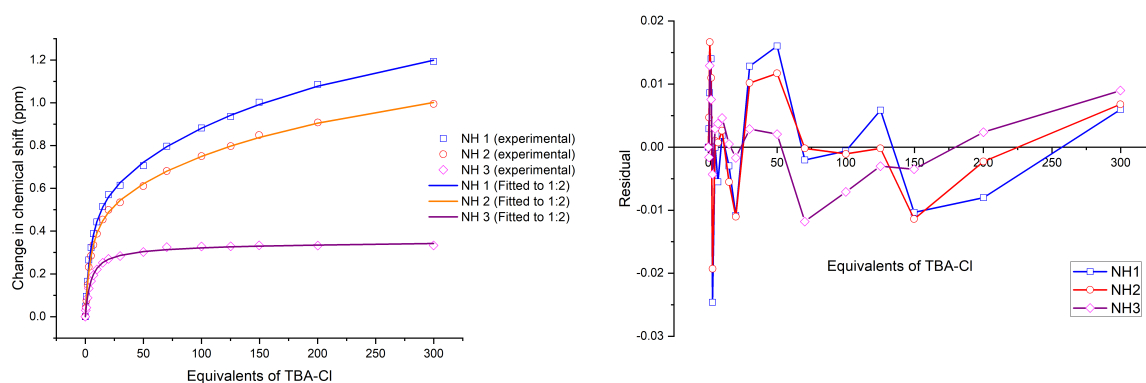

Figure S81. Fitted binding isotherm of 1,9-bis(4-nitrophenyl)thiourea-9(10H)-acridinone + TBACl showing the change in chemical shift of the NH protons fitted to the 1:2 binding model (left) K_{11} = 241.48 M^{-1}, K_{12} = 3.70 M^{-1}. Residual plot showing the random error obtained from the binding isotherm fitting (right). Covariance of fit (cov$_{fit}$) = 6.89×10^{-4}. Link to Bindfit fitting: http://app.supramolecular.org/bindfit/view/c8232517-f5fd-47a8-953b-0358f4a97324.
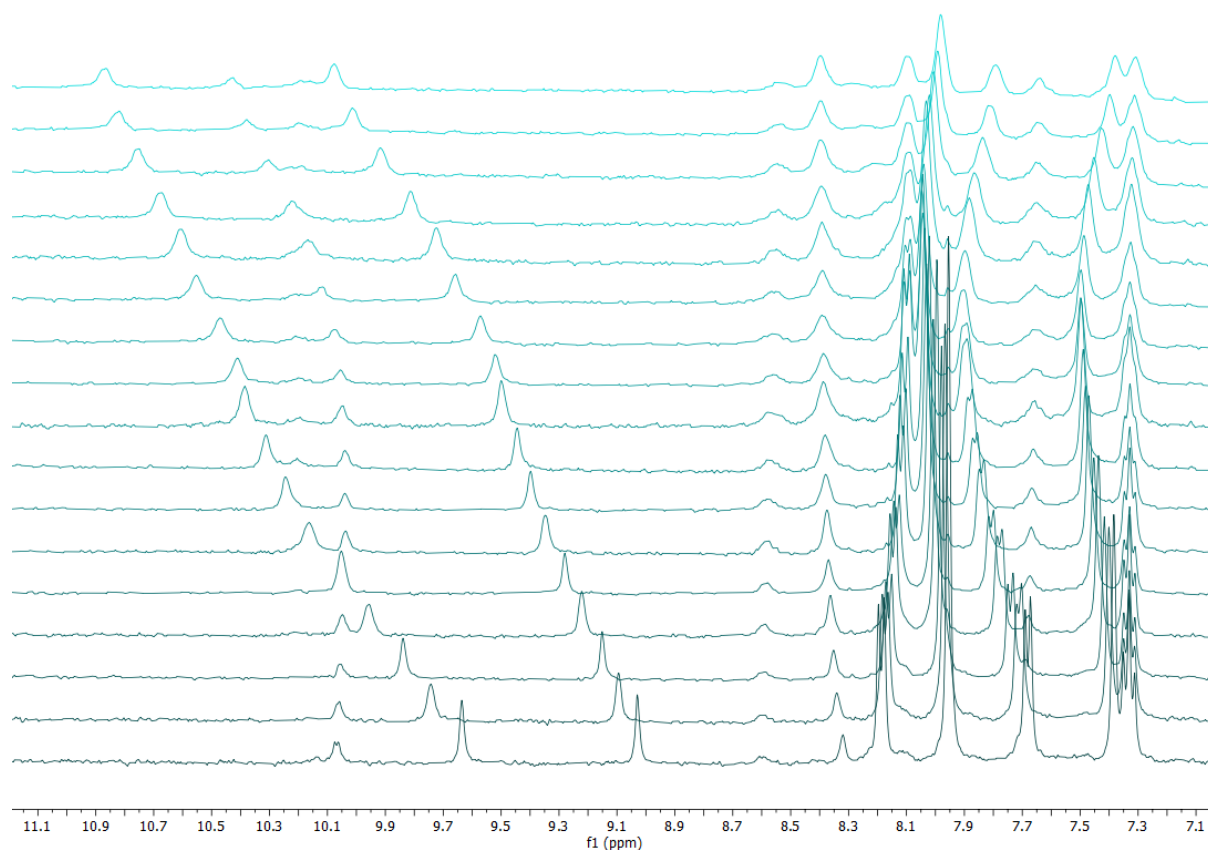
Figure S82. ^{1}H NMR titration spectra as a stack plot for 1,9-bis(3,5-bis-(trifluoromethyl)phenyl)urea-9(10H)-acridinone (1 mM) + TBACl in DMSO-d_6 /0.5% D$_2$O at 298 K.
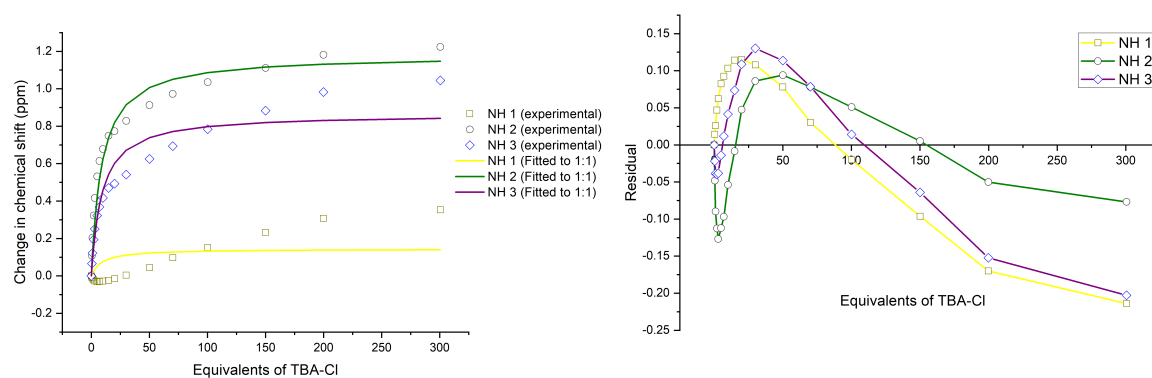
Figure S83. Fitted binding isotherm of 1,9-bis(3,5-bis-(trifluoromethyl)phenyl)urea-9(10H)-acridinone + TBACl showing the change in chemical shift of the NH protons fitted to the 1:1 binding model (left). K_a = 101.67 M^{-1}. Residual plot showing the random error obtained from the binding isotherm fitting (right). Covariance of fit (cov$_{fit}$) = 5.13×10^{-2}. Link to Bindfit fitting: http://app.supramolecular.org/bindfit/view/e5b07763-6eda-44e1-9743-bc2a88ef44dc.
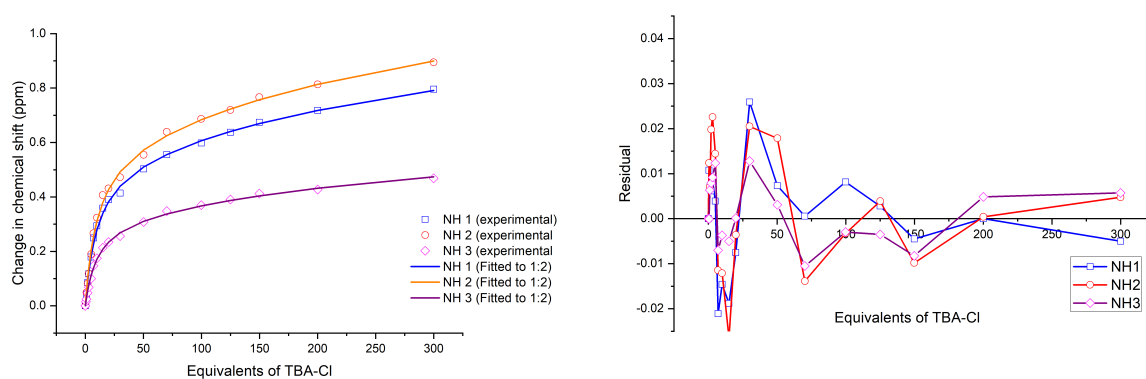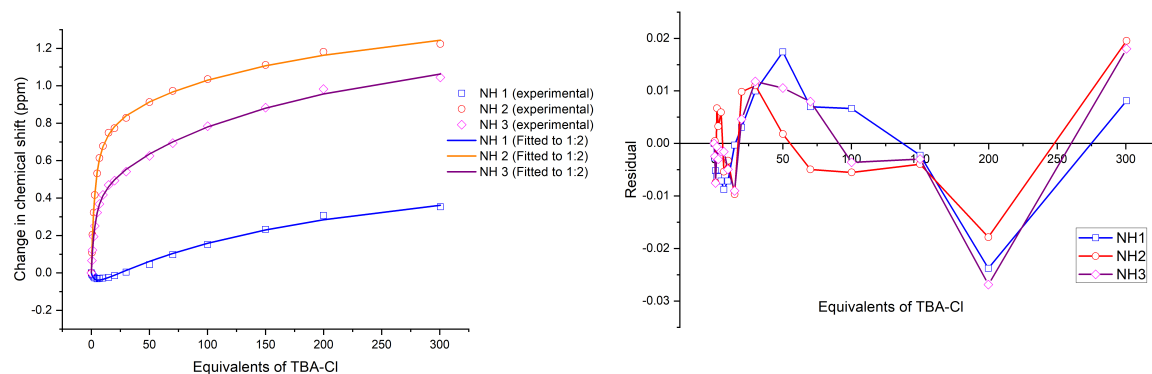
Figure S84. Fitted binding isotherm of 1,9-bis(3,5-bis-(trifluoromethyl)phenyl)urea-9(10H)-acridinone + TBACl showing the change in chemical shift of the NH protons fitted to the 1:2 binding model (left) K_{11} = 357.48 M^{-1}, K_{12} = 3.92 M^{-1}. Residual plot showing the random error obtained from the binding isotherm fitting (right). Covariance of fit (cov$_{fit}$) = 5.61×10^{-4}. Link to Bindfit fitting: http://app.supramolecular.org/bindfit/view/9693cda6-c60d-43d3-b96a-df4e1dd97295.
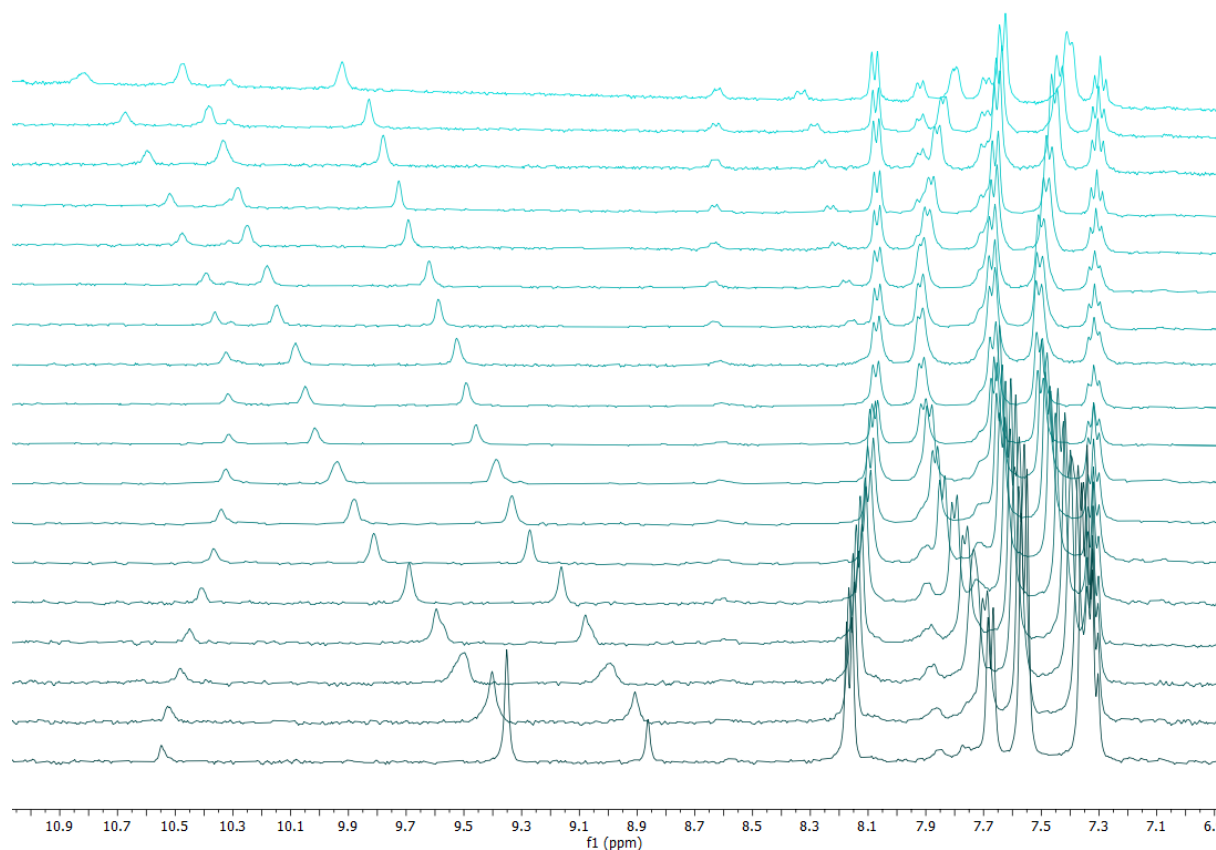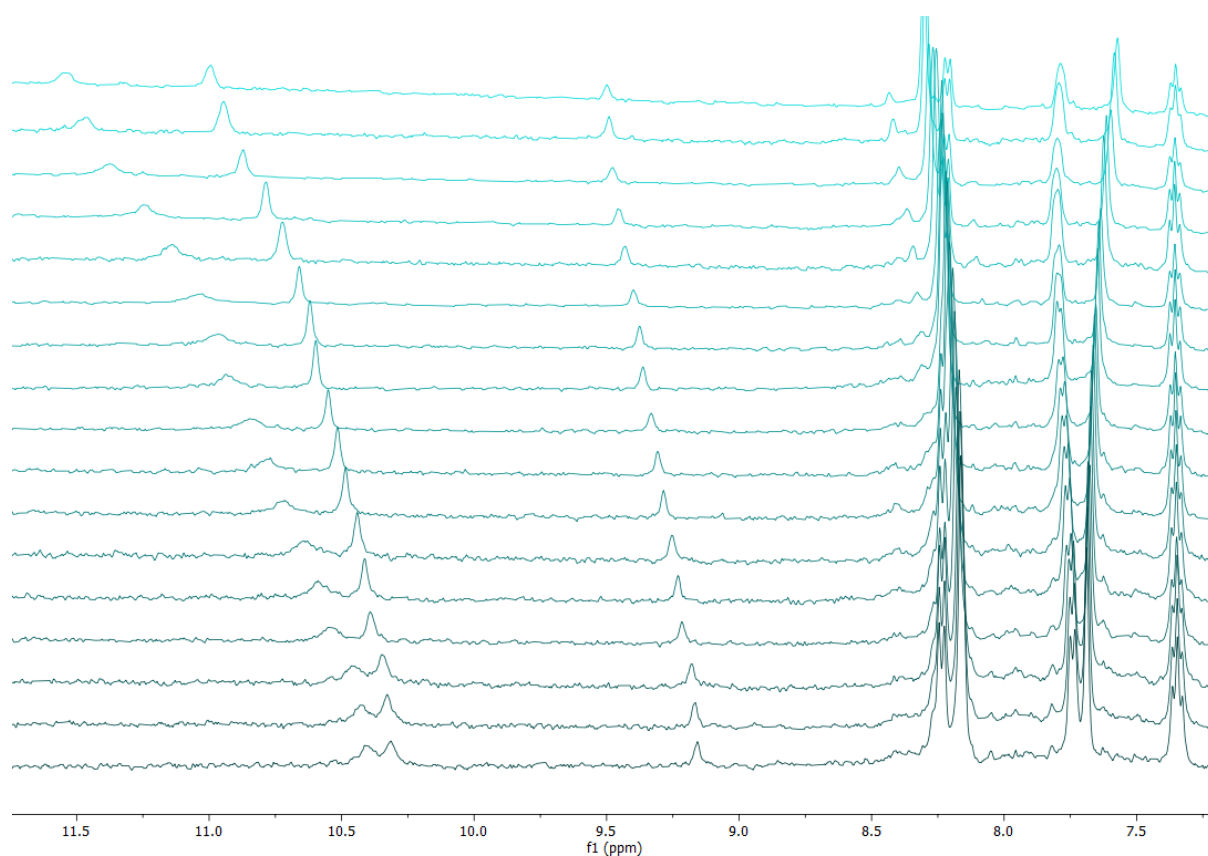

Figure S85. ^{1}H NMR titration spectra as a stack plot for 1,9-bis(3,5-bis-(trifluoromethyl)phenyl)thiourea-9(10H)-acridinone (1 mM) + TBACl in DMSO-d_6 /0.5% D$_2$O at 298 K.
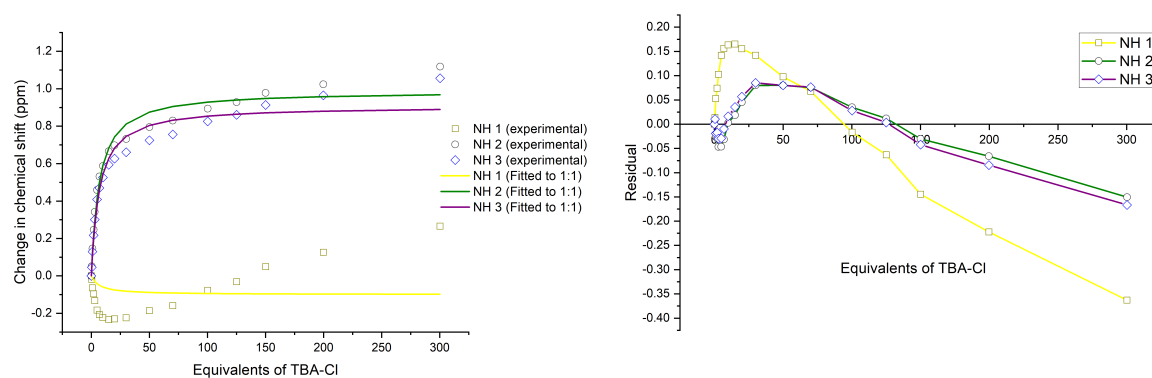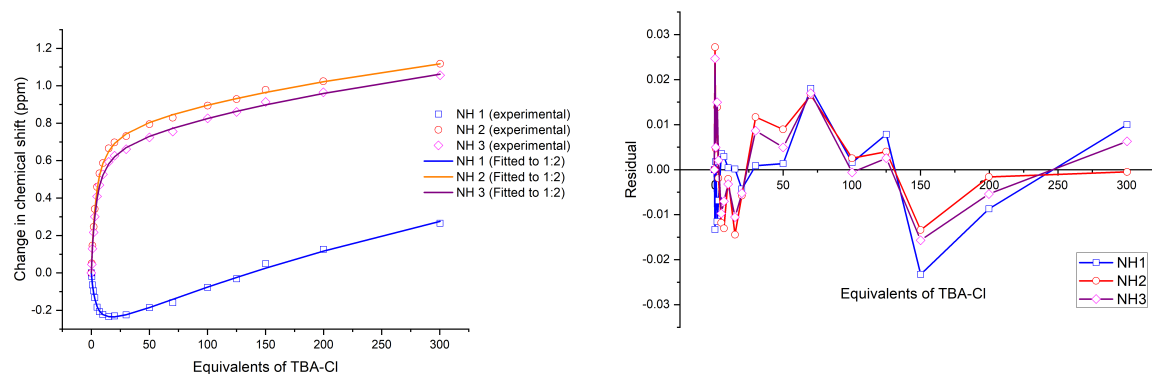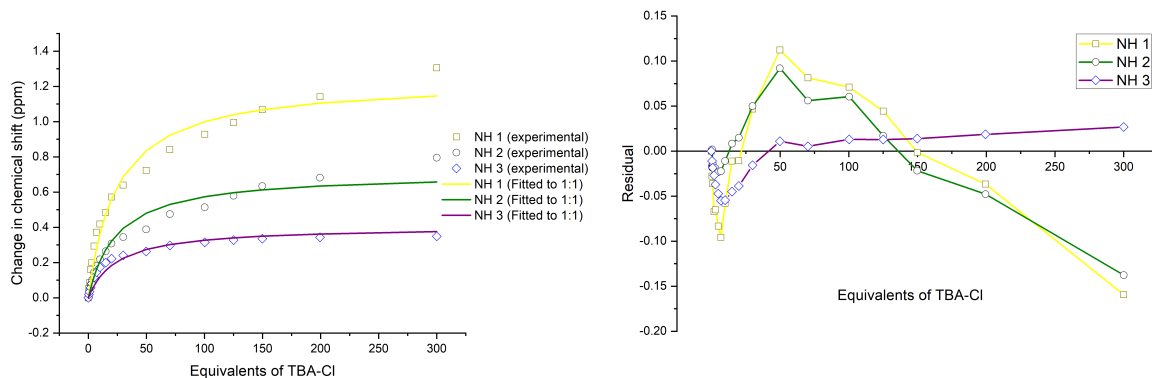
Figure S86. Fitted binding isotherm of 1,9-bis(3,5-bis-(trifluoromethyl)phenyl)thiourea-9(10H)-acridinone + TBACl showing the change in chemical shift of the NH protons fitted to the 1:1 binding model (left). K_a = 45.66 M^{-1}. Residual plot showing the random error obtained from the binding isotherm fitting (right). Covariance of fit (cov_{fit}) = 2.55×10^{-2}. Link to Bindfit fitting: http://app.supramolecular.org/bindfit/view/b2f52bdc-58e4-420a-912d-b5a6ecd978f0.
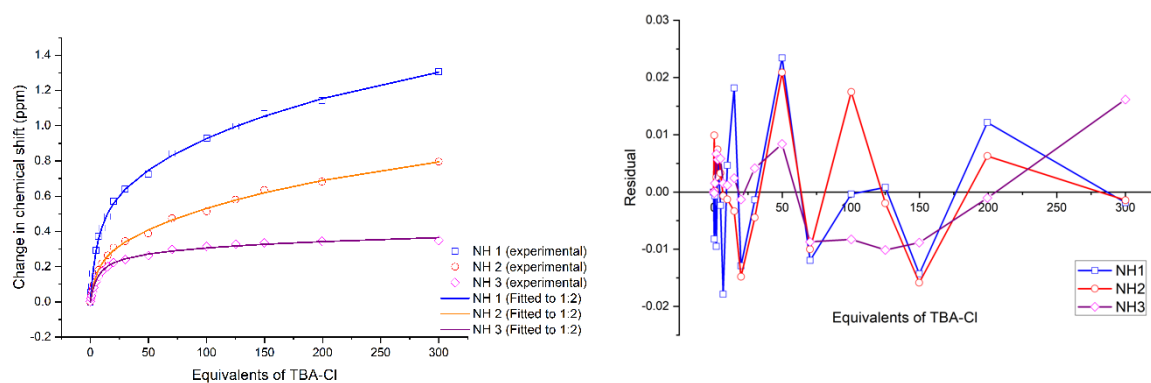
Figure S87. Fitted binding isotherm of 1,9-bis(3,5-bis-(trifluoromethyl)phenyl)thiourea-9(10H)-acridinone + TBACl showing the change in chemical shift of the NH protons fitted to the 1:2 binding model (left) K_{11} = 183.71 M^{-1}, K_{12} = 3.27 M^{-1}. Residual plot showing the random error obtained from the binding isotherm fitting (right). Covariance of fit (cov_{fit}) = 8.21×$^{-4}$. Link to Bindfit fitting: http://app.supramolecular.org/bindfit/view/99848803-c453-4c91-a18a-13252318ba88.
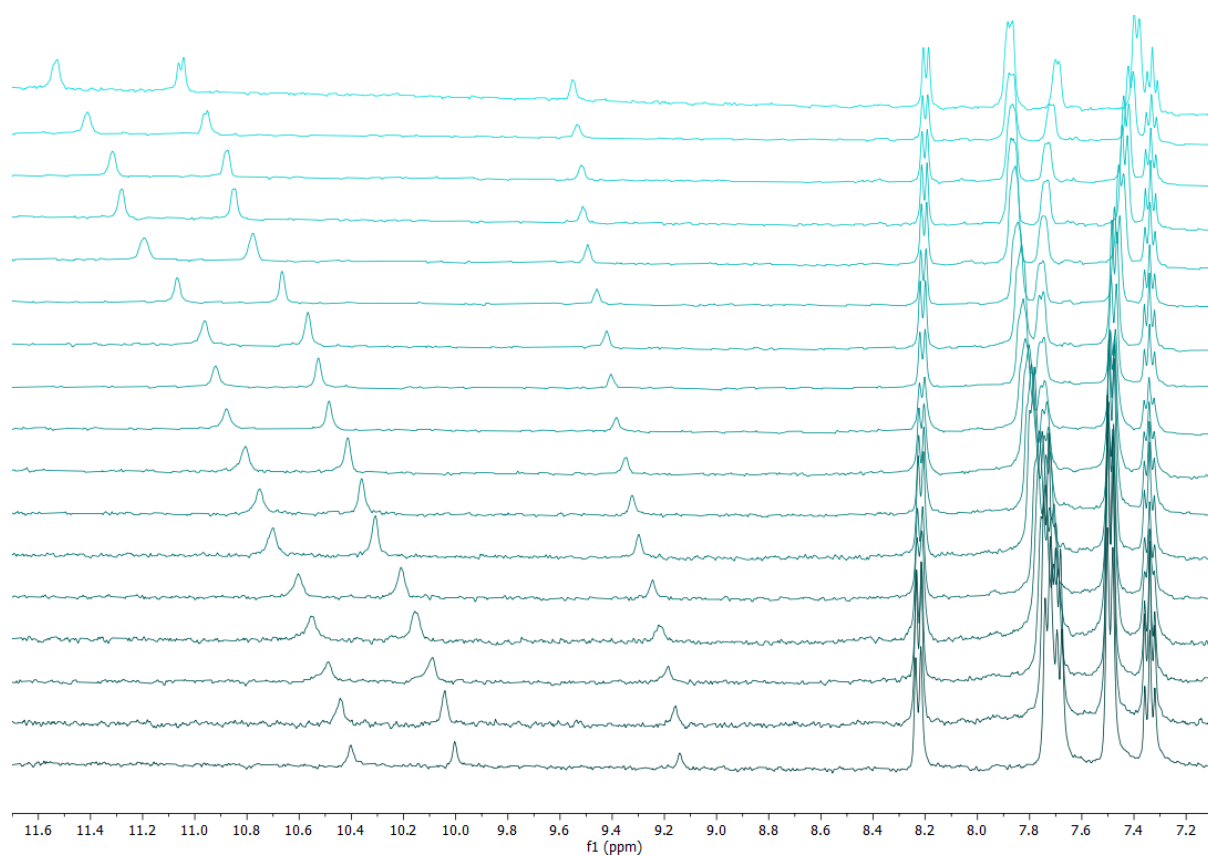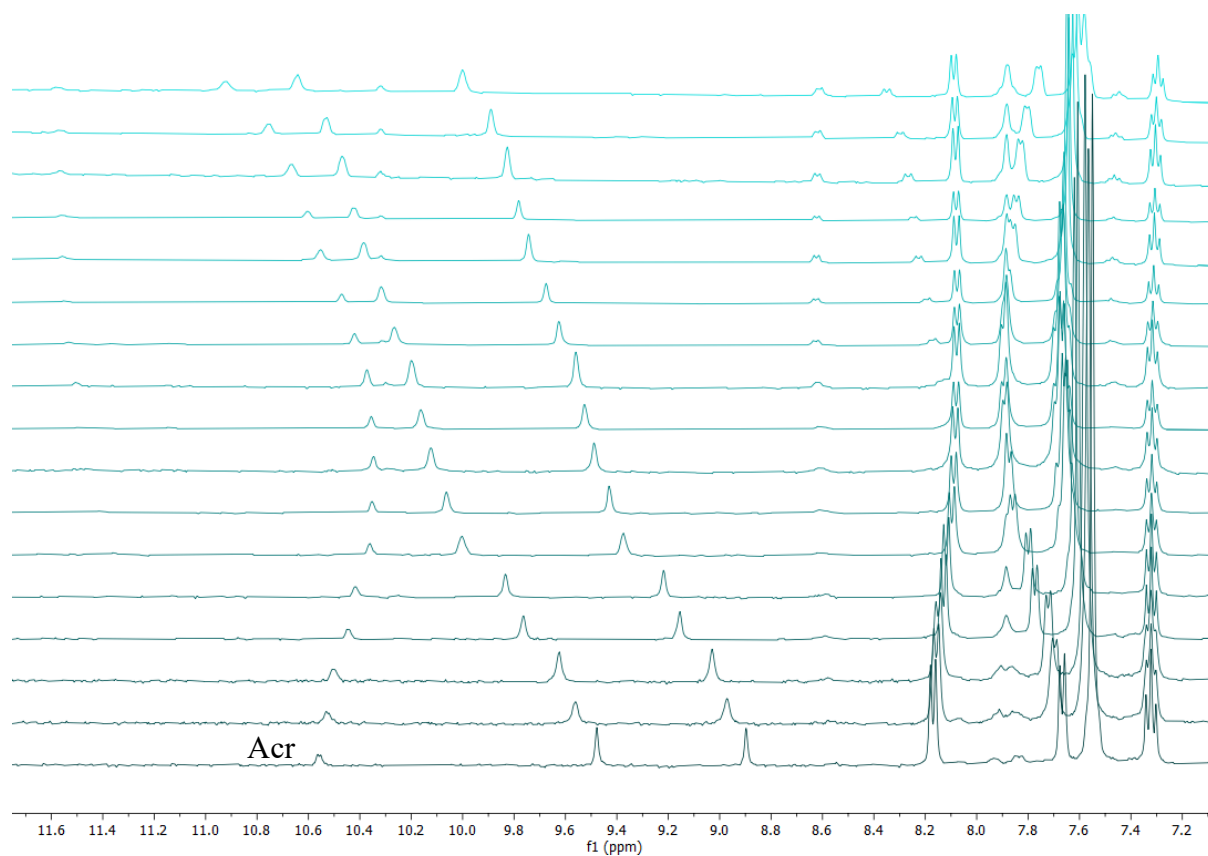
Figure S88. ^{1}H NMR titration spectra as a stack plot for 1,9-bis(4-(pentafluorosulfanyl)phenyl)urea-9(10H)-acridinone (1 mM) + TBACl in DMSO-d_6 /0.5% D$_2$O at 298 K.
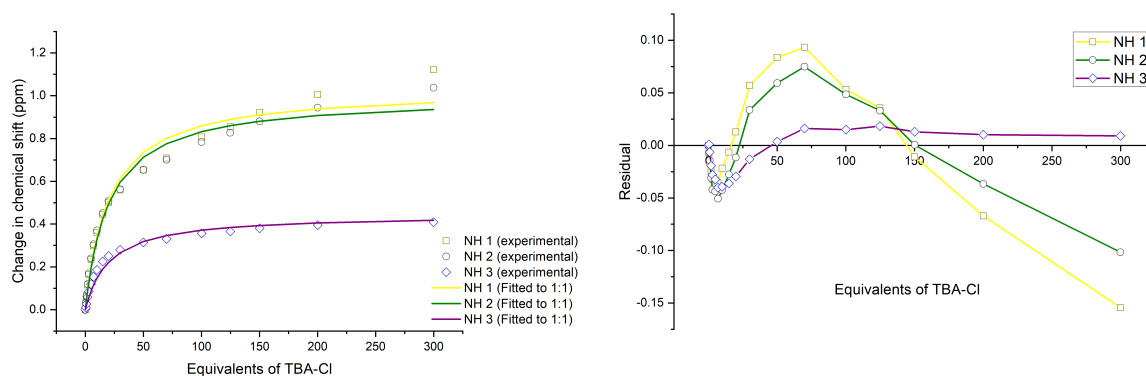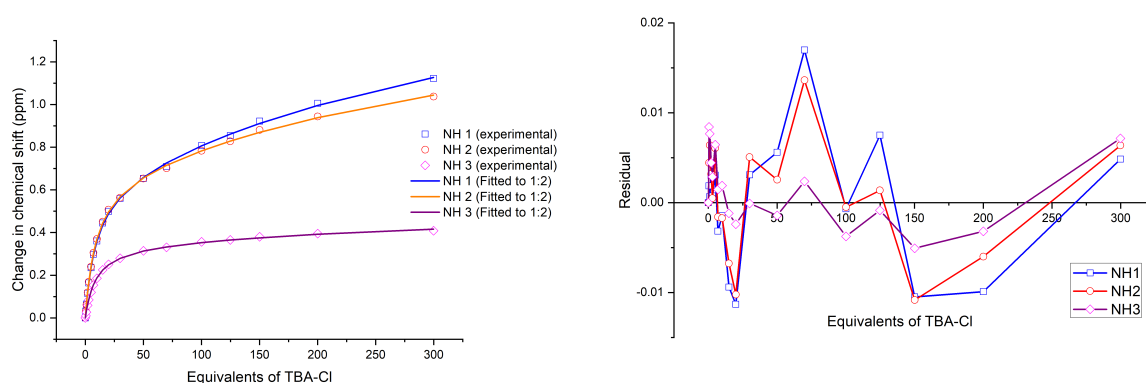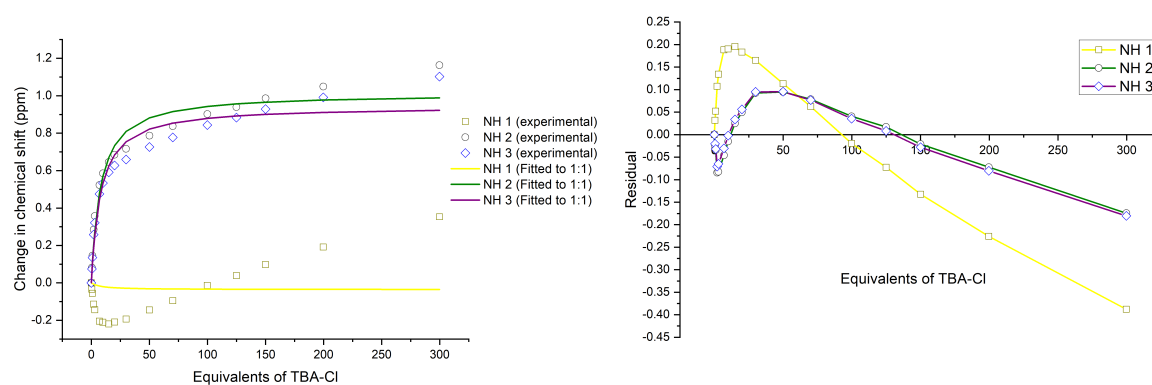

Figure S89. Fitted binding isotherm of 1,9-bis(4-(pentafluorosulfanyl)phenyl)urea-9(10H)-acridinone + TBACl showing the change in chemical shift of the NH protons fitted to the 1:1 binding model (left). K_a = 122.09 M^{-1}. Residual plot showing the random error obtained from the binding isotherm fitting (right). Covariance of fit (cov$_{fit}$) = 6.64×10^{-2}. Link to Bindfit fitting: http://app.supramolecular.org/bindfit/view/a72643d4-89a8-4b88-8b70-8ed84fbcc465.
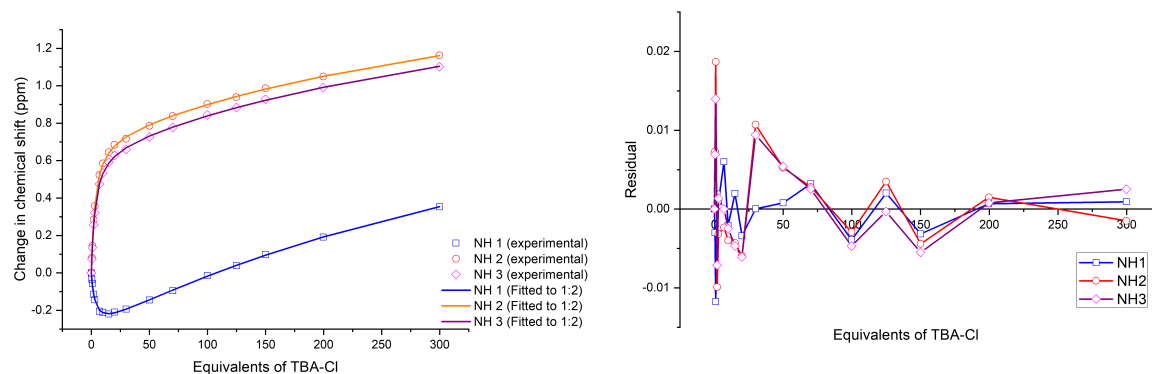
Figure S90. Fitted binding isotherm of 1,9-bis(4-(pentafluorosulfanyl)phenyl)urea-9(10H)-acridinone + TBACl showing the change in chemical shift of the NH protons fitted to the 1:2 binding model (left) K_{11} = 328.30 M^{-1}, K_{12} = 1.67 M^{-1}. Residual plot showing the random error obtained from the binding isotherm fitting (right). Covariance of fit (cov$_{fit}$) = 1.72×10^{-4}. Link to Bindfit fitting: http://app.supramolecular.org/bindfit/view/a39c1fbe-2b3e-46df-b194-ac952f49aeb7.
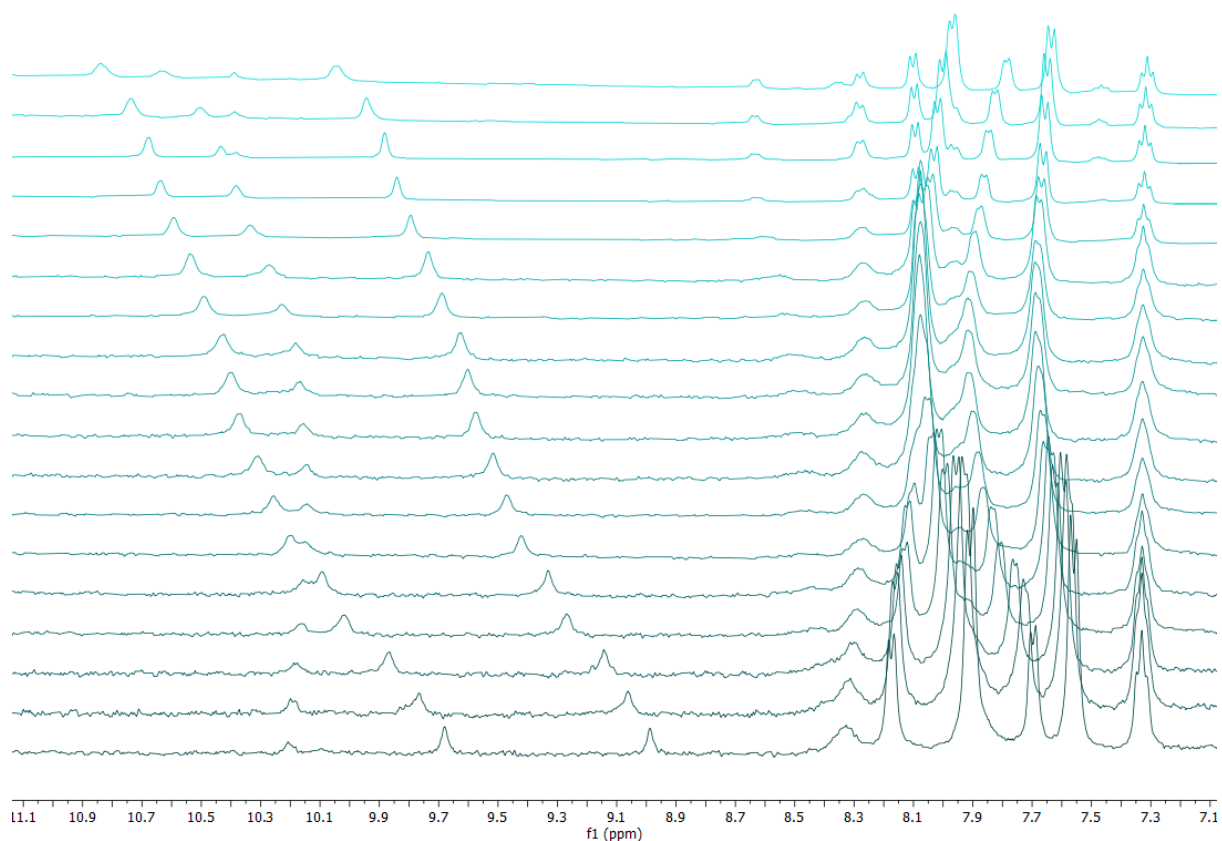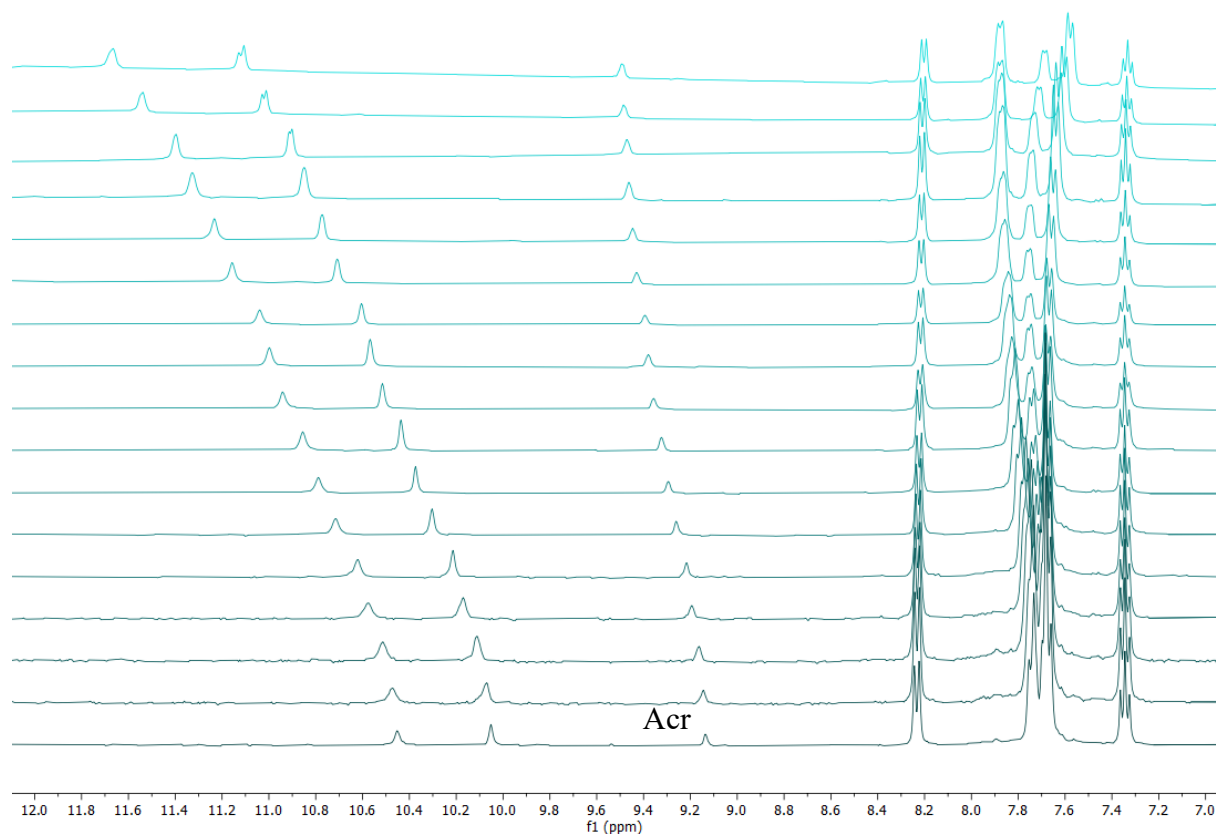

Figure S91. ^{1}H NMR titration spectra as a stack plot for 1,9-bis(4-(pentafluorosulfanyl)phenyl)thiourea-9(10H)-acridinone (1 mM) + TBACl in DMSO-d_6 /0.5% D$_2$O at 298 K.
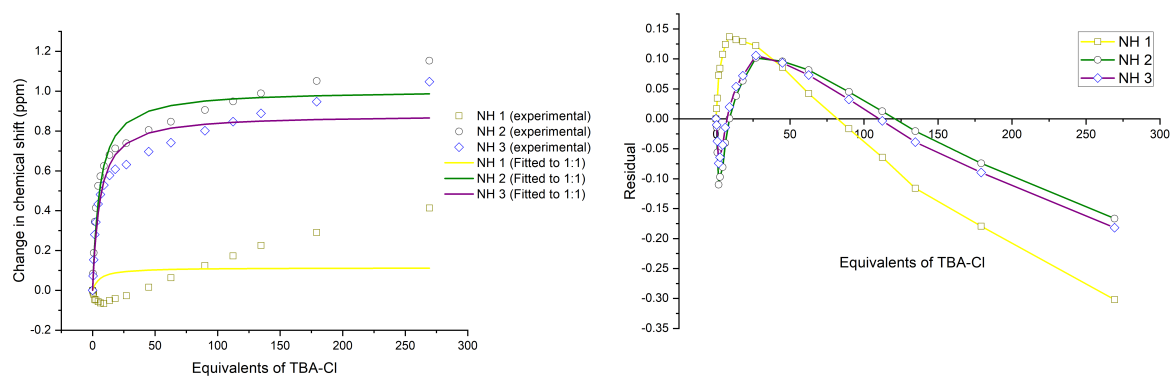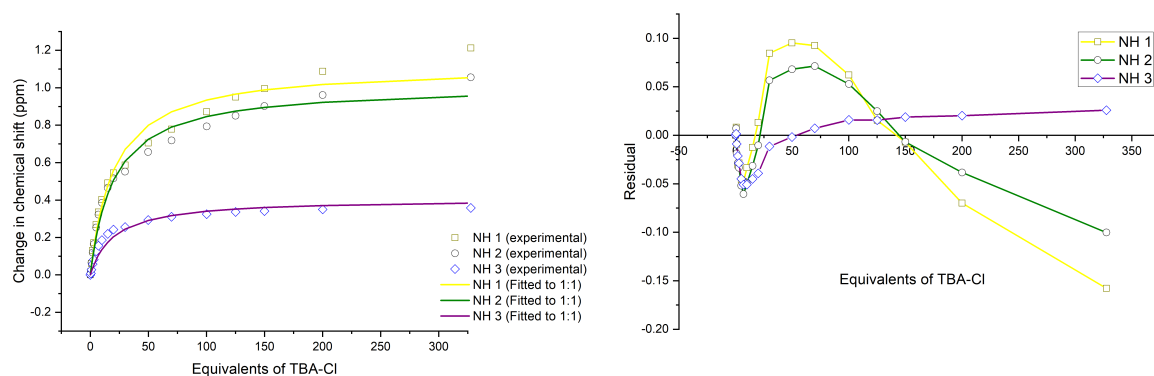
Figure S92. Fitted binding isotherm of 1,9-bis(4-(pentafluorosulfanyl)phenyl)thiourea-9(10H)-acridinone + TBACl showing the change in chemical shift of the NH protons fitted to the 1:1 binding model (left). K_a = 48.01 M^{-1}. Residual plot showing the random error obtained from the binding isotherm fitting (right). Covariance of fit (cov$_{fit}$) = 1.96×10^{-2}. Link to Bindfit fitting: http://app.supramolecular.org/bindfit/view/a72643d4-89a8-4b88-8b70-8ed84fbcc465.
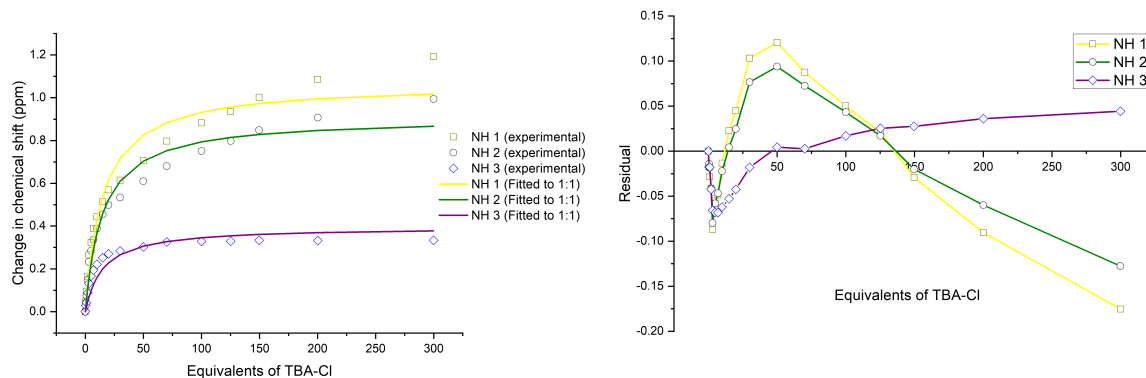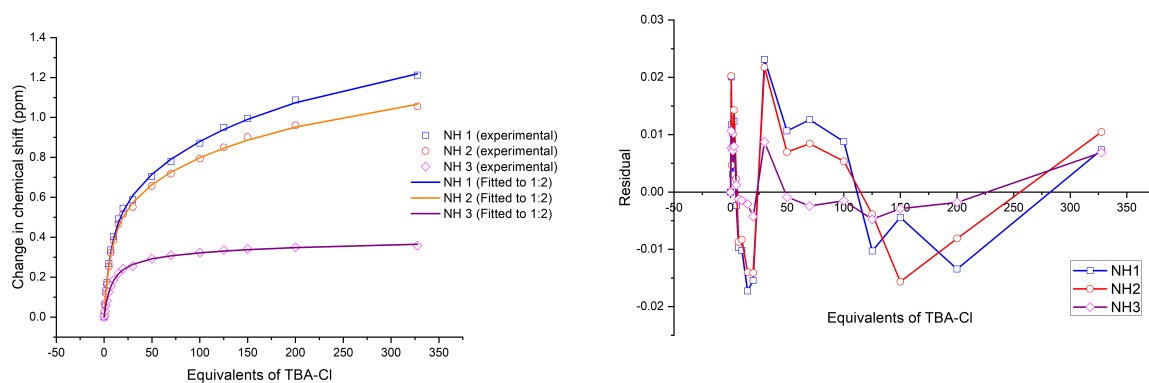

Figure S93. Fitted binding isotherm of 1,9-bis(4-(pentafluorosulfanyl)phenyl)thiourea-9(10H)-acridinone + TBACl showing the change in chemical shift of the NH protons fitted to the 1:2 binding model (left) K_{11} = 136.07 M^{-1}, K_{12} = 3.37 M^{-1}. Residual plot showing the random error obtained from the binding isotherm fitting (right). Covariance of fit (cov$_{fit}$) = 8.99×10^{-4}. Link to Bindfit fitting: http://app.supramolecular.org/bindfit/view/c5786123-3d87-4c52-8843-9b91a530b0e3.

Vesicle Studies

General Vesicle Preparation

Unilamellar vesicles were prepared following a procedure outlined previously by the Gale group.[6] A chloroform solution of POPC (37.5 mM, 4 mL) was transferred to a pre-weighed round-bottom flask, and the solvent was removed using a rotary evaporator. The pressure was lowered slowly to ensure the formation of a smooth lipid film. Subsequently, the film was dried *in vacuo* for 4−24 h, and the mass of lipid was recorded. The lipids were rehydrated with 4 mL of the respective internal solution (this number should correspond to the volume of POPC solution used initially) and vortexed until all lipids were removed from the sides of the flask and were suspended in solution. The lipids were subjected to 9 cycles of freeze-thaw by freezing using a dry ice/acetone bath and thawing in lukewarm water. Following this, the vesicles were left to rest at room temperature for 30 min. The lipids were extruded through a 200 nm polycarbonate membrane 25 times to form monodisperse vesicles. Only 1 mL of solution was extruded at a time before being collected. Finally, any residual unencapsulated salt from the internal solution was either removed via dialysis for 12 h in the desired external solution or through size-exclusion using a B19 column packed with hydrated G-25 Sephadex®, which had been pre-saturated with the respective external solution. The lipid suspensions were diluted with the external solution to afford a stock solution (10 mL) of a known concentration.

Electrode Calibration and Conversion of Raw Data

An Accumet chloride ion-selective electrode (ISE) was used for both the Cl^-/NO_3^- exchange assay and the cationophore coupled assay. Before the beginning of each set of experiments, calibration of the electrode was required to correct any drift between recorded datasets. The electrode was submerged in a sequence of NaCl solutions of increasing concentration (M), and the reading from the electrode was recorded after stabilising after 5−15 mins. The electrode potential reading, y, was plotted against NaCl concentration (M), x, and fitted to a simplified Nernst equation using *OriginPro 9.1*. The equation is given as followed:

$$y = (P_1 log_{10} x) + P_2$$

Equation 1. Calibration of electrode potential data using a simplified Nernst equation.

where P_1 and P_2 are the calibration parameters. The chloride ion concentration at any given time during the experiments can be calculated by substituting P_1, P_2 and y, the electrode

potential reading, into the equation and solving for x, the chloride ion concentration. By subtracting the chloride concentration at $t = 0$ from the concentration at a given time during the experiment, the total chloride concentration released from the vesicles at that given time can be calculated. Conversion to percentage chloride efflux was achieved by normalising the chloride concentration at time (t) using the 100% chloride efflux value recorded at the end of the experiment ($t = 420$ s) when the vesicles were lysed with a water dispersion of Triton X-100 (10% v/v).

Chloride/Nitrate Exchange ISE Assay

Dose-Response Hill Analysis

Vesicles were prepared using an internal solution of NaCl (487 mM) and buffered to pH 7.2 using a sodium phosphate salt buffer of NaH_2PO_4 (1.2 mM) and Na_2HPO4 (4mM). An external solution containing $NaNO_3$ (487 mM) was prepared separately with the same sodium phosphate salt buffer and adjusted to pH 7.2 using an aqueous solution of dilute NaOH. Following the freeze-thaw cycles and extrusion, the NaCl lipids were dialysed in the $NaNO_3$ external solution (~ 1600 mL) for 12h. The lipid stock solution (10 mL) was diluted with the external solution to give both a concentration and volume suitable for ISE experiments (1 mM, 5 mL).

Each receptor was added as a DMSO solution (10 µL) at $t = 0$ s, and the change in chloride concentration was recorded using an Accumet chloride ISE. At $t = 300$ s, a detergent solution (Triton X-100 (10% v/v in H_2O), 50 µL) was injected to lyse the vesicles, and a final chloride concentration reading was recorded at $t = 420$ s to provide a 100% chloride efflux reading for use in calibration.

Dose-response experiments were performed at six transporter concentrations and a blank DMSO run, and percentage efflux at $t = 270$ s was recorded for each concentration tested. The chloride efflux (%) at $t = 270$ s was plotted against receptor concentration (mol%, with respect to lipid concentration). The recorded data was fit to the Hill Equation, using *Origin 2021b (Academic)*, given as:

$$y = V_{max} \frac{x^n}{k^n + x^n}$$

Equation 2. The Hill equation.

where y represents the percentage of chloride efflux at $t = 270$ s, x is the transporter concentration (mol%, with respect to lipids concentration), and V_{max}, k and n are the parameters to be fitted. V_{max} represents the maximum chloride efflux (typically fixed to 100%), n can be interpreted as the Hill coefficient. A derived equation was used to calculate the EC_{50} value, the transporter concentration required to facilitate 50% chloride efflux, given as:

$$EC_{50} = k\left(\frac{50}{y_1 - y_0 - 50}\right)^{\frac{1}{n}}$$

Equation 3. The adapted EC_{50} equation.

where k and n are the derived parameters from the Hill equation, y_0 is the percentage chloride efflux at $t = 0$ s, and y_1 is the percentage chloride efflux at $t = 300$ s.

Maximum Rate

The maximum rate of chloride efflux was calculated for receptor **3** at 0.01 mol% and receptors **4**, **8**, and **9** at 0.05 mol% by fitting the efflux plot at the given concentration to a non-linear exponential decay function, in *Origin 2021b (Academic)*, given as:

$$y = A_1 e^{\left(\frac{-x}{t_1}\right)} + A_2 e^{\left(\frac{-x}{t_2}\right)} + y_0$$

Equation 4. A non-linear exponential decay function was used to fit the efflux plots of compounds **3**, **4**, **8** and **9**.

where y represents the percentage of chloride efflux (%), x is the receptor concentration (mol%), y_0 is the percentage chloride efflux at $t = 0$ s, and A_1, A_2, t_1, and t_2 are the derived parameters. The maximum rate was obtained by calculating the first derivative at $x = 0$, which is given as:

$$K_{initial} = \frac{-A_1}{t_1} - \frac{A_2}{t_2}$$

Equation 5. Derivative of the decay function used to determine the maximum rate given in %s^{-1}.

The maximum rate of chloride efflux was calculated for receptors **5** and **10** at 0.05 mol% by fitting the efflux plot at the given concentration to a non-linear Boltzmann curve function, in *Origin 2021b (Academic)*, given as:

$$y = A_2 + \frac{(A_1 - A_2)}{(1 + e^{(\frac{x - x_0}{dx})})}$$

Equation 6. The Boltzmann function was used for the fitting of the efflux plots for compounds **5** and **10**.

where y represents the percentage of chloride efflux (%), x is the receptor concentration (mol%), and A_1, A_2, x_0, and dx are the derived parameters. The maximum rate was obtained by calculating the first derivative at $x = 0$, which is given as:

$$K_{max} = \frac{A_2 - A_1}{4dx}$$

Equation 7. Derivative of the Boltzmann function used to determine the maximum rate given in $\%s^{-1}$.
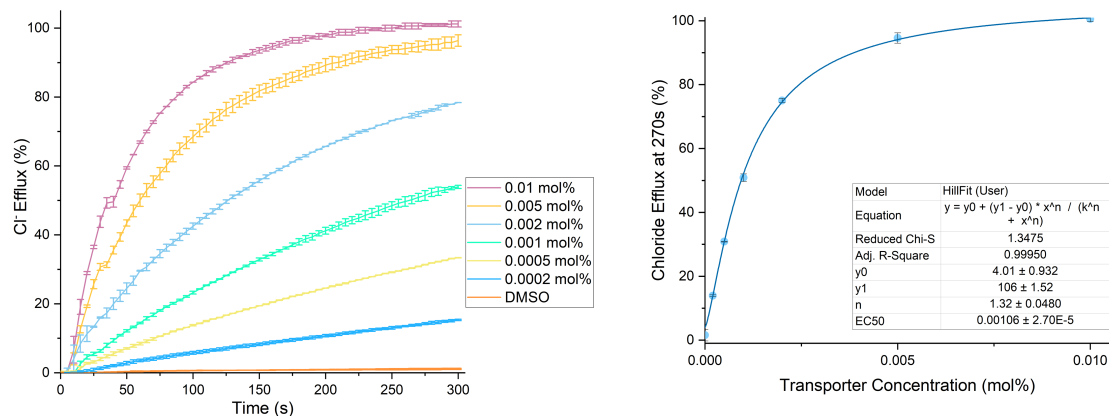
Figure S94. Hill analysis of Cl$^-$/NO$_3^-$ exchange facilitated by 1,9-bis(4-nitrophenyl)urea-9(10H)-acridinone. Each data point is the average of two repeats with error bars to show standard deviation. A run of pure DMSO was used as a control.
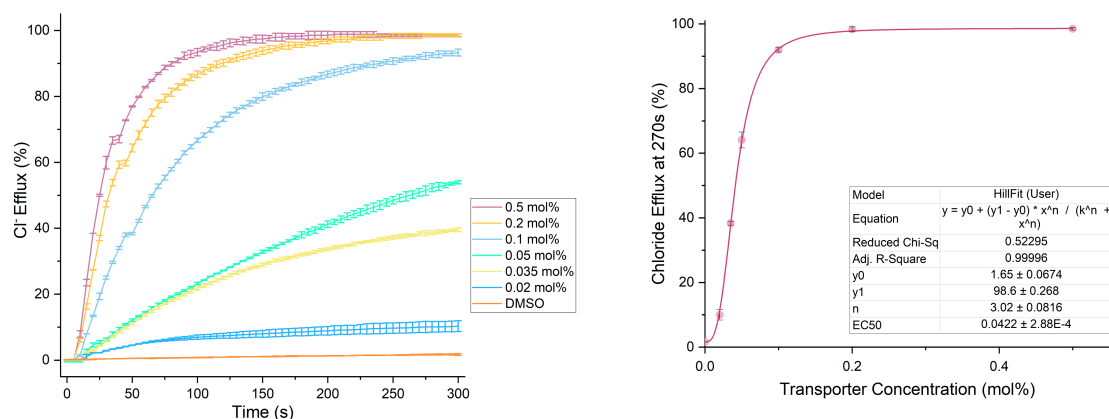
Figure S95. Hill analysis of Cl$^-$/NO$_3^-$ exchange facilitated by 1,9-bis(4-nitrophenyl)thiourea-9(10H)-acridinone. Each data point is the average of two repeats with error bars to show standard deviation. A run of pure DMSO was used as a control.
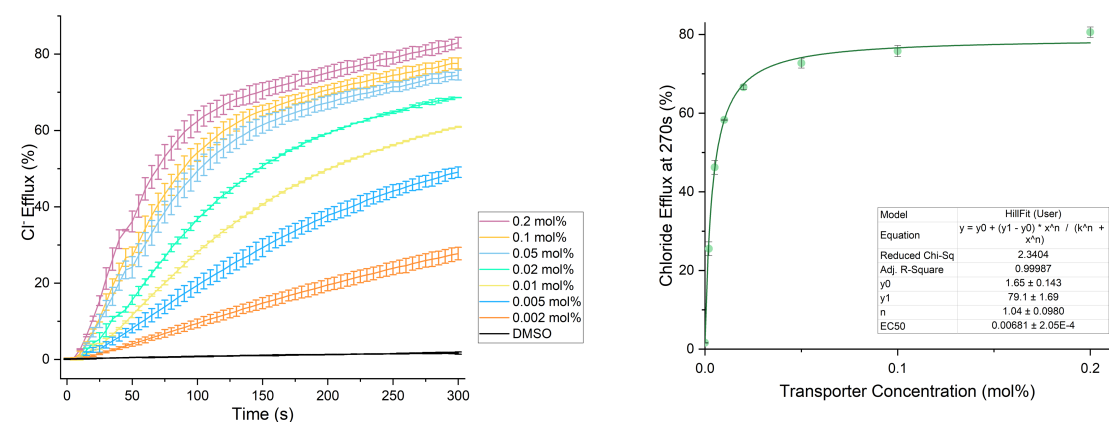
Figure S96. Hill analysis of Cl$^-$/NO$_3^-$ exchange facilitated by 1,9-bis(3,5-bis-(trifluoromethyl)phenyl)urea-9(10H)-acridinone. Each data point is the average of two repeats with error bars to show standard deviation. A run of pure DMSO was used as a control.
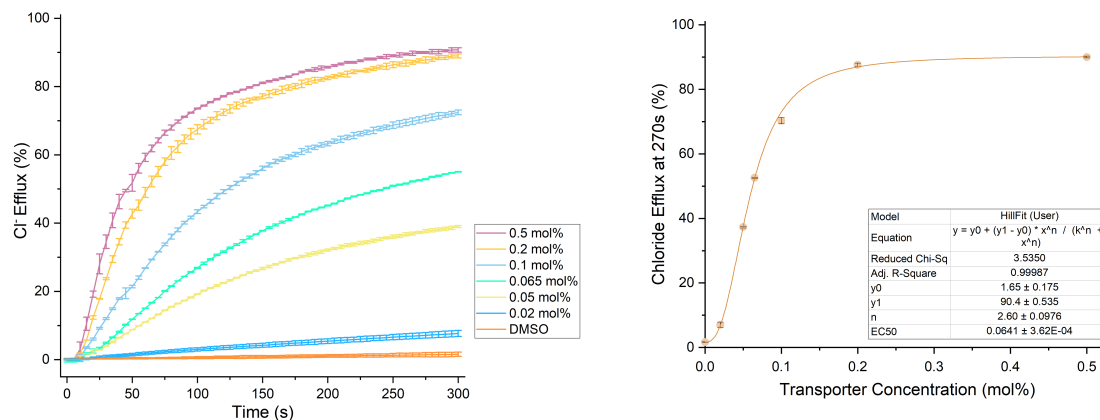
Figure S97. Hill analysis of Cl$^-$/NO$_3^-$ exchange facilitated by 1,9-bis(3,5-bis-(trifluoromethyl)phenyl)thiourea-9(10H)-acridinone. Each data point is the average of two repeats with error bars to show standard deviation. A run of pure DMSO was used as a control.
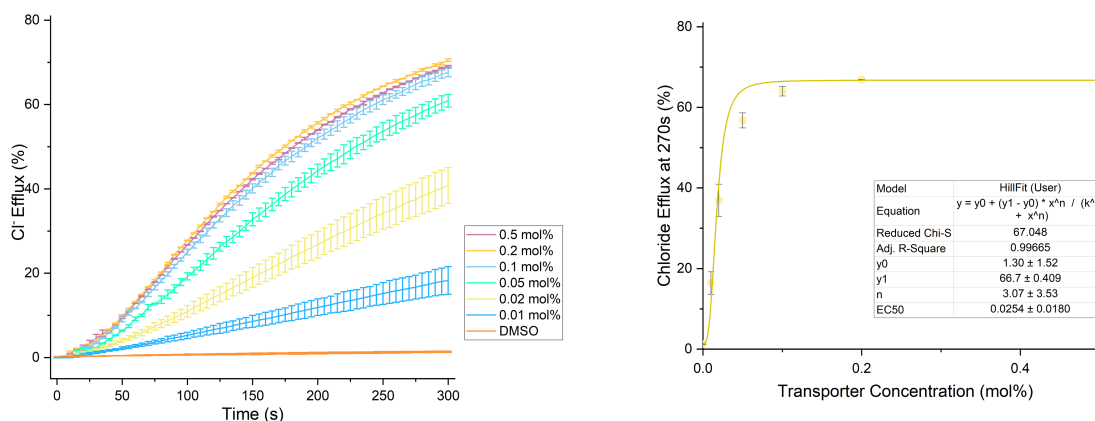
Figure S98. Hill analysis of Cl$^-$/NO$_3^-$ exchange facilitated by 1,9-bis(4-(pentafluorosulfanyl)phenyl)urea-9(10H)-acridinone. Each data point is the average of two repeats with error bars to show standard deviation. A run of pure DMSO was used as a control.
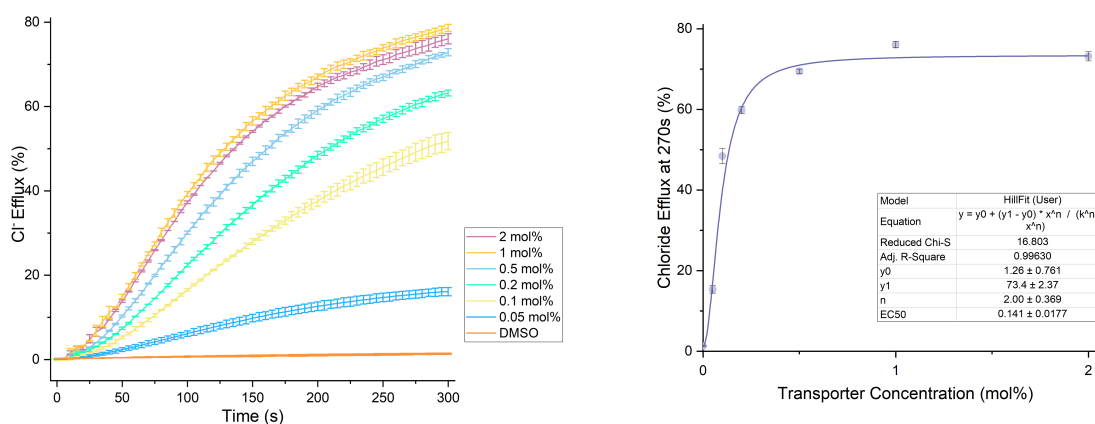
Figure S99. Hill analysis of Cl$^-$/NO$_3^-$ exchange facilitated by 1,9-bis(4-(pentafluorosulfanyl)phenyl)thiourea-9(10H)-acridinone. Each data point is the average of two repeats with error bars to show standard deviation. A run of pure DMSO was used as a control.

S77

ISE Cationophore Coupled Assay

Vesicles were prepared following the procedure described above (A2.3. Vesicle Studies, General Vesicle Preparation) with an internal solution of KCl (300 mM), with a sodium phosphate salt buffer consisting of NaH_2PO_4 (1.2 mM) and Na_2HPO4 (4mM), and adjusted to pH 7.2. Two external solutions were prepared and buffered to pH 7.2 with sodium phosphate salts (5 mM); one containing KNO_3 (333 mM) and the other a solution of KGlu (300 mM). Following extrusion, the vesicles were passed through a G-25 Sephadex® size-exclusion column which had been pre-rinsed with the KGlu external solution. The same solution was used as the eluent, and once the vesicles were collected, the volume was diluted to 10 mL using the KGlu external solution.

Each experiment was prepared by adding 0.5 mL of the vesicle solution to 4. 5 mL of either KNO_3 or KGlu solution. The transporter was added as a DMSO solution (10 µL) to initiate transport at $t = 0$ s. The transporter concentration was chosen to match the EC_{50} value determined in the Cl^-/NO_3^- exchange ISE assay. Efflux data was collected until $t = 300$ s using an Accumet chloride ISE before detergent (Triton X-100 (10% v/v in H_2O), 50 µL) was added to lyse the vesicles and release any remaining internal chloride solution. A final reading of the 100% chloride efflux value was recorded at $t = 420$ s for calibration purposes.

Cationophore coupled experiments were conducted by preparing an experimental solution of vesicle solution (0.5 mL) suspended in the KGluc external solution (4.5 mL). A DMSO solution of either valinomycin or monensin (10 µL) was added at $t = -30$ s to give a cationophore concentration of 0.1 mol% with respect to lipid concentration. The transporter was added as a DMSO solution (10 µL) at $t = 0$ s to initiate the experiments, and efflux was recorded as described in the paragraph above. Each experiment was completed in duplicate for the purposes of accuracy and data redundancy.
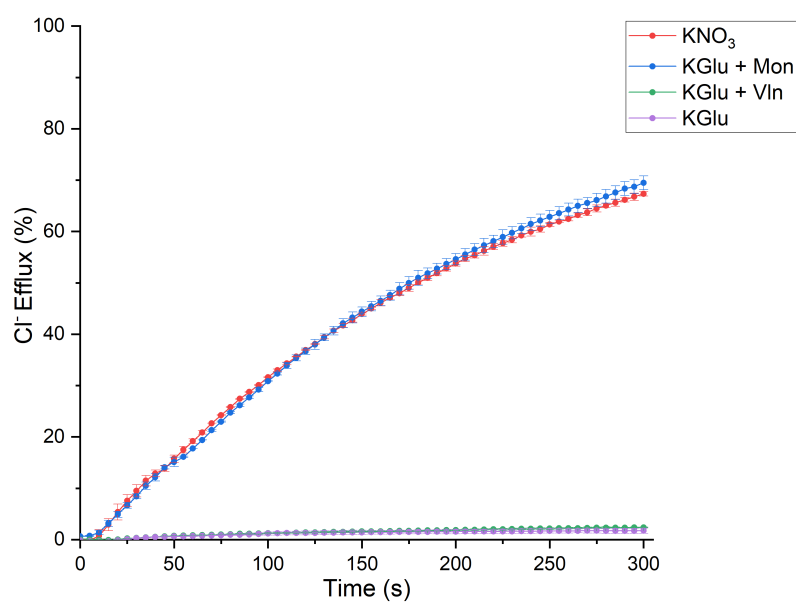
Figure S100. Chloride efflux facilitated by 1,9-bis(4-nitrophenyl)urea-9(10H)-acridinone (0.002 mol%) in POPC vesicles loaded with 300 mM KCl and suspended in an isotonic external solution containing KNO_3 (red), or containing KGlu in the presence of 0.1 mol% monensin (blue) and 0.1 mol% valinomycin (green). Each data point is the average of two repeats, with the error bars showing the standard deviation. Chloride efflux as a free transporter in an external KGlu solution is shown as the control (purple).
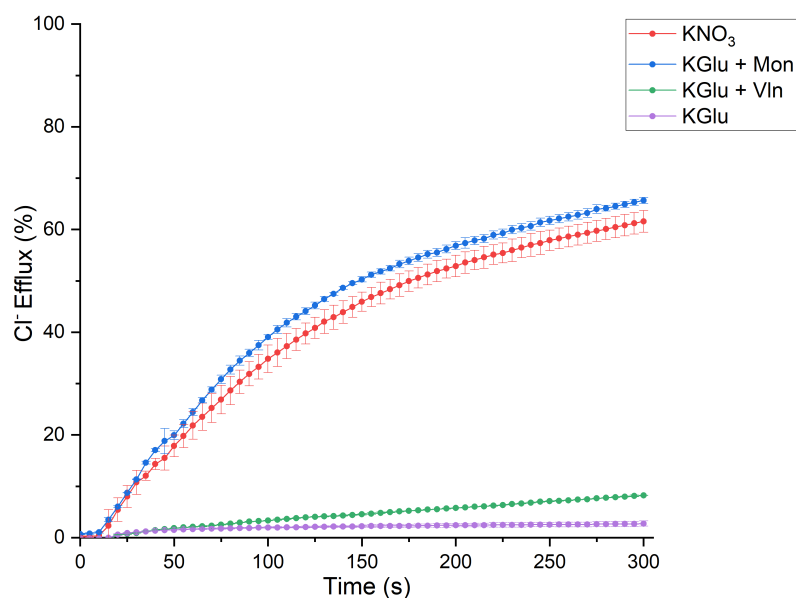
Figure S101. Chloride efflux facilitated by 1,9-bis(4-nitrophenyl)thiourea-9(10H)-acridinone (0.05 mol%) in POPC vesicles loaded with 300 mM KCl and suspended in an isotonic external solution containing KNO_3 (red), or containing KGlu in the presence of 0.1 mol% monensin (blue) and 0.1 mol% valinomycin (green). Each data point is the average of two repeats, with the error bars showing the standard deviation. Chloride efflux as a free transporter in an external KGlu solution is shown as the control (purple).
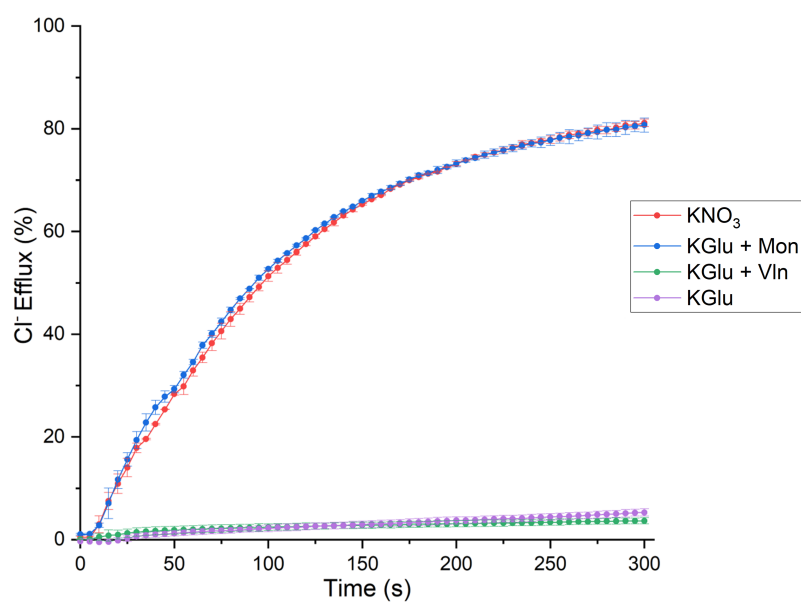
Figure S102. Chloride efflux facilitated by 1,9-bis(3,5-bis-(trifluoromethyl)phenyl)urea-9(10H)-acridinone (0.02 mol%) in POPC vesicles loaded with 300 mM KCl and suspended in an isotonic external solution containing KNO_3 (red), or containing KGlu in the presence of 0.1 mol% monensin (blue) and 0.1 mol% valinomycin (green). Each data point is the average of two repeats, with the error bars showing the standard deviation. Chloride efflux as a free transporter in an external KGlu solution is shown as the control (purple).
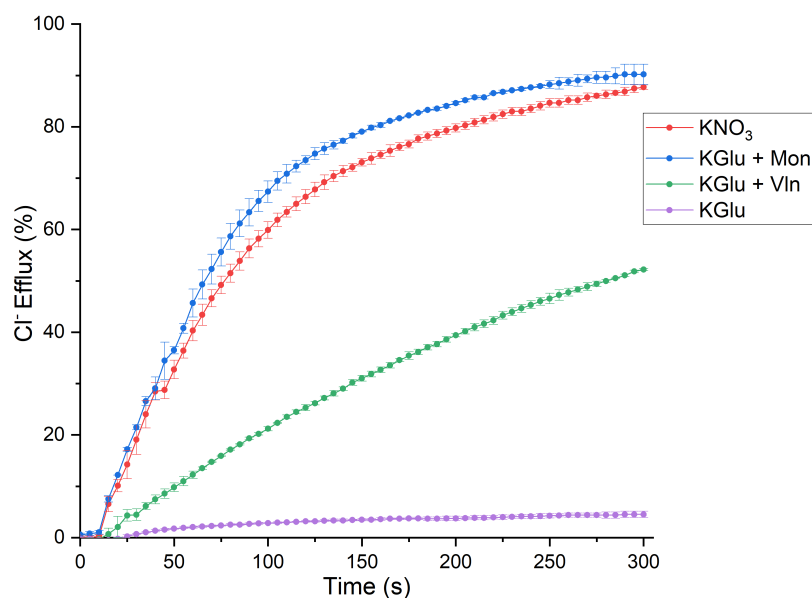
Figure S103. Chloride efflux facilitated by 1,9-bis(3,5-bis-(trifluoromethyl)phenyl)thiourea-9(10H)-acridinone (0.2 mol%) in POPC vesicles loaded with 300 mM KCl and suspended in an isotonic external solution containing KNO_3 (red), or containing KGlu in the presence of 0.1 mol% monensin (blue) and 0.1 mol% valinomycin (green). Each data point is the average of two repeats, with the error bars showing the standard deviation. Chloride efflux as a free transporter in an external KGlu solution is shown as the control (purple).
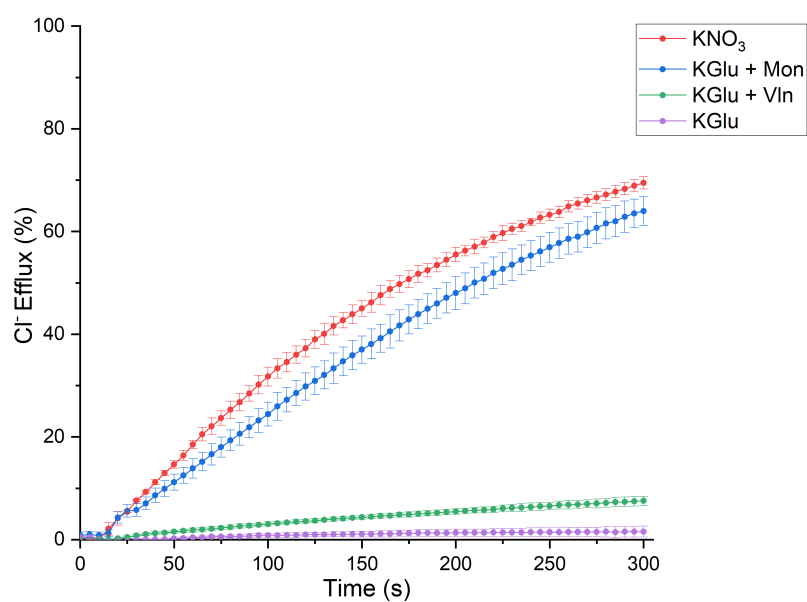
Figure S104. Chloride efflux facilitated by 1,9-bis(4-(pentafluorosulfanyl)phenyl)urea-9(10H)-acridinone (0.02 mol%) in POPC vesicles loaded with 300 mM KCl and suspended in an isotonic external solution containing KNO_3 (red), or containing KGlu in the presence of 0.1 mol% monensin (blue) and 0.1 mol% valinomycin (green). Each data point is the average of two repeats, with the error bars showing the standard deviation. Chloride efflux as a free transporter in an external KGlu solution is shown as the control (purple).
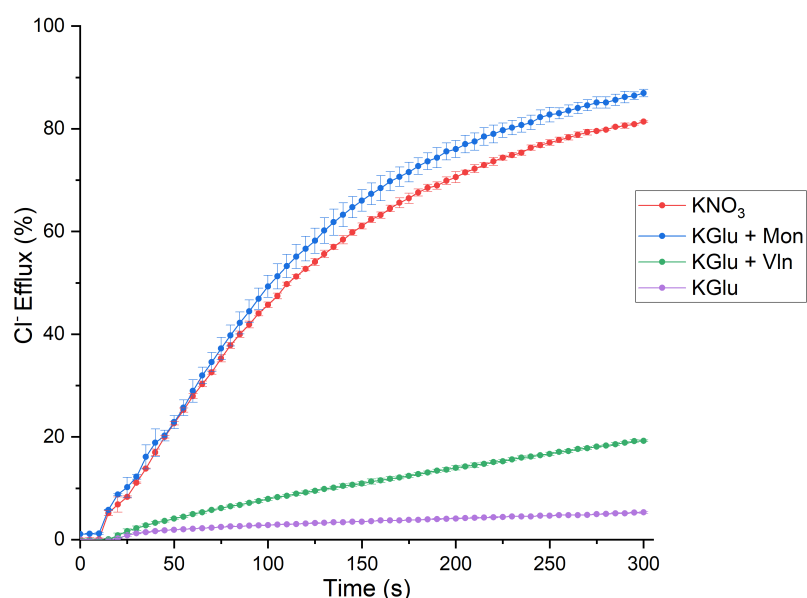
Figure S105. Chloride efflux facilitated by 1,9-bis(4-(pentafluorosulfanyl)phenyl)thiourea-9(10H)-acridinone (0.2 mol%) in POPC vesicles loaded with 300 mM KCl and suspended in an isotonic external solution containing KNO_3 (red), or containing KGlu in the presence of 0.1 mol% monensin (blue) and 0.1 mol% valinomycin (green). Each data point is the average of two repeats, with the error bars showing the standard deviation. Chloride efflux as a free transporter in an external KGlu solution is shown as the control (purple).

Figure S106. Chloride efflux facilitated by a blank DMSO run in POPC vesicles loaded with 300 mM KCl and suspended in an isotonic external solution containing KNO_3 (red) or containing KGlu in the presence of 0.1 mol% monensin (blue) and 0.1 mol% valinomycin (green). Each data point is the average of two repeats, with the error bars showing the standard deviation. Chloride efflux as a free transporter in an external KGlu solution is shown as the control (purple).
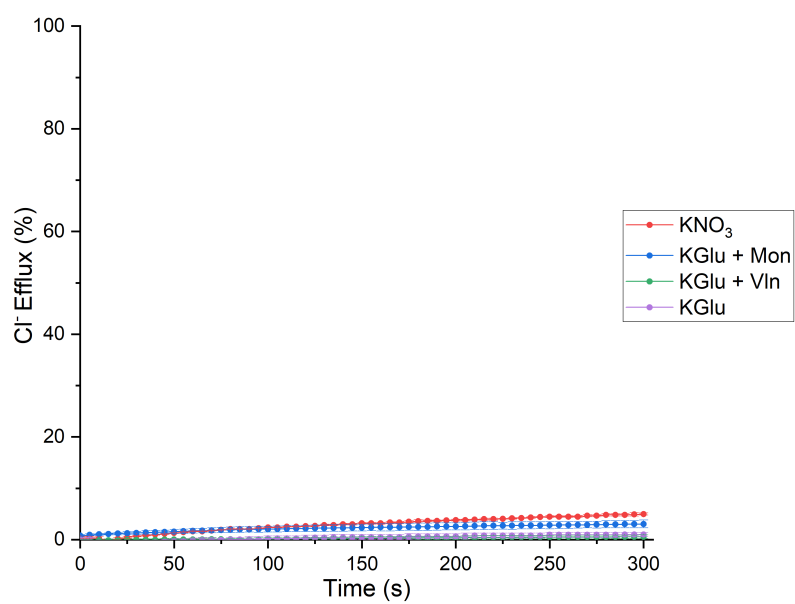
HPTS NMDG-Cl Assay

An external solution of NMDG-Cl (100 mM) was prepared with HEPES buffer (10mM) and adjusted to pH 7.0. An internal solution was prepared using the same external solution but with the addition of pH-sensitive fluorescent dye HPTS (1 mM). Vesicles were prepared following the procedure outlined above (A2.3. Vesicle Studies, General Vesicle Preparation). After extrusion, the vesicles were passed through a G-25 Sephadex® column that had been pre-rinsed with the external NMDG-Cl solution. The vesicles were collected and diluted with the external solution to a 10 mL volume with a known concentration.

For a given experiment, the prepared vesicles were diluted to a concentration of 0.1 mM in a 4.5 mL plastic cuvette. A pH gradient is required to drive transport through the vesicle membrane in these experiments before the transporter is added. An aliquot of aqueous NaOH solution (25 µL, 0.5 M) was added at approximately $t = -30$ s to increase the pH of the external solution by approx. one pH unit to pH 8.0. Transport was initiated with the addition of the transporter as a DMSO solution (5 µL) and ended with the addition of detergent (Triton X-100 (10% *v/v* in water), 25 µL) was added at $t = 210$ s to lyse the vesicles, and a final fluorescence intensity reading was recorded at $t = 300$ s to signify 100% proton efflux.

The changes in the fluorescent activity of intravesicular HPTS were used to detect pH changes during the experiments, and hence represent proton efflux. The acidic and basic forms of the HPTS probe were excited at $\lambda_{ex} = 403$ nm and $\lambda_{ex} = 460$ nm, respectively, and the fluorescence emission of both forms recorded at $\lambda_{em} = 510$ nm. The intensity ratio of basic form to acidic form was determined, and the fractional fluorescence intensity (I_F) was calculated using the equation:

$$I_F = \frac{R_t - R_0}{R_d - R_0}$$

Equation 8. Used for the conversion of raw HPTS data into fractional fluorescence intensity.

where R_t is the ratiometric fluorescence value at a given time (t), R_0 is the ratiometric fluorescence value at $t = 0$ s and R_d is the fluorescence ratiometric value recorded at $t = 360$ s following the addition of detergent.

Dose-response experiments were performed at six transporter concentrations plus a blank DMSO control run. The fractional fluorescence intensity (I_F) was plotted as a function of transporter concentration (mol%, with respect to lipid concentration). The I_F value at $t = 200$ s

for each tested transporter concentration was fit to an adapted Hill Equation, using *Origin 2021b (Academic)*, given as:

$$y = y_0 + (y_{max} - y_0)\frac{x^n}{k^n + x^n}$$

Equation 9. The modified Hill equation was employed in the NMDG-Cl assay.

where y_0 is the I_F value at $t = 200$ s for the DMSO blank run, y_{max} is the maximum I_F value, n is the Hill coefficient, and k is a derived parameter. EC$_{50}$ values were calculated by applying **Equation 3** used for the ISE dose-response studies.

Figure S107. Hill analysis of H$^+$/Cl$^-$ symport (or Cl$^-$/OH$^-$ antiport) facilitated by 1,9-bisphenylurea-9(10H)-acridinone in the NMDG-Cl assay. Each data point is the average of two repeats, with the error bars showing the standard deviation. A run of pure DMSO was used as a control.

Figure S108. Hill analysis of H$^+$/Cl$^-$ symport (or Cl$^-$/OH$^-$ antiport) facilitated by 1,9-bisphenylurea-9(10H)-acridinone in the NMDG-Cl assay. Each data point is the average of two repeats, with the error bars showing the standard deviation. A run of pure DMSO was used as a control.

Figure S109. Hill analysis of H^+/Cl^- symport (or Cl^-/OH^- antiport) facilitated by 1,9-bis(4-(trifluoromethyl)phenyl)urea-9(10H)-acridinone in the NMDG-Cl assay. Each data point is the average of two repeats, with the error bars showing the standard deviation. A run of pure DMSO was used as a control.
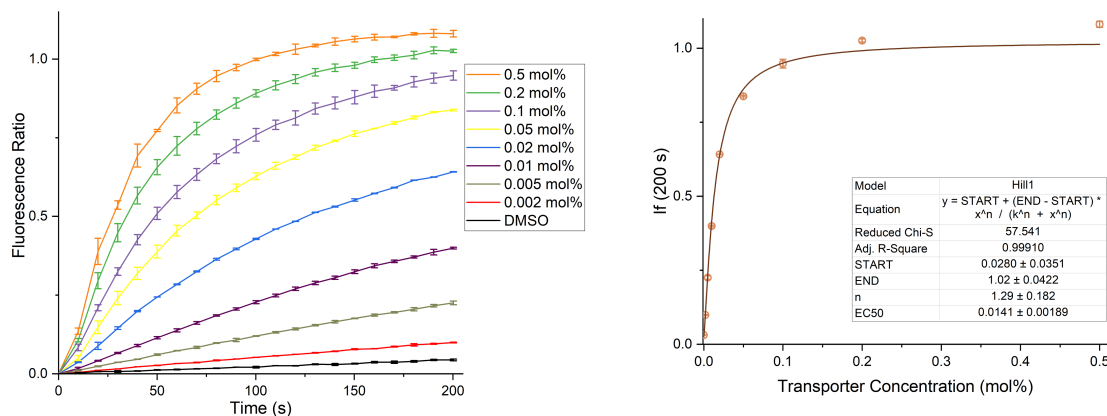
Figure S110. Hill analysis of H^+/Cl^- symport (or Cl^-/OH^- antiport) facilitated by 1,9-bis(4-(trifluoromethyl)phenyl)thiourea-9(10H)-acridinone in the NMDG-Cl assay. Each data point is the average of two repeats, with the error bars showing the standard deviation. A run of pure DMSO was used as a control.
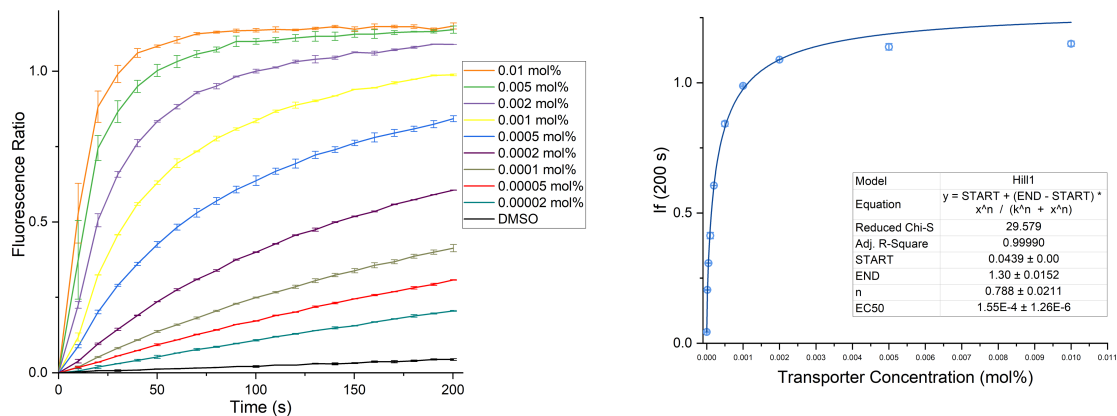
Figure S111. Hill analysis of H^+/Cl^- symport (or Cl^-/OH^- antiport) facilitated by 1,9-bis(4-nitrophenyl)urea-9(10H)-acridinone in the NMDG-Cl assay. Each data point is the average of two repeats, with the error bars showing the standard deviation. A run of pure DMSO was used as a control.
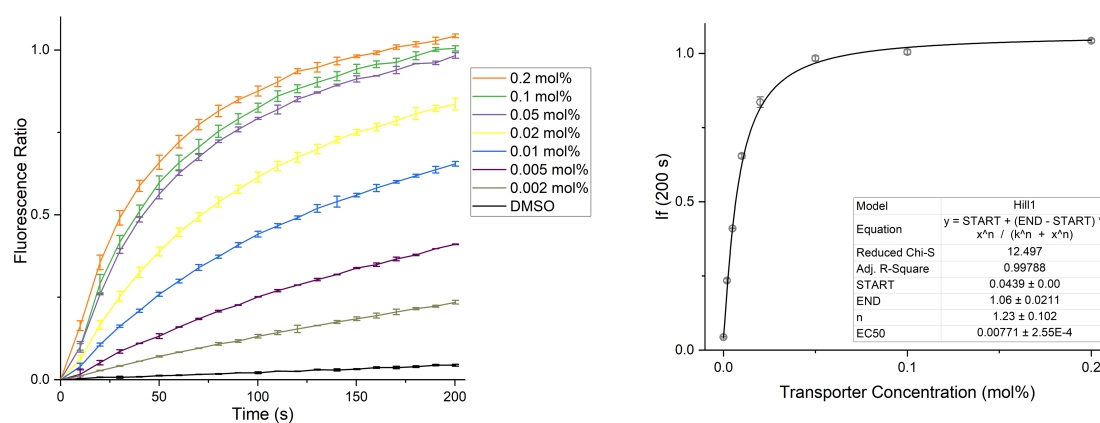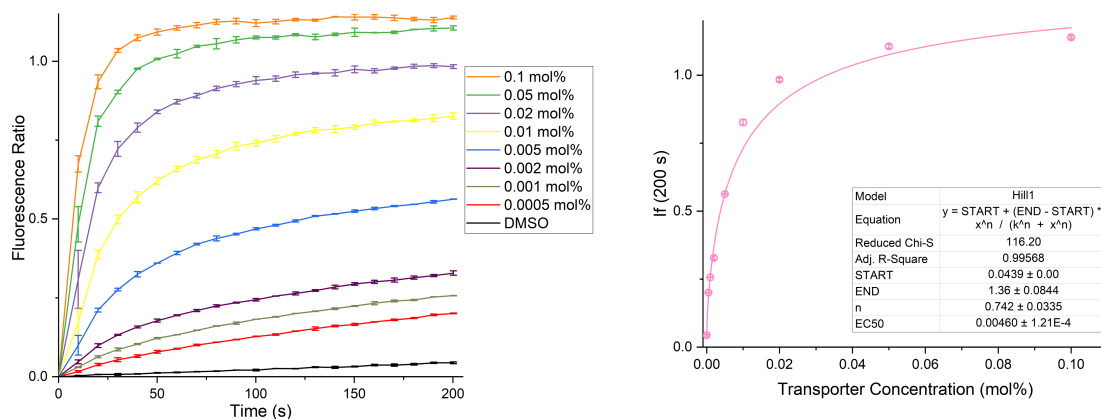

Figure S112. Hill analysis of H^+/Cl^- symport (or Cl^-/OH^- antiport) facilitated by 1,9-bis(4-nitrophenyl)thiourea-9(10H)-acridinone in the NMDG-Cl assay. Each data point is the average of two repeats, with the error bars showing the standard deviation. A run of pure DMSO was used as a control.
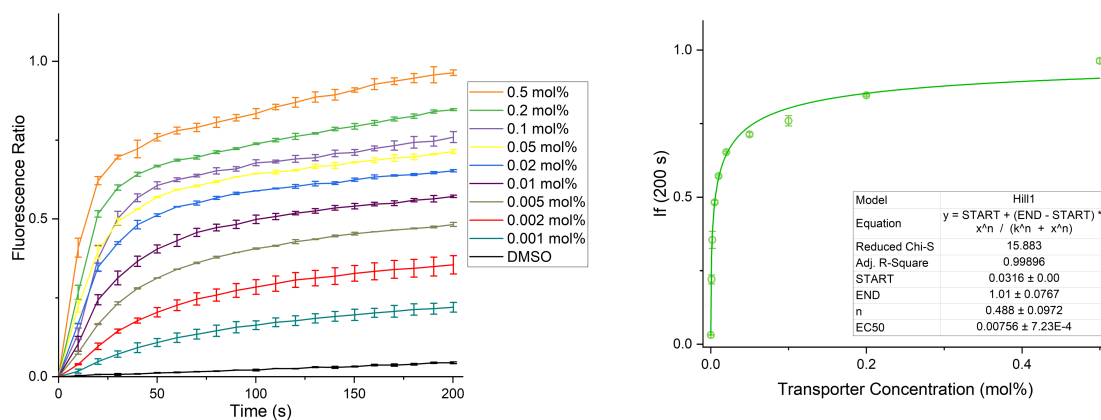
Figure S113. Hill analysis of H^+/Cl^- symport (or Cl^-/OH^- antiport) facilitated by 1,9-bis(3,5-bis-(trifluoromethyl)phenyl)urea-9(10H)-acridinone in the NMDG-Cl assay. Each data point is the average

of two repeats, with the error bars showing the standard deviation. A run of pure DMSO was used as a control.
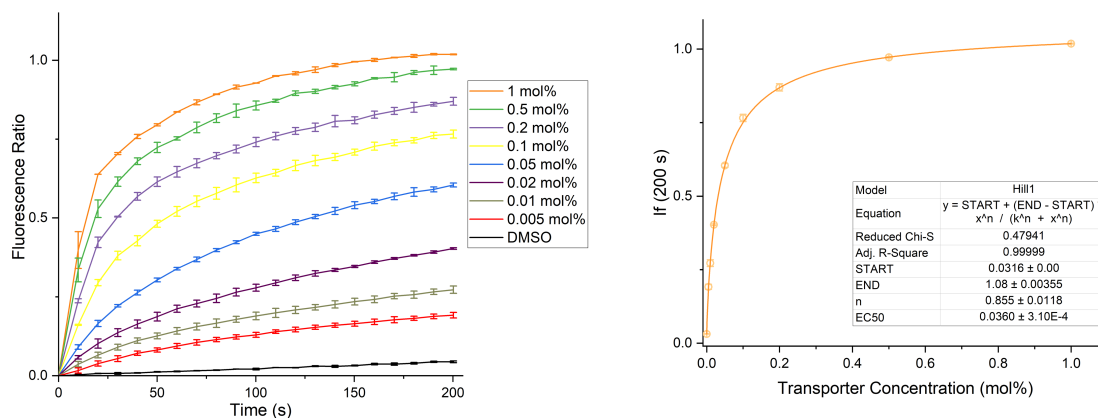
Figure S114. Hill analysis of H^+/Cl^- symport (or Cl^-/OH^- antiport) facilitated by 1,9-bis(3,5-bis-(trifluoromethyl)phenyl)thiourea-9(10H)-acridinone in the NMDG-Cl assay. Each data point is the average of two repeats, with the error bars showing the standard deviation. A run of pure DMSO was used as a control.
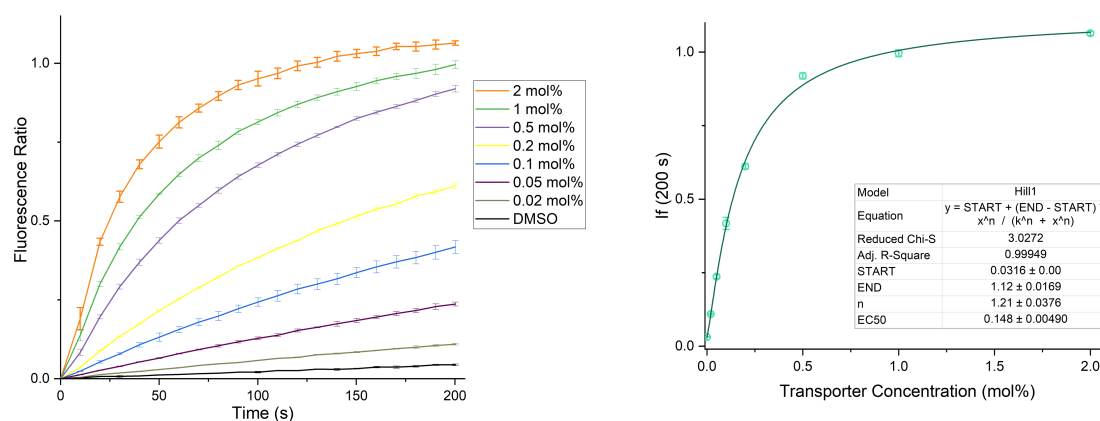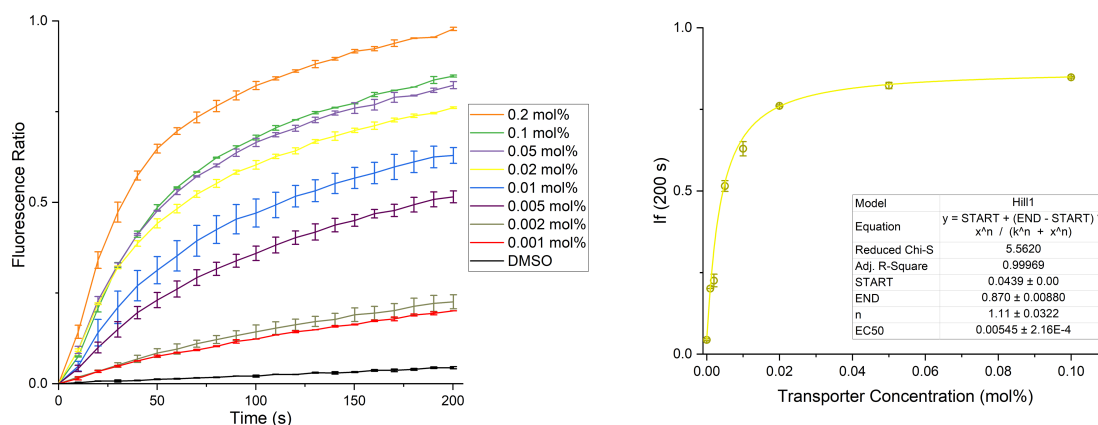

Figure S115. Hill analysis of H^+/Cl^- symport (or Cl^-/OH^- antiport) facilitated by 1,9-bis(4-(pentafluorosulfanyl)phenyl)urea-9(10H)-acridinone in the NMDG-Cl assay. Each data point is the average of two repeats, with the error bars showing the standard deviation. A run of pure DMSO was used as a control.
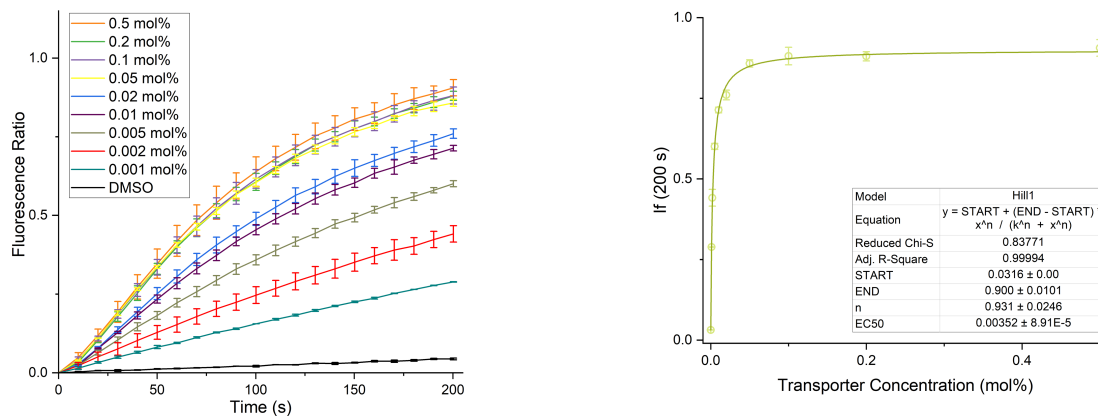
Figure S116. Hill analysis of H⁺/Cl⁻ symport (or Cl⁻/OH⁻ antiport) facilitated by 1,9-bis(4-(pentafluorosulfanyl)phenyl)thiourea-9(10H)-acridinone in the NMDG-Cl assay. Each data point is the average of two repeats, with the error bars showing the standard deviation. A run of pure DMSO was used as a control.
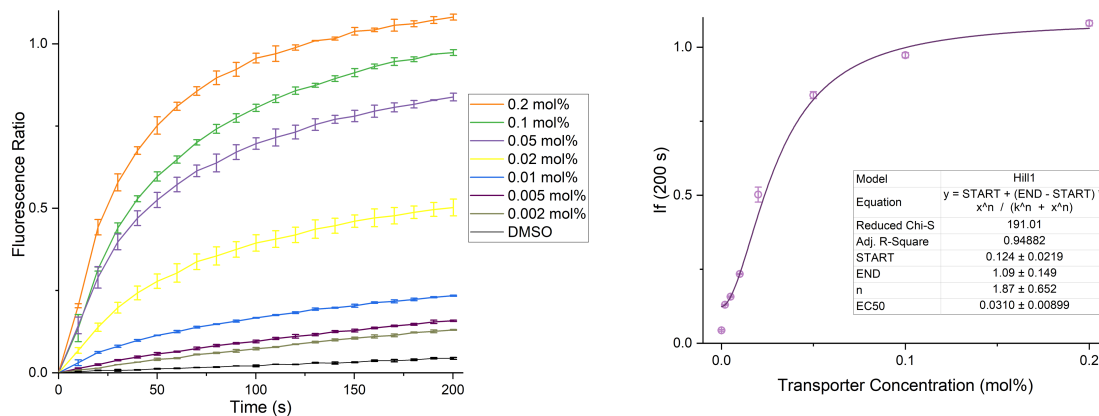
Voltage-Dependent Studies

Three sets of vesicles were prepared following the method described above (A2.3. Vesicle Studies, General Vesicle Preparation). The vesicles were loaded with mixtures of NaCl and KCl (with a total concentration of 100 mM) and HPTS (1 mM) before being suspended in an external solution of NaCl and KCl (with a total concentration of 100 mM). The cationophore valinomycin was added as a DMSO solution (5 µL, 0.1 mol%) before the NaOH (0.5 M) base pulse was added to induce a pH gradient. The salt compositions for the three experiments and resultant membrane potential can be viewed in **Error! Reference source not found.**. All solutions were buffered with HEPES (10 mM) and adjusted to pH 7.0. The fluorometric response of the HPTS probe is known to differ with ionic composition; however, no significant difference has been observed previously between NaCl and KCl.[7] Therefore, different compositions of these salts were used without affecting the HPTS response.

Table S 3. The membrane potential generated in each experiment in relation to both the internal and external K^+ ion concentrations.

$[K^+]_{internal}$ / mM	$[K^+]_{external}$ / mM	Membrane Potential / mV
100	100	0
1.0	100	118
100	1.0	−118

For each experiment, valinomycin was added as a DMSO solution (5 µL, 0.1 mol%) to generate the membrane potential before an aqueous NaOH base pulse (25 µL, 0.5 M) was added at approximately $t = -30$ s. The experiment was initiated with the addition of the transporter as a DMSO solution (5 µL) at a concentration matching the EC_{50} value determined in the NMDG-Cl HPTS assay. Detergent (Triton X-100 (10% v/v in H_2O), 25 µL) was added at $t = 210$ s to lyse the vesicles, and a final fluorometric reading was recorded at $t = 300$ s to signify 100% proton efflux. The ratiometric fluorescent response of the HPTS probe was converted to I_F using **Equation 8** and plotted against time to produce an efflux curve. Experiments were repeated in duplicate for the purposes of accuracy and data redundancy.

Figure S117. Voltage-dependent HPTS base pulse assay for 1,9-bisphenylurea-9(10H)-acridinone (0.01 mol%) at a neutral membrane potential (green), a positive membrane potential (red), and negative membrane potential (blue), generated using valinomycin based on a K^+ concentration gradient. Each data point is the average of two repeats, with the error bars showing the standard deviation.

Figure S118. Voltage-dependent HPTS base pulse assay for 1,9-bisphenylthiourea-9(10H)-acridinone (0.2 mol%) at a neutral membrane potential (green), a positive membrane potential (red), and negative membrane potential (blue), generated using valinomycin based on a K^+ concentration gradient. Each data point is the average of two repeats, with the error bars showing the standard deviation.

Figure S119. Voltage-dependent HPTS base pulse assay for 1,9-bis(4-(trifluoromethyl)phenyl)urea-9(10H)-acridinone (0.002 mol%) at a neutral membrane potential (green), a positive membrane potential (red), and negative membrane potential (blue), generated using valinomycin based on a K^+ concentration gradient. Each data point is the average of two repeats, with the error bars showing the standard deviation.

Figure S120. Voltage-dependent HPTS base pulse assay for 1,9-bis(4-(trifluoromethyl)phenyl)thiourea-9(10H)-acridinone (0.02 mol%) at a neutral membrane potential (green), a positive membrane potential (red), and negative membrane potential (blue), generated using valinomycin based on a K^+ concentration gradient. Each data point is the average of two repeats, with the error bars showing the standard deviation.
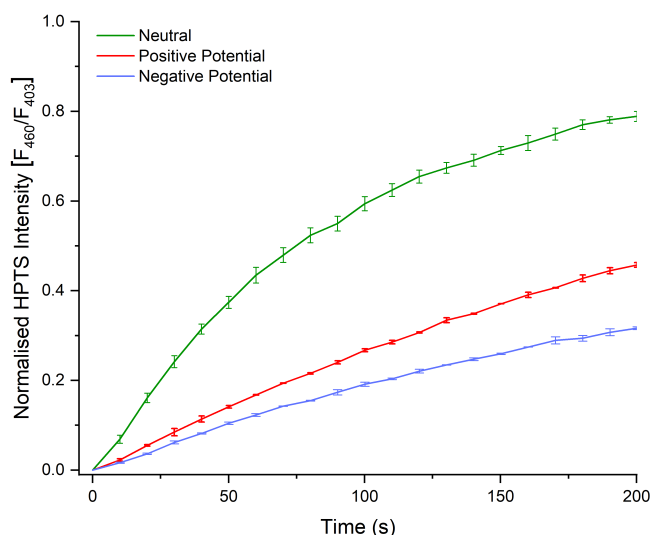
Figure S121. Voltage-dependent HPTS base pulse assay for 1,9-bis(4-nitrophenyl)urea-9(10H)-acridinone (0.00025 mol%) at a neutral membrane potential (green), a positive membrane potential (red), and negative membrane potential (blue) generated using valinomycin based on a K^+ concentration gradient. Each data point is the average of two repeats, with the error bars showing the standard deviation.
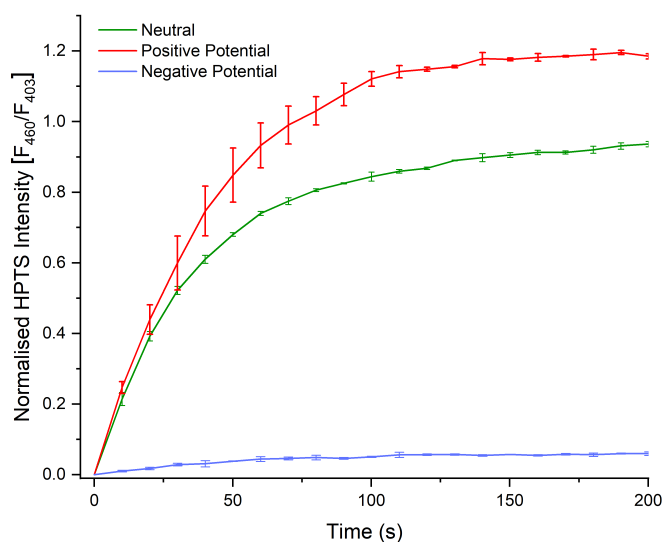

Figure S122. Voltage-dependent HPTS base pulse assay for 1,9-bis(4-nitrophenyl)thiourea-9(10H)-acridinone (0.005 mol%) at a neutral membrane potential (green), a positive membrane potential (red), and negative membrane potential (blue), generated using valinomycin based on a K^+ concentration gradient. Each data point is the average of two repeats, with the error bars showing the standard deviation.
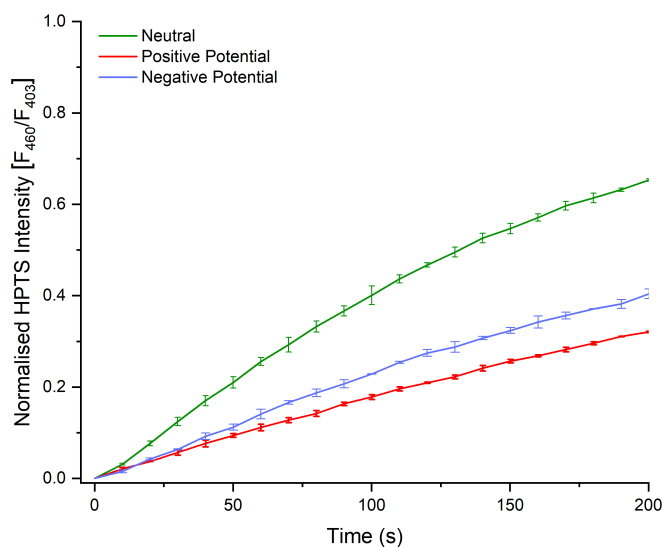
Figure S123. Voltage-dependent HPTS base pulse assay for 1,9-bis(3,5-bis-(trifluoromethyl)phenyl)urea-9(10H)-acridinone (0.01 mol%) at a neutral membrane potential (green), a positive membrane potential (red), and negative membrane potential (blue), generated using valinomycin based on a K^+ concentration gradient. Each data point is the average of two repeats, with the error bars showing the standard deviation.
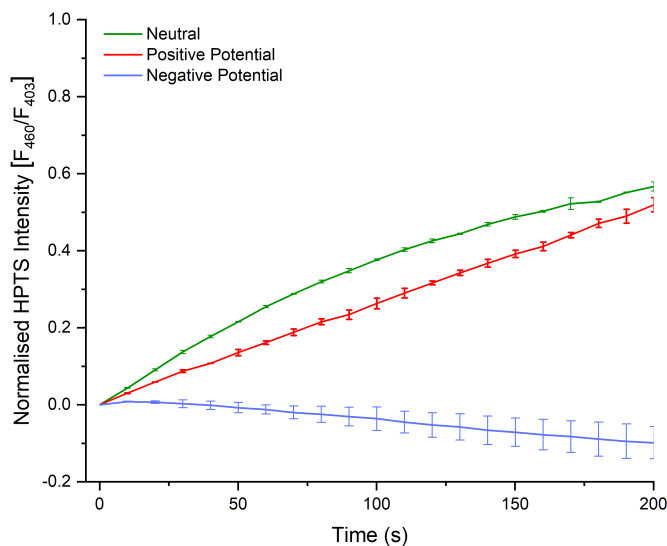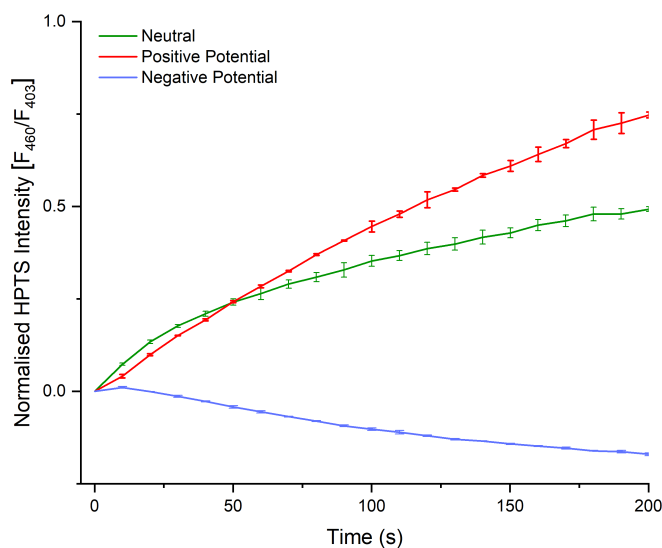

Figure S124. Voltage-dependent HPTS base pulse assay for 1,9-bis(3,5-bis-(trifluoromethyl)phenyl)thiourea-9(10H)-acridinone (0.02 mol%) at a neutral membrane potential (green), a positive membrane potential (red), and negative membrane potential (blue), generated using valinomycin based on a K^+ concentration gradient. Each data point is the average of two repeats, with the error bars showing the standard deviation.
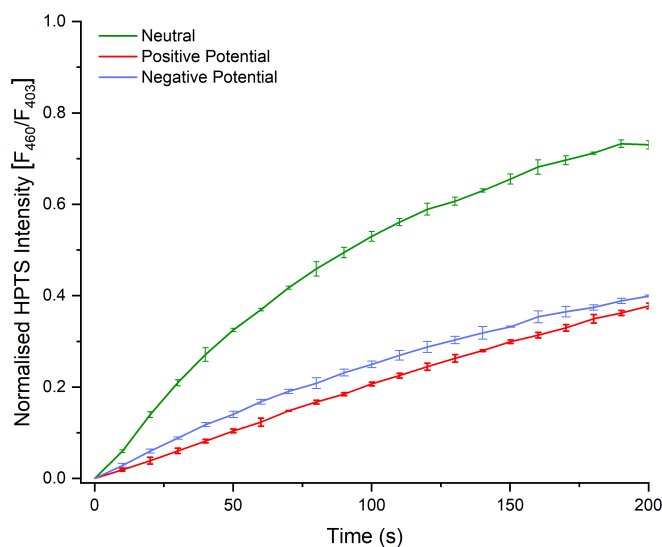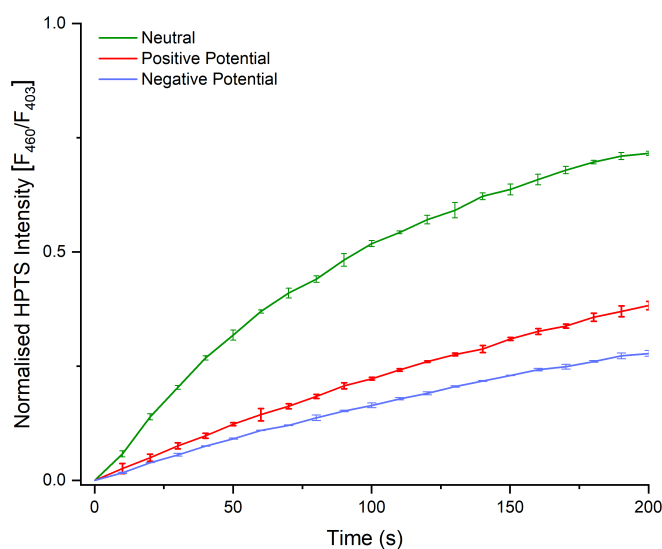
Figure S125. Voltage-dependent HPTS base pulse assay for 1,9-bis(4-(pentafluorosulfanyl)phenyl)urea-9(10H)-acridinone (0.005 mol%) at a neutral membrane potential (green), a positive membrane potential (red), and negative membrane potential (blue), generated using valinomycin based on a K^+ concentration gradient. Each data point is the average of two repeats, with the error bars showing the standard deviation.
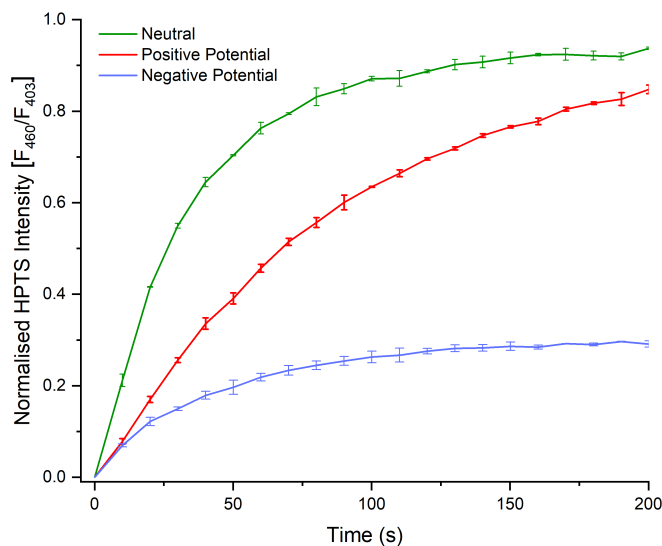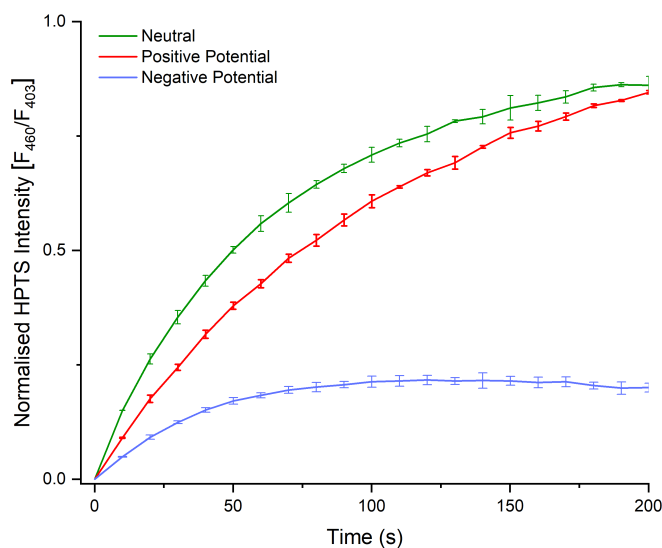

Figure S126. Voltage-dependent HPTS base pulse assay for 1,9-bis(4-(pentafluorosulfanyl)phenyl)thiourea-9(10H)-acridinone (0.05 mol%) at a neutral membrane potential (green), a positive membrane potential (red), and negative membrane potential (blue), generated using valinomycin based on a K^+ concentration gradient. Each data point is the average of two repeats, with the error bars showing the standard deviation.
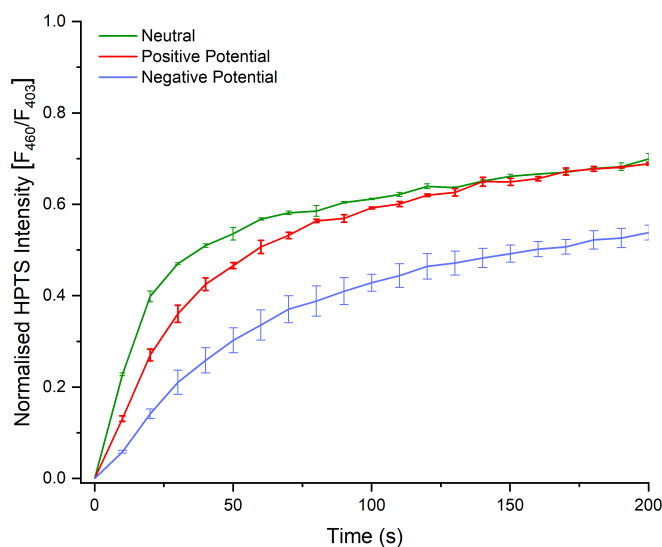
Figure S127. Voltage-dependent HPTS base pulse assay for a DMSO control at a neutral membrane potential (green), a positive membrane potential (red), and negative membrane potential (blue) generated using valinomycin based on a K^+ concentration gradient. Each data point is the average of two repeats, with the error bars showing the standard deviation.
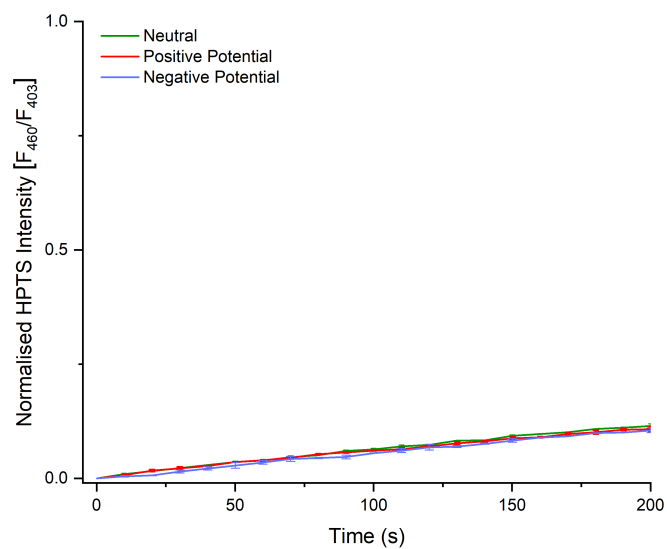
HPTS Mechanistic Studies

An external solution of KCl (100 mM) was prepared and adjusted to pH 7.0 using HEPES buffer (10 mM). An internal solution was prepared using the same external solution with the addition of the pH-sensitive fluorescent dye HPTS (1 mM). Vesicles were prepared following the procedure outlined above (A2.3. Vesicle Studies, General Vesicle Preparation). After extrusion, they were passed through a G-25 Sephadex® column that had been pre-rinsed with the external KCl solution. The vesicles were collected and diluted with the external solution to a 10 mL volume with a known concentration.

Untreated vesicle experiments were conducted by diluting the vesicle suspension with additional external solution to give afford a 0.1 mM concentration in 2.5 mL. An aliquot of the aqueous NaOH solution (25 µL, 0.5 M) was added at approximately $t = -30$ s before the experiment was initiated with the addition of the transporter DMSO solution (5 µL). The concentration of the transporter was determined by the EC_{50} calculated using the HPTS NMDG-Cl assay. Detergent (Triton X-100 (10% v/v in water), 25 µL) was added at $t = 210$ s to lyse the vesicles, and a final reading was recorded at $t = 300$ s to signify 100% proton efflux.

Experiments conducted with carbonyl cyanide m-chlorophenyl hydrazone (CCCP) were performed by adding the protonophore as a DMSO solution (25 µL, 1 mol%) prior to the addition of the base pulse, before following the experimental procedure outlined for the untreated vesicle experiments. Next, fatty acid free vesicles were produced by stirring a portion of the vesicle suspended solution for 30 min in the presence of 1 mol% bovine serum albumin (BSA), which sequestered the membrane-embedded fatty acids. The experimental procedure continued with the description outlined above for the untreated vesicles. Finally, a known quantity of fatty acids was added to the BSA-treated vesicles as an oleic acid solution (10 mol%), 5 min prior to the remaining set of experiments. A DMSO blank run was also performed, and experiments were repeated in duplicate.

Figure S128. HPTS KCl base pulse assay for 1,9-bisphenylurea-9(10H)-acridinone (0.01 mol%) in untreated vesicles (orange), coupled to CCCP (green), in vesicles treated with BSA (blue), and in BSA-treated vesicles after the addition of OA (pink). A DMSO control (grey) is also displayed. Each data point is the average of two repeats, with the error bars showing the standard deviation.

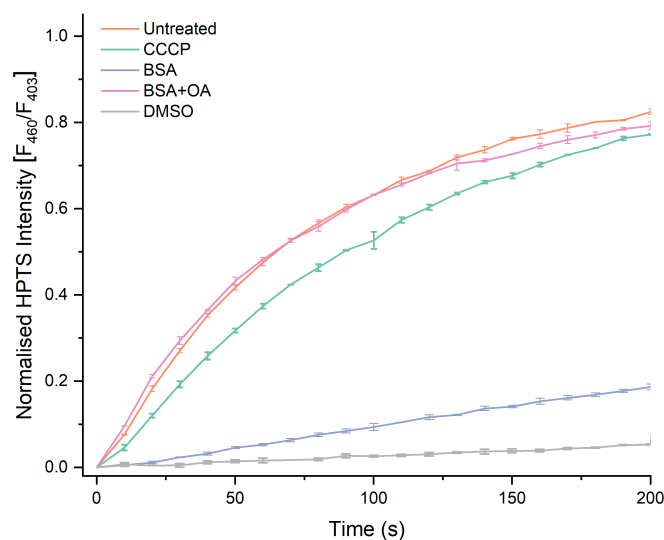Figure S129. Efflux plots for the HPTS KCl base pulse assay for 1,9-bisphenylthiourea-9(10H)-acridinone (0.2 mol%) in untreated vesicles (orange), coupled to CCCP (green), in vesicles treated with BSA (blue), and in BSA-treated vesicles after the addition of OA (pink). A DMSO control (grey) is also displayed. Each data point is the average of two repeats, with the error bars showing the standard deviation.

Figure S130. HPTS KCl base pulse assay for 1,9-bis(4-(trifluoromethyl)phenyl)urea-9(10H)-acridinone (0.002 mol%) in untreated vesicles (orange), coupled to CCCP (green), in vesicles treated with BSA (blue), and in BSA-treated vesicles after the addition of OA (pink). A DMSO control (grey) is also displayed. Each data point is the average of two repeats, with the error bars showing the standard deviation.

Figure S131. HPTS KCl base pulse assay for 1,9-bis(4-(trifluoromethyl)phenyl)thiourea-9(10H)-acridinone (0.02 mol%) in untreated vesicles (orange), coupled to CCCP (green), in vesicles treated with BSA (blue), and in BSA-treated vesicles after the addition of OA (pink). A DMSO control (grey) is also displayed. Each data point is the average of two repeats, with the error bars showing the standard deviation.
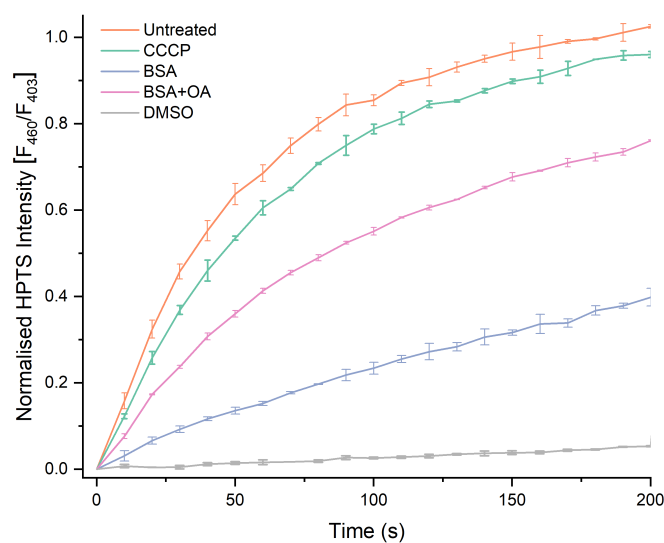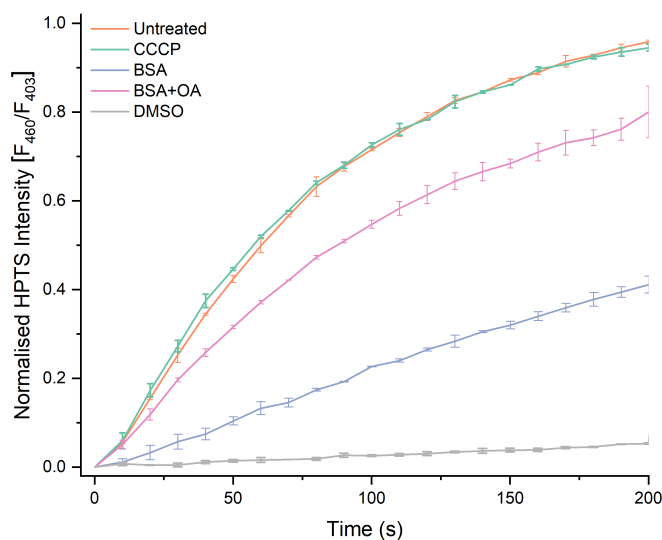
Figure S132. HPTS KCl base pulse assay for 1,9-bis(4-nitrophenyl)urea-9(10H)-acridinone (0.0002 mol%) in untreated vesicles (orange), coupled to CCCP (green), in vesicles treated with BSA (blue), and in BSA-treated vesicles after the addition of OA (pink). A DMSO control (grey) is also displayed. Each data point is the average of two repeats, with the error bars showing the standard deviation.
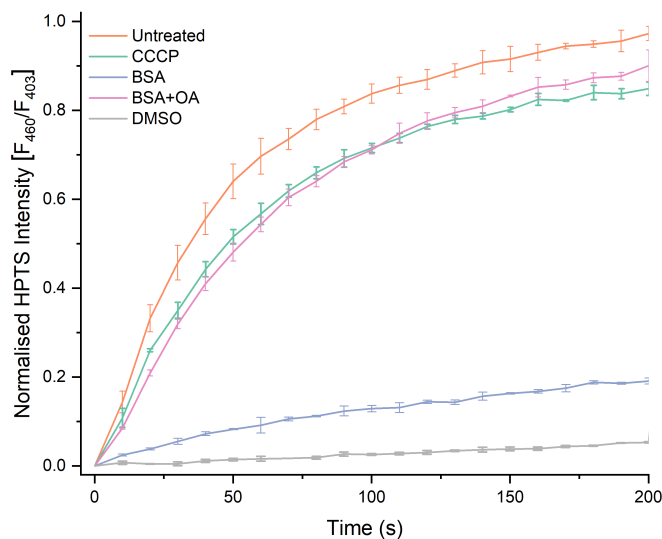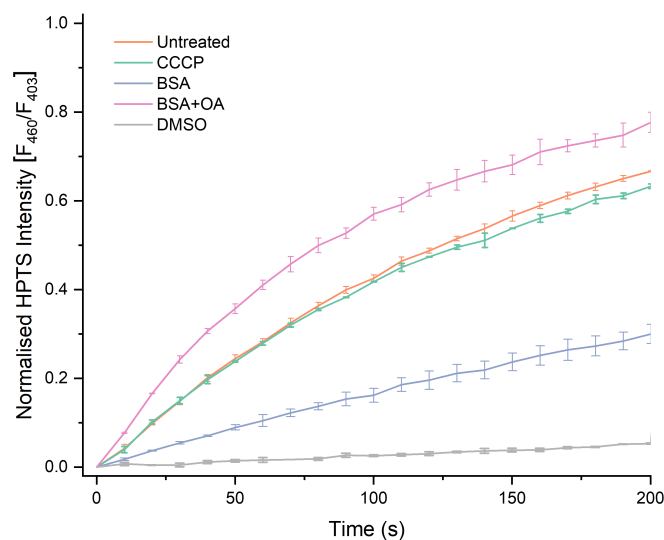

Figure S133. HPTS KCl base pulse assay for 1,9-bis(4-nitrophenyl)thiourea-9(10H)-acridinone (0.005 mol%) in untreated vesicles (orange), coupled to CCCP (green), in vesicles treated with BSA (blue), and in BSA-treated vesicles after the addition of OA (pink). A DMSO control (grey) is also displayed. Each data point is the average of two repeats, with the error bars showing the standard deviation.

Figure S134. HPTS KCl base pulse assay for 1,9-bis(3,5-bis-(trifluoromethyl)phenyl)urea-9(10H)-acridinone (0.01 mol%) in untreated vesicles (orange), coupled to CCCP (green), in vesicles treated with BSA (blue), and in BSA-treated vesicles after the addition of OA (pink). A DMSO control (grey) is also displayed. Each data point is the average of two repeats, with the error bars showing the standard deviation.
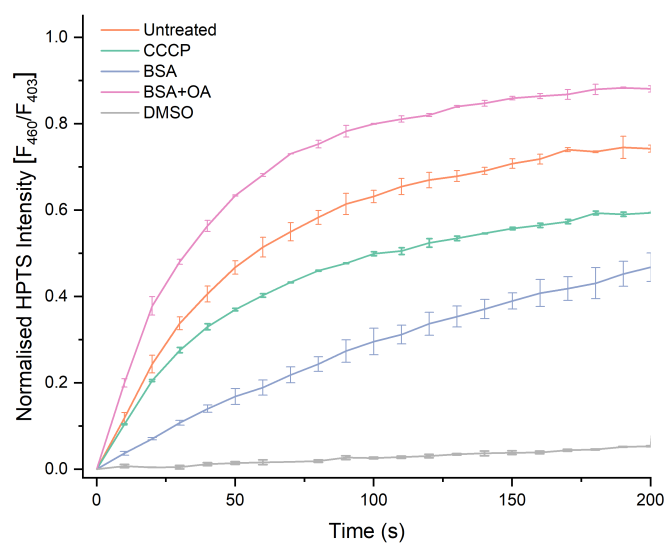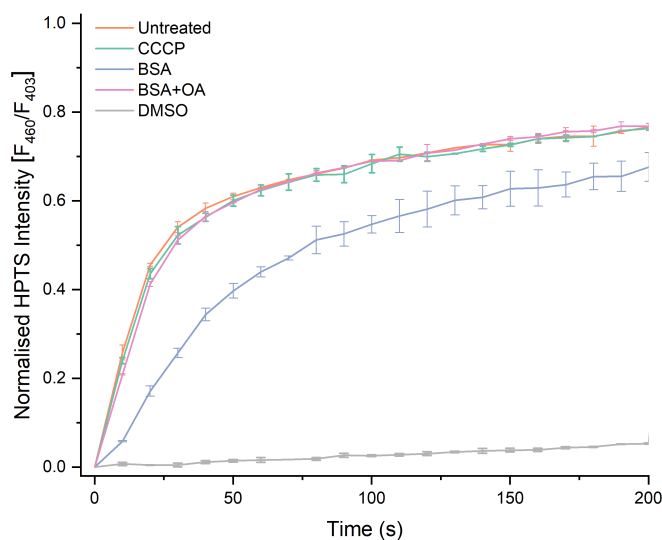

Figure S135. HPTS KCl base pulse assay for 1,9-bis(3,5-bis-(trifluoromethyl)phenyl)thiourea-9(10H)-acridinone (0.02 mol%) in untreated vesicles (orange), coupled to CCCP (green), in vesicles treated with BSA (blue), and in BSA-treated vesicles after the addition of OA (pink). A DMSO control (grey) is also displayed. Each data point is the average of two repeats, with the error bars showing the standard deviation.
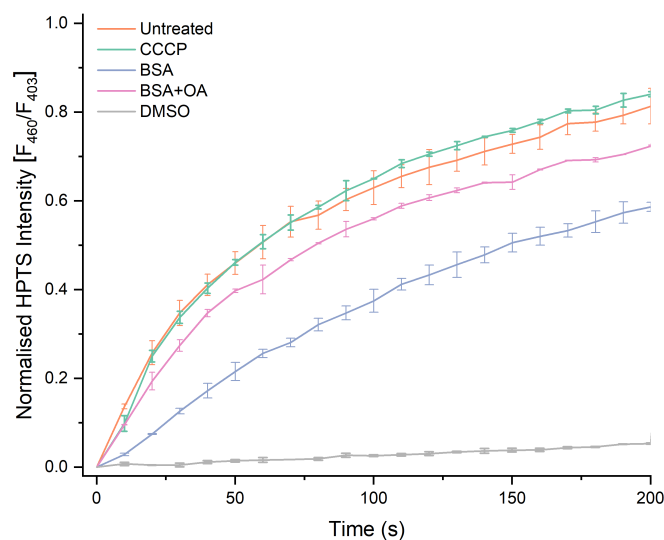
Figure S136. HPTS KCl base pulse assay for 1,9-bis(4-(pentafluorosulfanyl)phenyl)urea-9(10H)-acridinone (0.005 mol%) in untreated vesicles (orange), coupled to CCCP (green), in vesicles treated with BSA (blue), and in BSA-treated vesicles after the addition of OA (pink). A DMSO control (grey) is also displayed. Each data point is the average of two repeats, with the error bars showing the standard deviation.
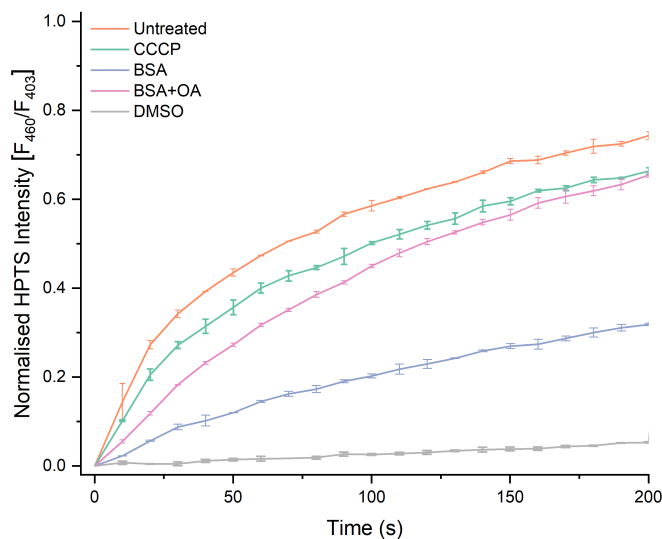

Figure S137. HPTS KCl base pulse assay for 1,9-bis(4-(pentafluorosulfanyl)phenyl)thiourea-9(10H)-acridinone (0.05 mol%) in untreated vesicles (orange), coupled to CCCP (green), in vesicles treated with BSA (blue), and in BSA-treated vesicles after the addition of OA (pink). A DMSO control (grey) is also displayed. Each data point is the average of two repeats, with the error bars showing the standard deviation.
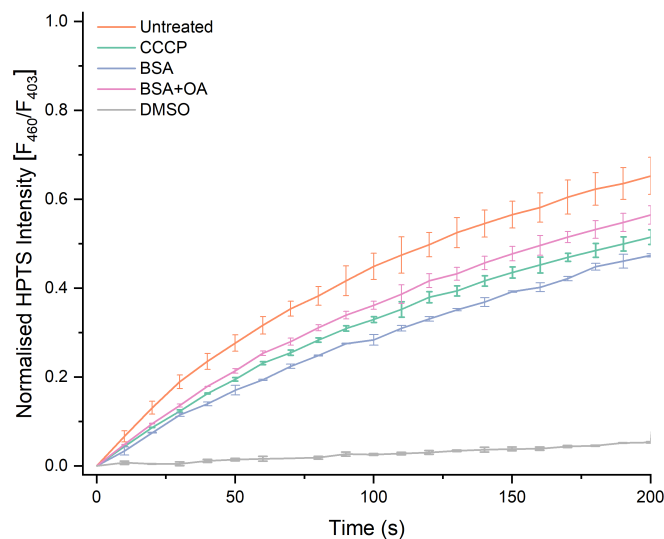
HPTS Anion Selectivity Assay

Vesicles were prepared via the method described above with an internal solution of NaCl (100 mM) and HPTS (1 mM), buffered with HEPES (10 mM) and adjusted to pH 7.0. Six separate external solutions were made in an isotonic HEPES buffer containing either NaCl, NaBr, NaI, NaNO₃ or NaClO₄, respectively (All at a concentration of 100 mM).[8] After extrusion, vesicles were eluted through a G-25 Sephadex® size-exclusion column pre-rinsed with the NaCl external solution, which was also used as the eluent. To a 4.5 mL plastic cuvette, and during each experiment, a vesicle suspension was made by diluting with the chosen external solution (0.1 mM, 2.5 mL). Anion exchange was initiated by adding the transporters as a DMSO solution (5 µL) at a concentration slightly higher than the EC_{50} value determined in the NMDG-Cl HPTS assay. Note that NaI contained elemental iodine impurities, which may act as a transporter for I^-. To account for this, rather than waiting approx. 30 s for system equilibration if the fluorescence ratios are too different, the transporter was added immediately. Conversion to I_F was performed using **Equation 8**. A DMSO control run was also performed, and experiments were repeated in duplicate for the purposes of accuracy and data redundancy.
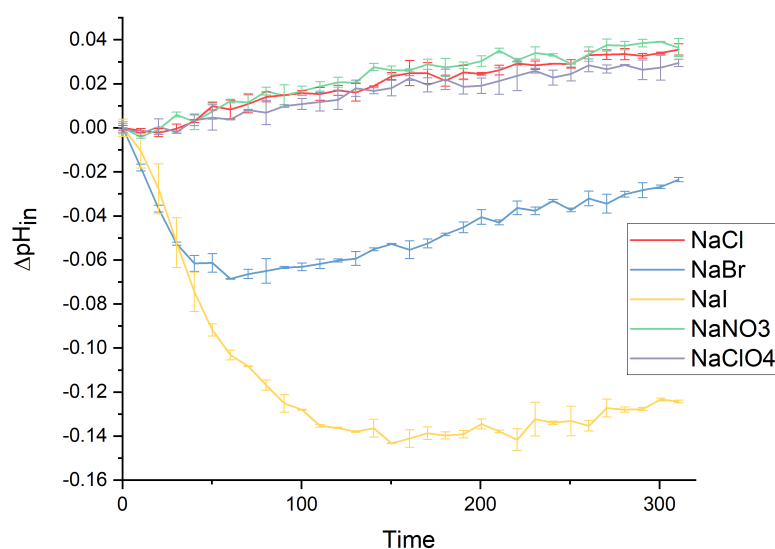

Figure S138. The anion selectivity assay for 1,9-bisphenylurea-9(10H)-acridinone (0.01 mol%, added at t = 0 s). Initial conditions: In: NaCl (100 mM), HPTS (1 mM), HEPES (10 mM), pH 7.0; Out: NaX(100 mM), HEPES (10 mM), pH 8.0. [POPC] = 0.1 mM, [DMSO] = 5 µL. Error bars represent standard deviations from two runs.
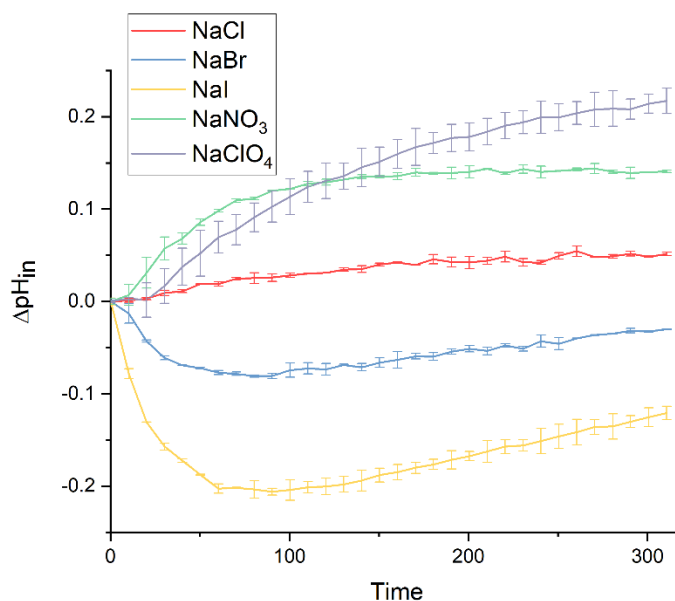
Figure S139. The anion selectivity assay for 1,9-bisphenylthiourea-9(10H)-acridinone (0.2 mol%, added at $t = 0$ s). Initial conditions: In: NaCl (100 mM), HPTS (1 mM), HEPES (10 mM), pH 7.0; Out: NaX(100 mM), HEPES (10 mM), pH 8.0. [POPC] = 0.1 mM, [DMSO] = 5 μL. Error bars represent standard deviations from two runs.

Figure S140. The anion selectivity assay for 1,9-bis(4-(trifluoromethyl)phenyl)urea-9(10H)-acridinone (0.002 mol%, added at $t = 0$ s). Initial conditions: In: NaCl (100 mM), HPTS (1 mM), HEPES (10 mM), pH 7.0; Out: NaX(100 mM), HEPES (10 mM), pH 8.0. [POPC] = 0.1 mM, [DMSO] = 5 μL. Error bars represent standard deviations from two runs.

Figure S141. The anion selectivity assay for 1,9-bis(4-(trifluoromethyl)phenyl)thiourea-9(10H)-acridinone (0.02 mol%, added at $t = 0$ s). Initial conditions: In: NaCl (100 mM), HPTS (1 mM), HEPES (10 mM), pH 7.0; Out: NaX(100 mM), HEPES (10 mM), pH 8.0. [POPC] = 0.1 mM, [DMSO] = 5 μL. Error bars represent standard deviations from two runs.
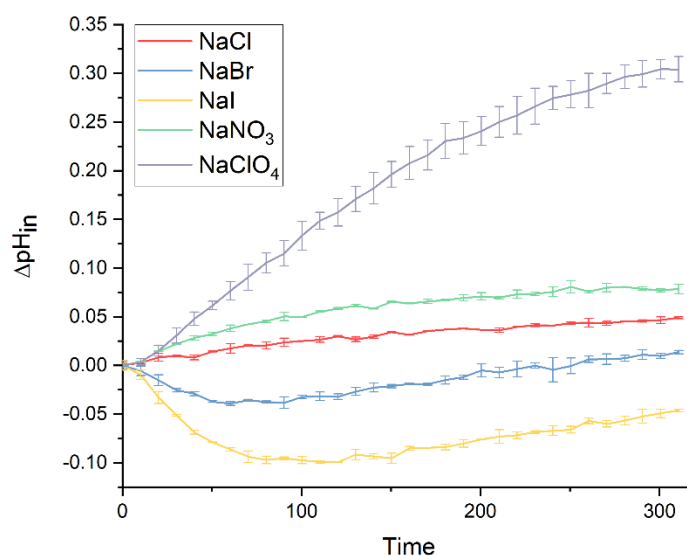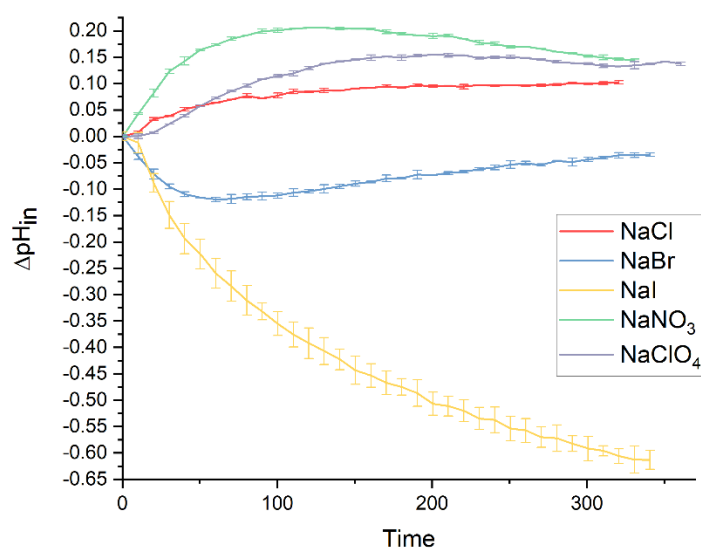

Figure S142. The anion selectivity assay for 1,9-bis(4-nitrophenyl)urea-9(10H)-acridinone (0.0002 mol%, added at $t = 0$ s). Initial conditions: In: NaCl (100 mM), HPTS (1 mM), HEPES (10 mM), pH 7.0; Out: NaX(100 mM), HEPES (10 mM), pH 8.0. [POPC] = 0.1 mM, [DMSO] = 5 μL. Error bars represent standard deviations from two runs.

Figure S143. The anion selectivity assay for 1,9-bis(4-nitrophenyl)thiourea-9(10H)-acridinone (0.01 mol%, added at $t = 0$ s). Initial conditions: In: NaCl (100 mM), HPTS (1 mM), HEPES (10 mM), pH 7.0; Out: NaX(100 mM), HEPES (10 mM), pH 8.0. [POPC] = 0.1 mM, [DMSO] = 5 μL. Error bars represent standard deviations from two runs.
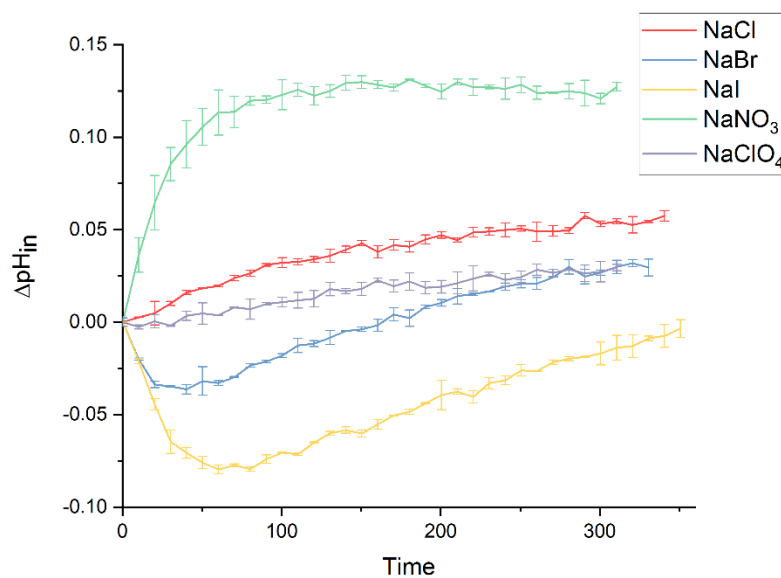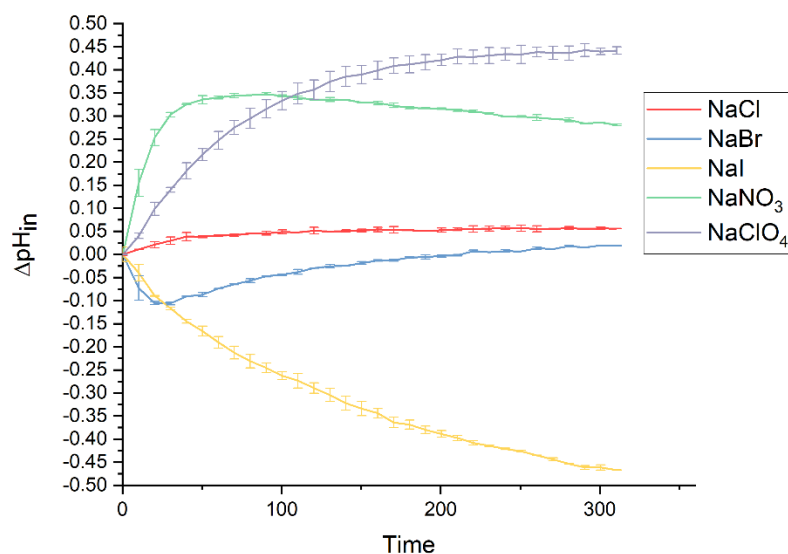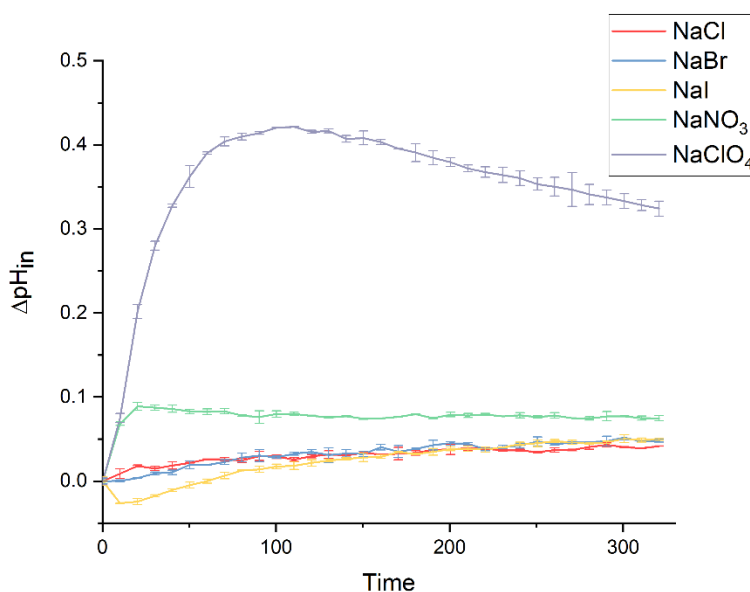

Figure S144. The anion selectivity assay for 1,9-bis(3,5-bis-(trifluoromethyl)phenyl)urea-9(10H)-acridinone (0.01 mol%, added at $t = 0$ s). Initial conditions: In: NaCl (100 mM), HPTS (1 mM), HEPES (10 mM), pH 7.0; Out: NaX(100 mM), HEPES (10 mM), pH 8.0. [POPC] = 0.1 mM, [DMSO] = 5 μL. Error bars represent standard deviations from two runs.
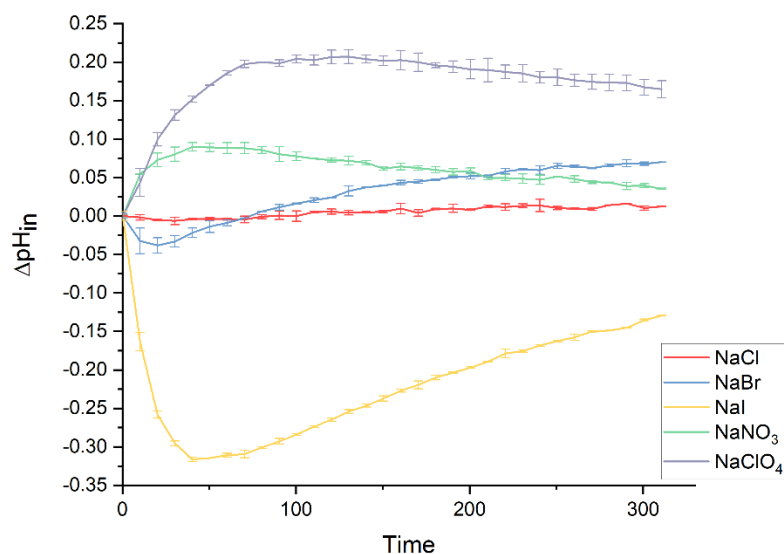
Figure S145. The anion selectivity assay for 1,9-bis(3,5-bis-(trifluoromethyl)phenyl)thiourea-9(10H)-acridinone (0.02 mol%, added at t = 0 s). Initial conditions: In: NaCl (100 mM), HPTS (1 mM), HEPES (10 mM), pH 7.0; Out: NaX(100 mM), HEPES (10 mM), pH 8.0. [POPC] = 0.1 mM, [DMSO] = 5 μL. Error bars represent standard deviations from two runs.

Figure S146. The anion selectivity assay for 1,9-bis(4-(pentafluorosulfanyl)phenyl)urea-9(10H)-acridinone (0.005 mol%, added at t = 0 s). Initial conditions: In: NaCl (100 mM), HPTS (1 mM), HEPES (10 mM), pH 7.0; Out: NaX(100 mM), HEPES (10 mM), pH 8.0. [POPC] = 0.1 mM, [DMSO] = 5 μL. Error bars represent standard deviations from two runs.

Figure S147.The anion selectivity assay for 1,9-bis(4-(pentafluorosulfanyl)phenyl)thiourea-9(10H)-acridinone (0.05 mol%, added at $t = 0$ s). Initial conditions: In: NaCl (100 mM), HPTS (1 mM), HEPES (10 mM), pH 7.0; Out: NaX(100 mM), HEPES (10 mM), pH 8.0. [POPC] = 0.1 mM, [DMSO] = 5 μL. Error bars represent standard deviations from two runs.

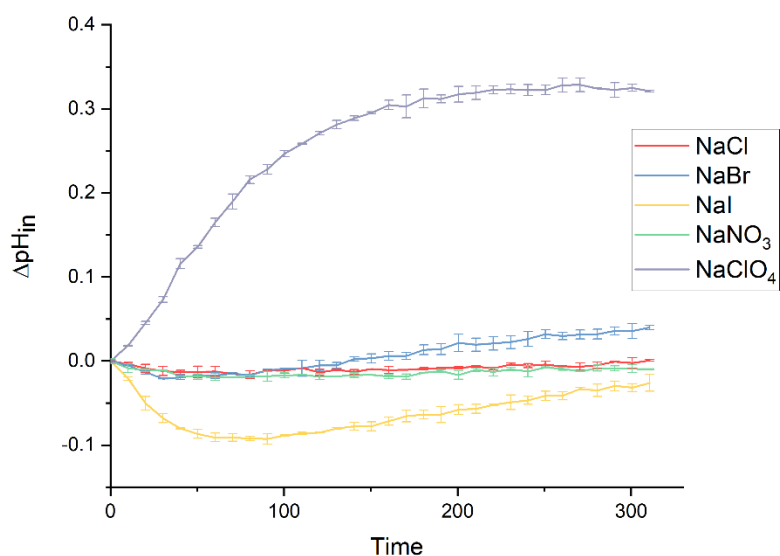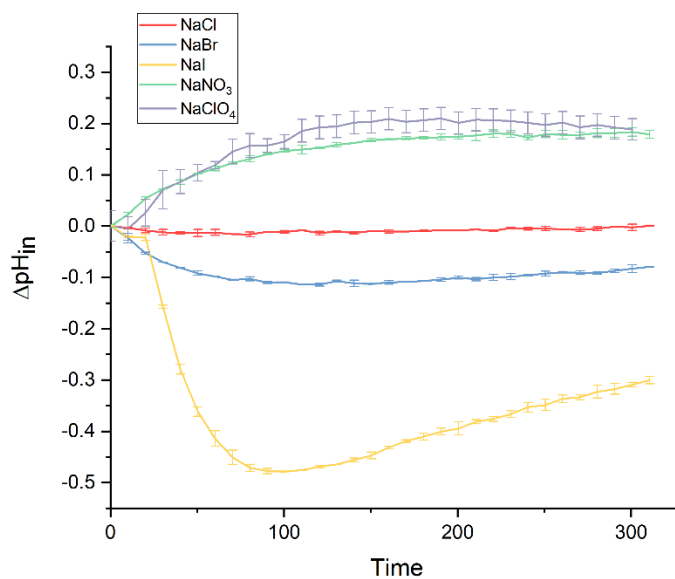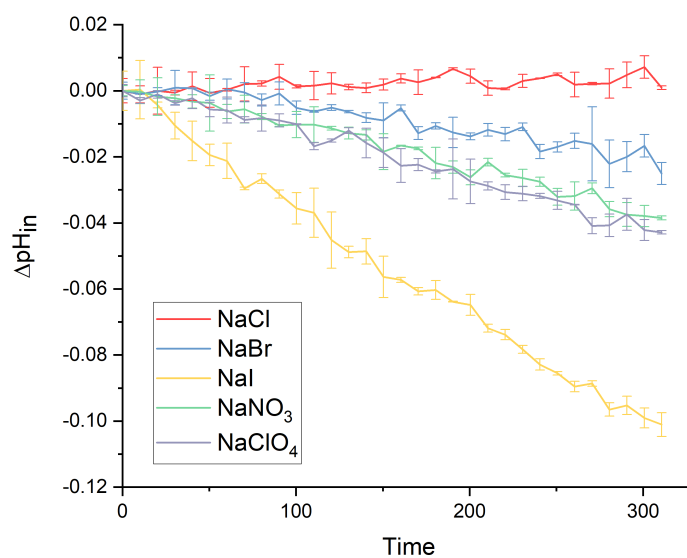Figure S148. The anion selectivity assay for DMSO blank, added at $t = 0$ s. Initial conditions: In: NaCl (100 mM), HPTS (1 mM), HEPES (10 mM), pH 7.0; Out: NaX(100 mM), HEPES (10 mM), pH 8.0. [POPC] = 0.1 mM, [DMSO] = 5 μL. Error bars represent standard deviations from two runs.

Molecular Modelling

A PM6 semi-empirical model was calculated for compounds **3** and **8** in the presence of Cl⁻ using Spartan '14 to elucidate the equilibrium geometry of the binding modes for each receptor.
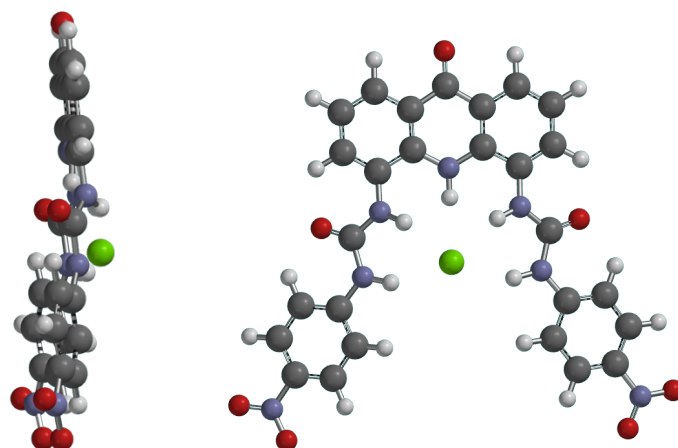

Figure S149. Ground-state equilibrium geometry calculated for compound **3** in the presence of Cl⁻. The molecule can adopt a near-flat conformation.
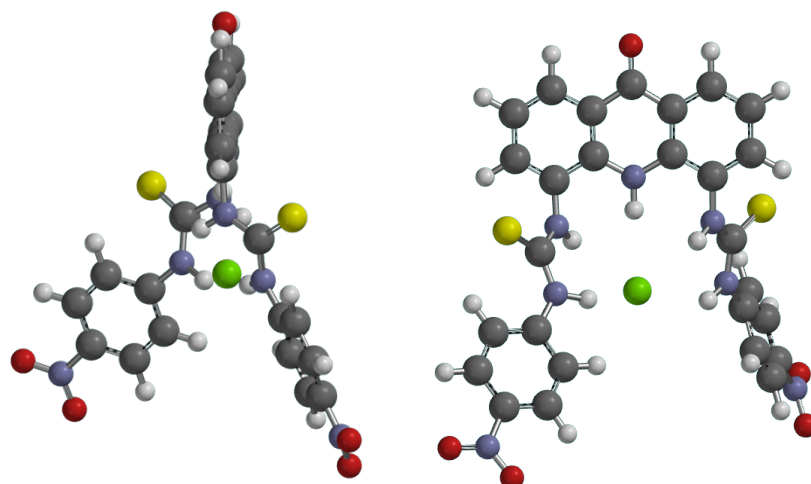

Figure S149. Ground-state equilibrium geometry calculated for compound **8** in the presence of Cl⁻. The sulfur atoms are almost perpendicular to the acridinone plane.

References

1.   McPhillips, T. M.; McPhillips, S. E.; Chiu, H. J.; Cohen, A. E.; Deacon, A. M.; Ellis, P. J.; Garman, E.; Gonzalez, A.; Sauter, N. K.; Phizackerley, R. P.; Soltis, S. M.; Kuhn, P., Blu-Ice and the Distributed Control System: software for data acquisition and instrument control at macromolecular crystallography beamlines. *J Synchrotron Radiat* **2002,** *9* (Pt 6), 401-6.

2.   Kabsch, W., Automatic processing of rotation diffraction data from crystals of initially unknown symmetry and cell constants. *J. Appl. Crystallogr.* **1993,** *26* (6), 795-800.

3.   Sheldrick, G., A short history of SHELX. *Acta Crystallogr., Sect. A* **2008,** *64* (1), 112-122.

4.   Sheldrick, G., Crystal structure refinement with SHELXL. *Acta Crystallogr., Sect. C* **2015,** *71* (1), 3-8.

5.   Dolomanov, O. V.; Bourhis, L. J.; Gildea, R. J.; Howard, J. A. K.; Puschmann, H., OLEX2: a complete structure solution, refinement and analysis program. *Journal of applied crystallography* **2009,** *42* (2), 339-341.

6.   Jowett, L. A.; Gale, P. A., Supramolecular methods: the chloride/nitrate transmembrane exchange assay. *Supramolecular Chemistry* **2019,** *31* (5), 297-312.

7.   Wu, X.; Small, J. R.; Cataldo, A.; Withecombe, A. M.; Turner, P.; Gale, P. A., Voltage-Switchable HCl Transport Enabled by Lipid Headgroup–Transporter Interactions. *Angewandte Chemie International Edition* **2019,** *58* (42), 15142-15147.

8.   Wu, X.; Gale, P. A., Measuring anion transport selectivity: a cautionary tale. *Chemical Communications* **2021,** *57* (33), 3979-3982.